MATHEMATICAL MODELLING OF THE MICROSTRUCTURAL EVOLUTION DURING THE HOT ROLLING OF AA5083 ALUMINUM ALLOYS

by

Simon P. Jupp

B.A.Sc., The University of British Columbia, 1999

A THESIS SUBMITTED IN PARTIAL FULFILLMENT OF
THE REQUIREMENTS FOR THE DEGREE OF

MASTER OF APPLIED SCIENCE

in

THE FACULTY OF GRADUATE STUDIES
DEPARTMENT OF METALS AND MATERIALS ENGINEERING

We accept this thesis as conforming
to the required standard

THE UNIVERSITY OF BRITISH COLUMBIA

August 2001

In presenting this thesis in partial fulfilment of the requirements for an advanced degree at the University of British Columbia, I agree that the Library shall make it freely available for reference and study. I further agree that permission for extensive copying of this thesis for scholarly purposes may be granted by the head of my department or by his or her representatives. It is understood that copying or publication of this thesis for financial gain shall not be allowed without my written permission.

Department of ___Metals and Materials Engineering___

The University of British Columbia
Vancouver, Canada

Date ___Sept. 6, 2001___

DE-6 (2/88)

Abstract

A mathematical model to predict the through-thickness temperature, strain and strain rate distribution after a single hot rolling stand was developed and applied to two commercially significant alloys, AA5083 and AA5056 aluminum alloys. For the AA5083 aluminum alloy application a microstructure component was added to model the microstructure evolution that occurred in the strip in the time between the roll bite exit and the quench.

The deformation model was developed using a commercial finite element package, ABAQUS™, which couples the thermal and deformation phenomena that occur during strip rolling. The model is able to predict the temperature, strain and strain rate distribution at any position in the strip and any time during the roll bite.

The microstructure model is a "user-defined" subroutine within ABAQUS™ that uses semi-empirical equations from in the literature quantifying the microstructure (fraction recrystallised) changes that occur between the roll bite exit and the quench. The microstructure model uses roll bite exit values for deformation temperature and strain, as well as the mean strain rate for at the through-thickness locations. The thermal history of the strip in the interpass region is predicted by ABAQUS™ based on convective heat transfer between the strip and the environment. This is used in the microstructure model to predict recrystallisation kinetics.

Validation of the model using a literature comparison and industrial data indicated reasonable predictions for temperature, strain and rolling loads. However, the microstructure model using Raghunathan's equation is not able to consistently predict the fraction recrystallised. A sensitivity analysis indicated that the microstructure model used to predict recrystallisation kinetics was extremely sensitive to the deformation temperature as well as the fitting parameters used in the equation.

Table of Contents

List of Tables

List of Figures

List of Symbols

$\dot{\varepsilon}$	Strain rate	s^{-1}
Q_{def}	Activation energy of deformation	$J\ mol^{-1}$
R	Gas constant	$J\ mol^{-1}\ K^{-1}$
T_{def}	Deformation temperature	K
Z	Zener-Hollomon parameter	s-1
X_V	Fraction recrystallised	
β	JMAK equation constant	
n	Exponent	
t	Time	s
$t_{0.5}$	Time to 50% recrystallised	s
a,b,c,d,e	Microstructure equations fitting coefficients	
d_o	Initial grain size	μm
ε	Strain	
Q_{rex}	Activation energy of recrystallisation	$J\ mol^{-1}$
T_{rex}	Recrystallisation temperature	K
d_{rex}	Recrystallised grain size	μm
C_t	Fitting constant	
M_{GB}	Grain boundary mobility	
P_D	Grain boundary driving pressure	J
N_v	Number of recrystallised grain nucleation sites	
θ	Sub-grain boundary angle	°
θ_m	Grain boundary angle	°
M	Sub-grain boundary mobility	
d_{gg}	Recrystallised grain after grain growth	μm
A	Constant	
p_c	Critical particle diameter	μm

T	Temperature	K
P_z	Zener-drag pressure	Pa
γ	Surface energy	kJ
f	Particle volume fraction	
r	Particle radius	μm
r^*	Critical particle size for nucleation	μm
K	Geometric constant	
$\bar{\dot{\varepsilon}}$	Mean strain rate	s^{-1}
[t]	Traction force matrix per unit area	N m^{-2}
[δu]	Displacement field	
S	Surface area	m^2
[f]	Force matrix per unit volume	N m^{-3}
V	Volume	m^3
[σ]	True stress matrix	Pa
[x]	Direction matrix	
k	Thermal conductivity	W m^{-1}°C^{-1}
$\dot{Q}$	Rate of heat generation	W
ρ	Density	kg m^{-3}
C_p	Heat capacity	J kg^{-1} °C^{-1}
η	Efficiency term	
$\bar{\sigma}_{flow}$	Effective flow stress	Pa
[C_P]	Heat capacity matrix	J kg^{-1} °C^{-1}
$\{\dot{T}\}$	Rate of temperature change vector	°C s^{-1}
[K_C]	Heat conduction matrix	
$\{T\}$	Temperature vector	°C
$\{Q\}$	Heat flux vector	J m^{-2}
α	Stress multiplier	
A	Hyperbolic sine coefficient	

r	radial location	mm
h	Interface heat transfer coefficient	$W\ m^{-2}\ K^{-1}$
P	Pressure	$kg\ mm^{-2}$ or Pa
τ_{crit}	Critical shear stress	Pa
μ	Coulomb friction coefficient	
δt_i	Time increment	s
W	Temperature compensated time parameter	
$W_{0.5}$	Temperature compensated time to 50% recrystallisation	

Acknowledgements

Chapter 1 Introduction

The demand by customers for stringent property specifications along with maximising production requirements to remain efficient and economically viable in an increasingly competitive market is continuously driving aluminum sheet manufacturers forward. In order to remain competitive and efficient it is critical that aluminum producers understand the influence of their processing operation on the properties that are produced in the final product.

One method of achieving this is to develop mathematical models that simulate the microstructure and texture evolution at each stage of the process and thereby achieve a greater understanding of the effect of the process variables on the properties of the final product. Mathematical models of this nature attempt to embody the complex interactions among plasticity, heat flow, microstructural and texture changes that occur during an industrial manufacturing process. Microstructural engineering, which focuses on quantitatively linking the microstructure and texture development in a material to its processing parameters using fundamentally based mathematical models, is key to meeting this challenge.

1.1 Modelling

During the past two decades, computer simulation of the microstructure evolution during thermomechanical processing, and in particular hot rolling, of carbon-manganese and microalloyed steels has received considerable attention. The incentive for the steel industry behind this research has been the need to optimize their processing conditions by understanding the relationship between the processing variables (strain, strain rate and temperature), the resulting microstructure and the final mechanical properties of the material.

This same approach of combining models of the thermal and deformation history of the metal with the microstructure changes, has recently been applied to the hot rolling

of aluminum and aluminum alloys [1-3], but it is a relatively new activity with only a few studies published in the open literature. Part of the reason microstructure models of industrial hot rolling of aluminum have lagged behind those for steel is because: 1) microstructure modelling, in particular recrystallisation, of aluminum is complex and requires a greater understanding of the physical mechanisms in order to make accurate microstructure predictions and 2) texture evolution during aluminum recrystallisation has a significant impact on the final properties. In fact it has proved to be difficult to describe recrystallisation during hot rolling of aluminum with the same simplified approach that has been used for steels [4].

The interactions between stress/strain, temperature and microstructure during hot deformation are very complex.
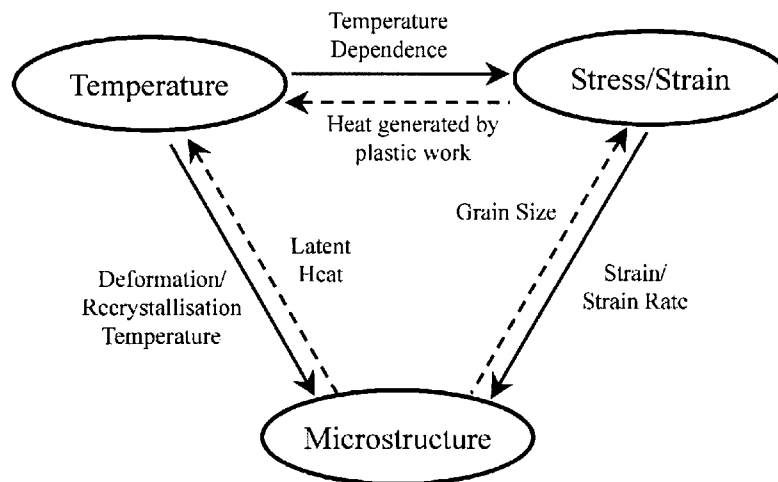
Figure 1.1 - Schematic illustrating complex relationship between stress/strain, temperature and microstructure.

As shown in Figure 1.1, each parameter will have an effect on the other parameters and hence a model must accurately reflect these dependencies. For example, the temperature of the strip is influenced by both the latent heat released during recrystallisation and heat generated by plastic work. In turn, the temperature will affect the microstructure evolution during rolling and in the interstand region. Also the stress/strain conditions, i.e.

2

the deformation, will strongly affect the recrystallisation microstructure by affecting the amount of stored energy in the material. The temperature at which the material is deformed will affect the stresses and strains since the constitutive behaviour of aluminum is significantly influenced by temperature.

In general a hot rolling model will consist of two distinct regions: the roll bite, where the deformation occurs, and the interstand region, shown in Figure 1.2.
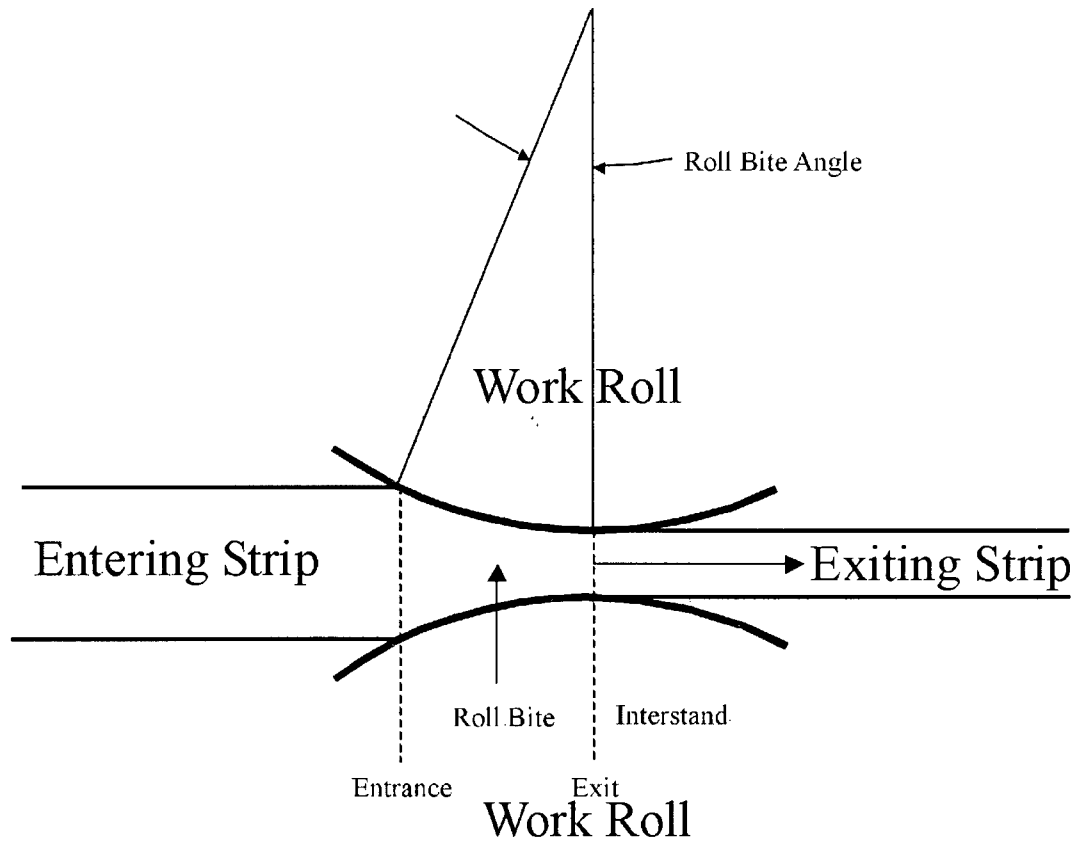
Figure 1.2 - Schematic of roll bite and interstand regions.

1.2 Manufacturing

Although aluminum sheet processing will vary from producer to producer the general process path is shown in Figure 1.3 [1]. Typically ingots, produced by direct chill (DC) casting, are scalped and homogenised prior to rolling. Breakdown rolling is a reversible hot rolling process where the thickness of the initial ingot is reduced to

3

approximately 25 mm from 500 mm. The number of passes required to achieve this reduction can vary from 9 to 25 depending on the size of the mill.

Thickness of slab   Temperature of slab

$\approx 700°C$

Casting $\approx 670°C$

$\approx 510mm$ ————————————— $\approx 25°C$

Scalping

$\approx 500mm$ ———————————— $\approx 25°C$

Homogenising $\approx 610°C$

$\approx 550°C$

Break-down rolling

$\approx 25mm$ ———————————— $\approx 430°C$

Tandem rolling

$\approx 2.5mm$ ——————————— $\approx 350°C$

Inter-annealing $\approx 350°C$

$\approx 25°C$

Cold rolling $\approx 100°C$

$\approx 0.33mm$ ——————————

Heat Treatment $\approx 150°C$
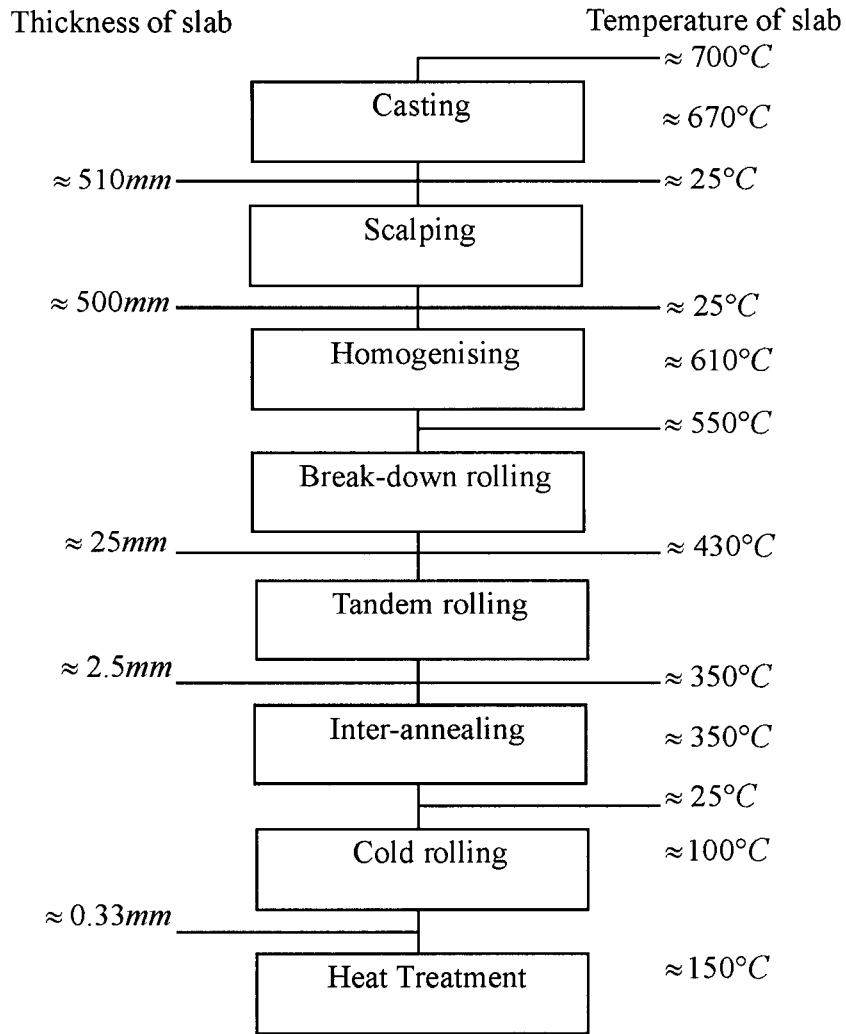
Figure 1.3 - Typical aluminum production flow chart [1].

Industrial tandem hot rolling of aluminum strip, with a typical initial thickness of 15-25 mm and temperature of 400°C-450°C, involves 2-5 rolling stands with the strip experiencing strains of up to one per stand and strain rates of 10-100 s^{-1} before exiting with a thickness of 2-3 mm at an approximate temperature of 300-350°C [1]. The hot tandem rolling not only has to economically convert the slab to the required dimensions

4

but also has to achieve specified properties. These properties may include such features as yield strength, tensile strength, surface finish, grain size and texture [2]. Examples of applications for hot rolled aluminum products are welded pressure vessels and ferry superstructures.

In applications that require higher strengths or thinner gauges, the strip is cold rolled and followed by a heat treatment. Examples of applications that are made from cold rolled aluminum are aluminum foil and automobile body panels.

1.3 Rolled Aluminum Production

The world market for rolled aluminum products is significant, as shown in Table 1.1. Furthermore, the use of rolled aluminum products in Europe is growing, as demonstrated by Figure 1.4. The use of rolled products has been gradually increasing since 1996 and this trend is expected to continue in the near future; in 2001 the growth in demand for rolled products is estimated at 0.6%, with 2002 being rated at 2.3% [6]. Overall from 1994 to 2000, the use of aluminium rolled products in Europe increased by 6.6%, to reach the level of 3.4 million tonnes.

Table 1.1 - Rolled product shipments (in thousands of metric tonnes)[5].

	2000				2001	
	Q2	Q3	Q4	Year	Q1	Q2
North America	288	274	244	1083	279	269
South America	41	44	50	165	55	46
Asia	64	65	71	239	68	68
Europe	171	167	189	696	208	197
Total	564	550	554	2183	610	580
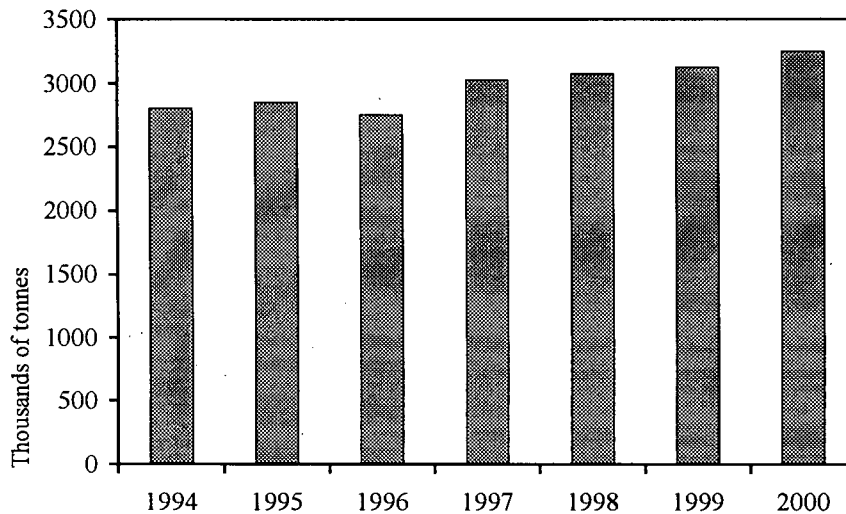
Figure 1.4 - Consumption of rolled aluminum products in Europe [6].

In part as a result of expanding market demand of rolled products in Europe, a collaborative project between the University of British Columbia and the CORUS Group plc. was initiated to develop a mathematical model capable of accurately predicting the temperature, plasticity and microstructural changes that occur during hot rolling of AA5XXX aluminum alloys.

1.4 References

1   van der Winden, M.R. "Laboratory simulation and modelling of the break-down rolling of AA3104", Ph.D. Thesis, Sheffield University, 1999

2   Wells, M.A. "Mathematical modelling of the microstructure and texture changes during hot tandem rolling of AA5182 and AA5052 aluminum alloys" Ph.D. Thesis, University of British Columbia, 1995

3   Chen, B.K., Choi, S.K. and Thomson, P.F. "Simulation of evolution of microstructure in a thermo-mechanical analysis of the hot rolling of aluminium" Res Mechanica, 31, pp. 455-469, 1991

4   Sellars, C.M. "Modelling Microstructural Development During Hot Rolling", Materials Science and Technology, Vol. 6, November 1990, 1072-1081.

5   Alcan 2nd Quarter Results Analyst Presentation, New York, July 16th, 2001

6   European Aluminum Association Press Release, April 27, 2001

Chapter 2   Literature Review

2.1   Microstructural Evolution During Hot Tandem Rolling

Over the years there has been a proliferation of computer models developed to simulate hot rolling processes. Most of these models have been applied to plain carbon and micro-alloyed steels but in recent years a similar approach has been applied to simulate hot rolling of aluminum alloys [1-7]. The details of the hot deformation parameters (i.e. strain, strain rate and deformation temperature), in conjunction with quantitative relationships describing microstructure changes and the temperature at time after deformation, form the basis from which microstructure models can be developed.

Energy stored by deformation is typically released by three mechanisms, recovery, recrystallisation and grain growth [8]. Recovery occurs by mutual annihilation of dislocations of opposite sign and rearrangement of the remaining dislocations to minimise the energy of the system. In general, recrystallisation includes all processes involving grain boundary migration [8]. Primary recrystallisation involves grain boundary migration driven by the residual stored energy after recovery.

There are two distinct processes that take place during hot rolling, dynamic changes that take place in the roll bite and static changes that take place outside of the roll bite in the interstand regions.

2.1.1 Dynamic Changes

2.1.1.1 Dynamic Recovery

The ability of a system to dynamically recover is determined by stacking fault energy (γ) and the temperature at which deformation occurs. In a material with a high stacking fault energy, such as aluminum, the dislocations are more easily able to climb or cross-slip out of their slip plane, which allows dislocation rearrangements to occur and hence, recover. A list of stacking fault energy for selected metals is shown in Table 2.1; the stacking fault energy of copper is considered a medium value while the stacking fault energy of aluminum is considered to be a high value.

8

Table 2.1 – Summary of stacking fault energy for selected metals [9].

Metal	γ (mJ m^{-2})	Metal	γ (mJ m^{-2})
Zirconium	240	Gold	45
Aluminum	166	Silver	22
Zinc	140	304 Stainless Steel	21
Nickel	128	70 Cu: 30 Zn	20
Magnesium	125	Cobalt (fcc)	15
Copper	78	91 Cu: 9 Si	5

Additionally, since dislocation climb is a thermally activated process, higher temperatures will enhance recovery [8]. Therefore dynamic recovery in aluminum alloys is rapid at high temperatures and usually the only form of dynamic restoration that occurs. The stress-strain curve is typically characterised by a rise to a plateau followed by a constant or steady-state stress beyond a specific strain, as shown in Figure 2.1 [9].
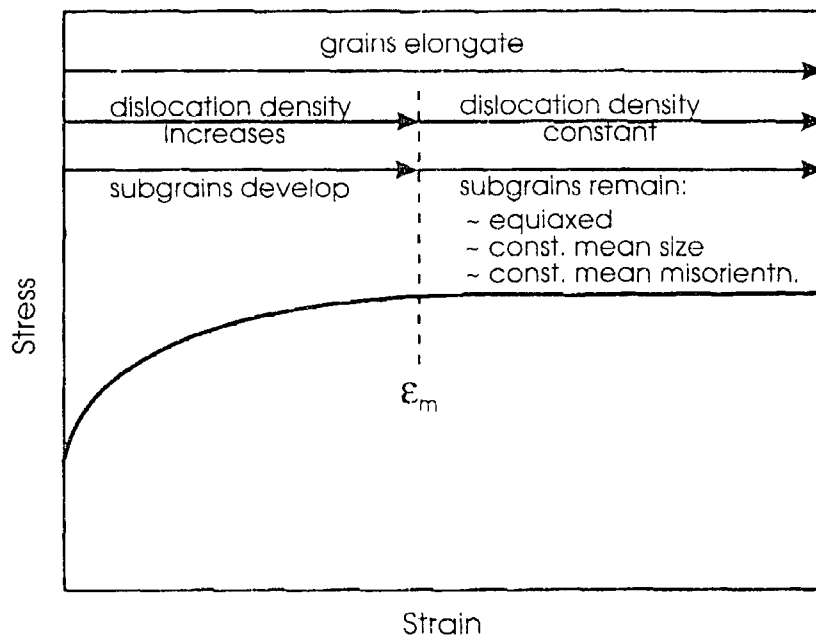
Figure 2.1 – Typical stress/strain curve of a material undergoing dynamic recovery [9].

2.1.1.2 Dynamic Recrystallisation

During hot rolling of metals with lower stacking fault energy, the combination of strain energy and elevated temperature can cause dynamic recrystallisation during the application of strain. Since aluminum is a high stacking fault energy material dynamic recrystallisation does not generally occur [9]. However, McQueen and co-workers [10-13] have observed three types of dynamic recrystallisation in aluminum alloys: discontinuous, continuous and geometric. The difference between them is the amount of grain boundary migration involved. In discontinuous dynamic recrystallisation the nuclei of new grains grow by long-range boundary migration. Continuous dynamic recrystallisation occurs by continuous rotation of sub-grains transforming the low-angle grain boundary into large-angle grain boundaries. Geometric dynamic recrystallisation results from the increase in grain boundary area necessitated by the continuing deformation to prevent the formation of voids. Both continuous and geometric dynamic recrystallisation will occur without nucleation. In the absence of discontinuous and continuous dynamic recrystallisation, geometric dynamic recrystallisation will eventually occur, as Blum *et al.* [11] have shown to be the case for an AA5083 aluminum alloy. Geometric dynamic recrystallisation was observed under hot-working compression conditions at strains of around 2. However, the fine grain structure formed by geometric dynamic recrystallisation may quickly be destroyed by static recrystallisation if the cooling rate to room temperature is insufficient.

2.1.2 Static changes

2.1.2.1 Static Recovery

Since dynamic recovery has already taken place during the hot rolling of aluminum, further microstructural changes due to static recovery are usually small [9]. In general, static recovery mechanisms slowly change dislocation tangles within the sub-grains into neat arrays and the sub-grains may grow larger as some of the sub-grain boundaries disappear. Often the dislocations are attracted into arrays of similar dislocations, thereby increasing the misorientation caused by the array. If this process continues, some sub-grain boundaries may obtain a misorientation angle greater than

approximately 10° and become a grain boundary capable of migrating or nucleating a recrystallised grain.

2.1.2.2 Static Recrystallisation

The majority of the microstructure changes associated with hot rolling of aluminum take place as a result of static recrystallisation. Static recrystallisation is a heterogeneous process with well-defined starting and finishing points [8]. Static recrystallisation follows a set of rules that were first proposed by Mehl in 1948 and refined by Burke and Turnbull in 1952. These rules predict the effect of the initial microstructure (grain size) and processing parameters (strain, strain rate and temperature) on recrystallisation kinetics and recrystallised grain size and are summarized below [14]:

1. A minimum amount of deformation is necessary to produce recrystallisation
2. Increasing the annealing time decreases the temperature necessary for recrystallisation
3. The final grain size depends chiefly on the degree of deformation and to a lesser extent on the annealing temperature.
4. The larger the original grain size, the greater is the amount of deformation required to give an equivalent recrystallisation temperature and time as a smaller initial grain.
5. Temperature, strain and strain rate all have a strong influence on the kinetics of recrystallisation, fraction recrystallised and recrystallised grain size.

The amount of strain is a parameter that has a large influence on the recrystallisation kinetics and the recrystallised grain size. In lab-scale rolling experiments conducted by Raghunathan et al. [15] on AA5056 and AA5083 aluminum alloys, the effect of strain on the recrystallised grain size was found to saturate after an approximate strain of 1.5, shown in Figure 2.2.

11
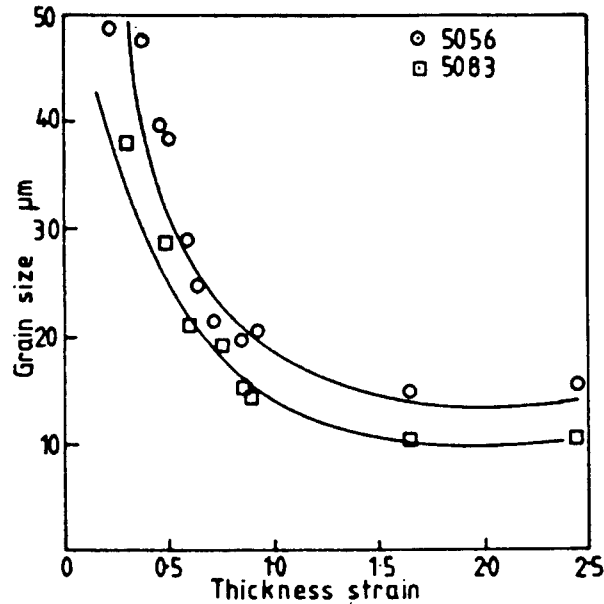
Figure 2.2 - Effect of strain on recrystallised grain size [15].

According to Raghunathan *et al.* [15], the strain saturation is a result of the dependence of recrystallised grain size on the nucleation rate and growth rate. This dependence can be explained since for a given recrystallisation temperature, the growth rate will remain constant while the nucleation rate will increase with strain. At low strain levels the deformation is heterogeneously distributed near the grain boundaries and particles, resulting in a smaller number of nuclei per unit volume because the potential nuclei are widely distributed [15]. As the strain increases there will be a corresponding increase in the number of nuclei per unit volume since the potential nuclei sites are more closely spaced [15]. At some point the inter-nuclei distance cannot be further reduced, therefore the increased strain will no longer affect the recrystallised grain size. Similarly, recrystallisation kinetics will only depend on strain up to a finite amount [16].

Humphreys *et al.* [9] have shown that in general a fine grained material will recrystallise more rapidly than a coarse-grained material. The effect of initial grain size on the recrystallised grain size is similar to the effect on the recrystallisation kinetics. However, the recrystallised grain size does not always depend on the initial grain size. Raghunathan *et al.* [15] reported that a finer initial grain will result in a finer

12

recrystallised grain but this is not true for all aluminum alloys [1,4,15]. The dependence of the initial grain size for the AA5056 and AA5083 aluminum alloys has been attributed to grain boundary nucleation [15]. Hence a decrease in parent (initial) grain size would increase the boundary area per unit volume, thereby increasing the density of potential nuclei. Therefore the recrystallised grain size will be proportional to the initial grain size, as shown in Figure 2.3.
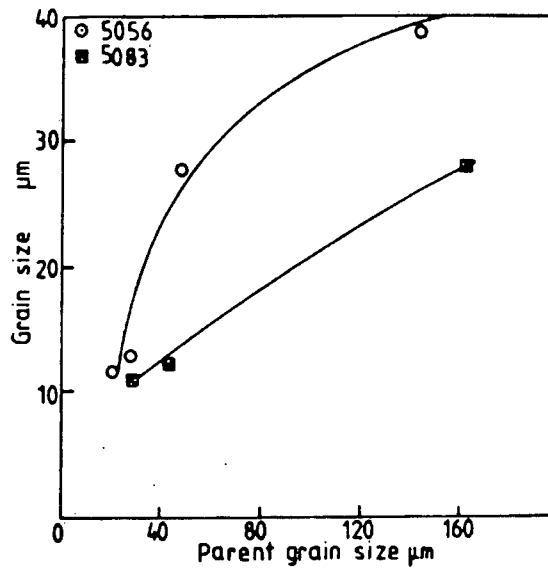
Figure 2.3 - Effect of parent (initial) grain size on the recrystallised grain size [15].

In addition, if the initial grain size is coarse there may be the formation of deformation bands, which are able to act as nucleation sites for new grains due to their favourable misorientation angle across the boundaries [15]. Two types of deformation bands have been identified in high stacking fault energy materials [9]. The first type of deformation band results from the strain being accommodated by more than one set of slip systems. The second type of deformation band is due to the different regions of the grain experiencing different strains when the work done within the bands is less than that required for homogeneous deformation and the bands can be arranged so that the net strain matches the overall deformation [9].

13

The effect of deformation temperature and strain rate on the kinetics of recrystallisation have been combined into what is known as the Zener-Hollomon parameter, Z, in the form given by:

$$Z = \dot{\varepsilon} \cdot \exp\left(\frac{Q_{def}}{R \cdot T_{def}}\right)$$ (2.1)

where $\dot{\varepsilon}$ is the strain rate (in s^{-1}), Q_{def} is the activation energy of deformation (in kJ mol^{-1}), R is the gas constant (in J mol^{-1} K^{-1}) and T_{def} is the deformation temperature (in K). At low strain rates and high temperatures there will be less stored energy available for recrystallisation processes and hence the kinetics will be slower. The effect of the Zener-Hollomon parameter on the recrystallised grain size can be seen from the work done by Raghunathan et al. [15] on AA5056 and AA5083 aluminum alloys, shown in Figure 2.4.
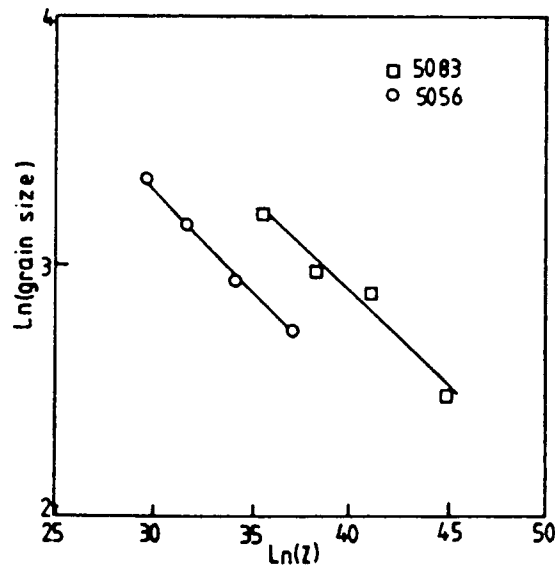
Figure 2.4 - Effect of Z parameter on recrystallised grain size [15].

As would be expected, decreasing Z will increase the recrystallised grain size since there is less energy available to promote the nucleation required for a new grain to form. Similarly for recrystallisation kinetics, decreasing Z will increase the time required for recrystallisation [16].

14

2.2 Static Recrystallisation Modelling

Static recrystallisation is a heterogeneous process of grain nucleation and growth, however it has a very well defined starting and finishing points. There have been a number of approaches taken to modelling recrystallisation kinetics and recrystallised grain size, including the Johnson-Mehl-Avrami-Kolgormorov (JMAK) model, a modified JMAK approach taken by Vatne *et al.* [4] and the Cellular Automaton model.

2.2.1 JMAK Model

The classic JMAK model is a semi-empirical approach that encompasses recrystallised grain nucleation and grain growth mechanisms in a single equation. The JMAK model assumes that recrystallised nuclei form randomly, the rates of nucleation and growth remain constant and the growth of recrystallised nuclei is isotropic.

In general, the JMAK model follows an Avrami-type equation, shown below [9]:

$$X_V = 1 - \exp\left(-\beta \cdot t^n\right) \tag{2.2}$$

where X_v is the fraction recrystallised, β is a constant, t is the time and n is the JMAK exponent, which is a function of both nucleation and growth rates. Experimentally there has been reasonable agreement between researchers [1,7,15,17] for the JMAK exponent for hot rolled aluminum alloys, which are typically around 2. According to JMAK theory in 2-D, n will equal 2 if all nucleation is assumed to occur at the beginning of recrystallisation (i.e. site saturated nucleation) or n will equal 3 if the nucleation rate remains constant [9]. Marthinsen *et al.* [18] have shown that the variations in the experimental JMAK exponents could represent varying degrees of particle clustering. However, the different values for the Avrami exponent could also be accounted for by decreases in the nucleation rates, non-uniform distribution of stored energy of deformation, non-random distribution of recrystallised nuclei and anisotropic growth.

One method to estimate the recrystallisation kinetics for hot deformed aluminum alloys is to quantify the amount of time required for 50% recrystallisation to occur ($t_{0.5}$), given in the form shown in Equation 2.3. This equation quantifies the $t_{0.5}$ based on the deformation parameters.

15

$$t_{0.5} = a \cdot d_o^b \cdot \varepsilon^c \cdot Z^d \cdot \exp\left(\frac{Q_{rex}}{RT_{rex}}\right) \qquad (2.3)$$

where d_o is the initial grain size (in μm), ε is the strain, Q_{rex} is the activation energy of recrystallisation (in kJ mol^{-1}), R is the gas constant (in J mol^{-1} K^{-1}), T_{rex} is the recrystallisation temperature (in K), a-d are experimentally determined material constants and Z is the Zener-Hollomon parameter. Some recrystallisation kinetics equation coefficients for selected aluminum alloys are summarized in Table 2.2.

Table 2.2 - Summary of recrystallisation kinetics coefficients for aluminum alloys.

Researcher	Material	a	b	c	d	Q_{rex} (kJ/mol)	Q_{def} (kJ/mol)
Sellars [7]	Al-1%Mg	9.8×10^{-6}	1.35	-0.27	-1.1	230	156
Gutierrez [19]	CP Al	1.5×10^{-4}	0	-1.5	-0.75	220	158
Raghunathan	AA5056	9.1×10^{-12}	1.58	*	-0.38	212	166.9
et al. [15,16]	AA5083	2.7×10^{-10}	2.45	**	-0.58	183	175
Wells *et al.*	AA5182	8.34×10^{-7}	1.35	-0.93	-0.73	200	196
[1]	AA5052	1.25×10^{-6}	1.35	-1.023	-0.66	200	196

* modified $(0.0286 + 1.8\,\varepsilon^2)^{-1}$

** modified $(9.73 + 3.82\varepsilon^2)^{-1}$

According to Raghunathan *et al.* [15], the amount of stored energy for recrystallisation will not increase past a finite strain. The power law fit for strain dependence used by the researchers is typically derived from laboratory experiments of constant temperatures and low levels of deformation and does not take the saturation of strain energy into consideration. In hot rolling operations the strip temperatures are not constant and higher levels of strain can be obtained in multi-pass scenarios. Consequently, Raghunathan *et al.* [15,16] determined an alternative relationship and estimated the parameters by assuming a value for the strain exponent and fitting the experimental data with a straight line, repeating this procedure until the best fit was obtained.

Once the $t_{0.5}$ has been calculated the fraction recrystallised can be estimated for any time using the JMAK equation in the following form:

$$X_v = 1 - \exp\left(-0.693\left(\frac{t}{t_{0.5}}\right)^n\right)$$ (2.4)

where t is the time (in s), $t_{0.5}$ is the time to 50% recrystallisation (in s) and n is the JMAK exponent. Typically this approach has been used to develop equations representing the recrystallisation behaviour in experimentally deformed materials where the temperature and strain rate during the deformation is constant. When applying these equations to industrial rolling mills both the temperature and the strain rate change during the deformation and the choice of which temperature and strain rate to use to represent the deformation behaviour becomes difficult. In fact, some researchers have applied exit values for temperature and strain rate [2] whereas others have used average values [3,7].

An estimate of the recrystallised grain size, d_{rex}, has been determined from the empirical equation shown in Equation 2.5 [1,7,16,19].

$$d_{rex} = a \cdot d_0^b \cdot \varepsilon^c \cdot Z^d$$ (2.5)

where d_0 is the initial grain size (in μm), ε is the strain, Z is the Zener-Hollomon parameter and a,b,c,d are experimentally determined material dependent coefficients. The equation coefficients for selected aluminum alloys are summarised in Table 2.3. Commercially pure (CP) aluminum recrystallised grain size equations have an additional Arrhenius-type annealing temperature dependence, with an activation energy of 30 kJ mol^{-1} [7,19]. For both Sellars [7] and Guitierrez [19] modelling CP aluminum, the effect of the annealing temperature will modify the apparent effect of the Zener-Hollomon parameter, reducing the exponent to -0.14 when the annealing temperature does not equal the deformation temperature [19], as is the case for a hot rolling process.

17

Table 2.3 - Summary of final recrystallised grain size coefficients for selected aluminum alloys.

Researcher	Material	a	b	c	d
Sellars [7]	Al-1%Mg	435	1.3	-0.39	-0.24
	CP Al	11500	0	-0.5	-0.33
Gutierrez [19]	CP Al	1.15	0	-0.5	-0.33
Raghunathan et al.	AA5056	101.7	1.00	*	-0.075
[16]	AA5083	4.79	0.67	**	-0.064
Wells et al. [1]	AA5182	12690	0	-0.37	-0.17
	AA5052	8463	0	-0.78	-0.113

$* \ (3.72 + 1.12\varepsilon^2)^{-1}$

$** \ (24.42 + 7.52\varepsilon^2)^{-1}$

The JMAK method for estimating microstructure for a wide range of processing conditions has been shown to adequately describe the recrystallisation kinetics and recrystallised grain sizes for aluminum. The wide variation in coefficients between similar alloys would suggest that there is a strong influence of alloying elements, which has yet to be quantified. Another area that has yet to be considered is second phase particles.

2.2.2 Vatne Approach

Some researchers [4,5,17,20,21] have quantified recrystallisation from a more physical point-of-view, although the fraction recrystallised is still calculated using the JMAK equation. The more fundamental approach considers the driving pressure for recrystallisation in the form of stored energy, nucleation theory and grain boundary mobility. The equation developed to predict the recrystallisation kinetics is as follows:

$$t_{0.5} = \frac{C_t}{M_{GB}P_D}\left(\frac{1}{N_v}\right)^{\frac{1}{3}} \qquad\qquad (2.6)$$

where C_t is a modelling constant, M_{GB} is the grain boundary mobility, P_D is the amount of stored energy and N_v is the number of nucleation sites.

Although some of the input parameters for the model, such as grain boundary mobility, are not well known, a formula for estimating the mobility of grain boundaries has been proposed by Humphreys [22,23] in the following form:

$$M = M_m\left\{1-\exp\left(-B\cdot\left(\frac{\theta}{\theta_m}\right)^{n}\right)\right\} \qquad\qquad (2.7)$$

where M_m is the mobility of a high angle boundary, B is approximately 5, θ is the sub-grain boundary angle, θ_m is the critical angle (approximately 10° to 15°) and n is approximately 4 for aluminum.

Some model predictions using this method are compared to plane strain compression (PSC) experimental results, as shown in Figure 2.5. As shown in Figure 2.5a, the model is able to reasonably predict the recrystallisation kinetics with constant strain rates. However, strain rates will vary in industrial rolling, which has been considered in work done by Furu et al. [24] and Baxter et al. [25]. Their results have demonstrated that the current models are not able to accurately describe the effects of the variation in strain rates throughout a process on the $t_{0.5}$, as shown in Figure 2.5b.

a) Constant strain rate
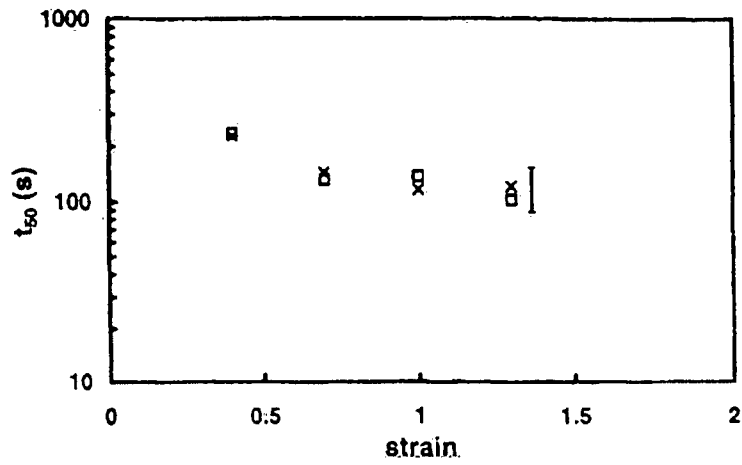
□ 2.5 s^{-1} (measured)

× 2.5 s^{-1} (predicted)

b) Changing strain rate
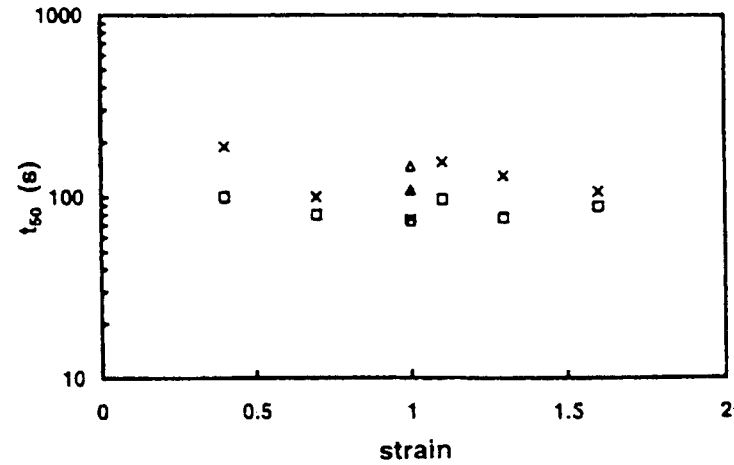
△ increasing (measured)

▲ increasing (predicted)

□ decreasing (measured)

× decreasing (predicted)

Figure 2.5 – Al-1%Mg model predictions and experimental data for $t_{0.5}$ for a) Constant strain rate (typical uncertainty in the model is shown by the error bar) and b) Changing strain rates [24].

The equation for recrystallised grain size, given by Furu *et al.* [17] as a function of grain nucleation sites, is shown below:

$$d_{rex} = \left(\frac{1}{N_v}\right)^{\frac{1}{3}}$$

(2.8)

where N_v is the number of nucleation sites (μm^{-3}). An example of the predictions using the model developed by Vatne *et al.* [20] for recrystallised grain size predictions is shown in Figure 2.6. The modelling constants were determined to fit the model predictions with the first set of measured PSC testing results, shown as the circle symbol. Remaining model predictions used these modelling constants, shown as the solid line, were then compared to a second set of experimental results.

Recrystallized grain size [μm]
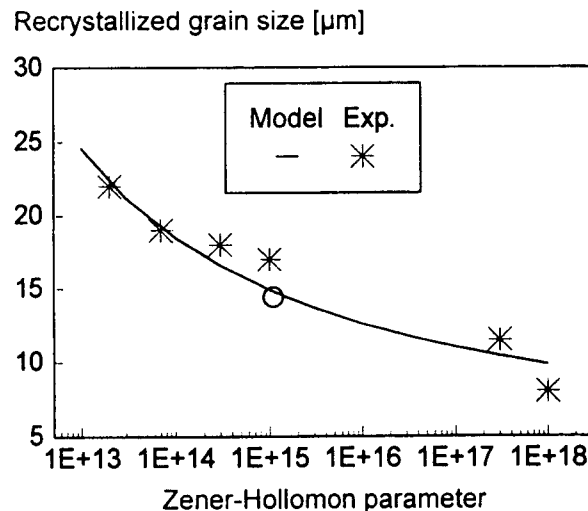
Figure 2.6 - Recrystallised grain size predictions compared to PSC result under different Zener-Hollomon parameters (Al-Mg-Mn material, $\varepsilon=2$, $d_o=30$ μm) [20].

Vatne and coworkers [4,5,17,20] have been able to show that these models are able to reasonably predict the recrystallisation kinetics and recrystallised grain size with constant strain rates. Advantages of the Vatne approach are the dependence upon more fundamental properties of the material, i.e. dislocation densities, while disadvantages include the difficulty in accurately measuring some of the input parameters and the lack

21

of information concerning the behaviour of some parameters, i.e. grain boundary mobility.

2.2.3 Cellular Automaton Model

A relatively new approach to modelling static recrystallisation is the cellular automaton (CA) method [26]. The CA model is a probabilistic method that can predict grain structures with kinetics. Historically CA has been applied to solidification and dendrite growth processes but in recent years has been applied to phase transformations and recrystallisation for both steel and aluminum [26,27].

There have been two distinctly different approaches taken for modelling recrystallisation using the CA method. The approach taken by Davies et al. [26,28,29], Marx et al. [30] and Hesselbarth et al. [31] involves assigning nucleation rules and grain growth velocities based on calculated probabilities. The approach taken by Geiger et al. [32] involves assigning a random grain number (i.e. a sub-grain) and a texture component to every cell at the beginning of the model. The resulting energy differences of the grain boundaries formed by the different cells then determine the grain growth.

The three-dimensional CA model developed by Davies [26] was compared to experimental data of CP aluminum of Gutierrez et al. [19] that had been torsion tested at 325°C to a total strain of 2.98 and a Z value of 6.13×10^{13} s^{-1}, then annealed at 410 °C. The results are shown in Figure 2.7.
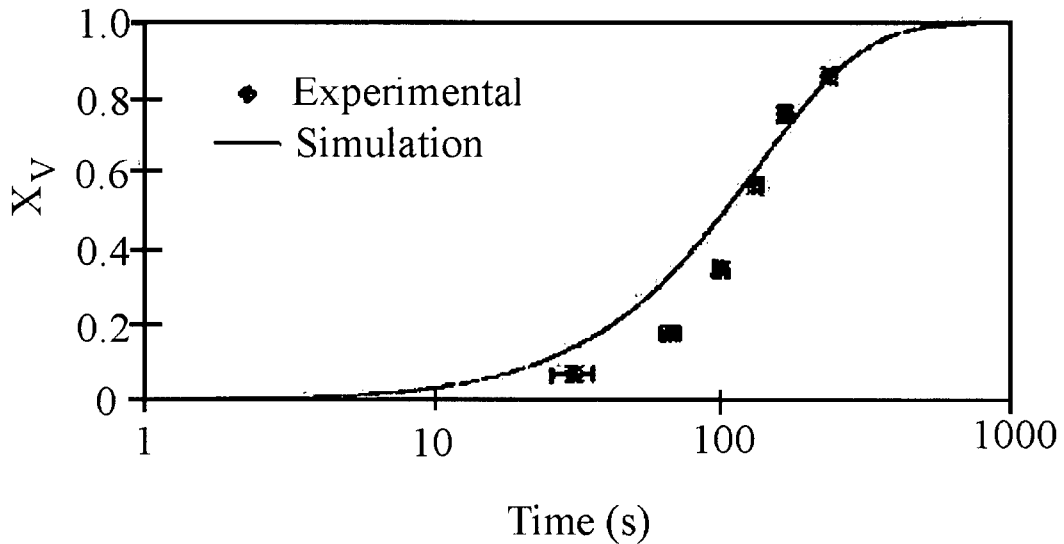
Figure 2.7 - Static recrystallisation kinetics resulting from Davies [26] simulations compared to experimental results by Gutierrez *et al.*[19].

As can be seen from Figure 2.7, the CA method shows reasonable agreement with experimental data. For aluminum alloys, grains of different textures are known to grow at different rates; it is conjectured that the grains whose growth rate is initially the most rapid would be the easiest to measure at low fractions transformed and thus would skew the grain boundary velocity to higher values. Therefore the simulation develops at a more rapid rate than occurs in reality [26], shown by the simulations reduced incubation time compared to the experimental data.

The use of energy terms makes the Geiger method very attractive as a fundamental study, however the approach taken by Davies, Marx and Hesselbarth is a simpler method compared to Geiger. However, there are a couple of unresolved issues with the probabilistic approach, primarily the quantification of the grain boundary velocity which affects the models ability to predict the amount of fraction recrystallised at the lower fractions and the large number of small grains, which would likely be consumed by larger grains in a real system.

2.2.4 Grain Growth

Grain growth occurs after recrystallisation to reduce the amount of grain boundary energy and is a function of time and temperature for a given alloy. In general, the average grain size will increase with time at all temperatures [9]. Also, for smaller strain conditions before recrystallisation the growth rate during the subsequent grain growth stage is slightly lower [15].

As a first approximation, grain growth can be fitted to an empirical equation given by:

$$d_{gg} = A \cdot t^n \qquad (2.9)$$

where d_{gg} is the grain size after grain growth, A and n are material constants for a given temperature and strain condition. The values of A and n found by Raghunathan *et al.* [15] for AA5083 aluminum alloys at 80% strain are summarised in Table 2.4.

Table 2.4 - Grain growth coefficients for AA5083 [15].

Temperature (°C)	A	n
490	8.17	0.043
540	9.13	0.066

As can be seen by the small values for n, there is a very small effect of grain growth on AA5083 alloys primarily due to the presence of solute atoms of manganese, iron and silicon. Also due to the presence of precipitate's pinning the grain boundaries.

Furthermore, Ryum *et al.* [33] have investigated the grain growth of AA5XXX aluminum alloys and found that the magnesium serves to reduce the rate of grain growth after recrystallisation, shown in Figure 2.8. Since grain growth is not a significant process in the Al-Mg alloys for the brief periods of time available for static recrystallisation it will not be further considered.
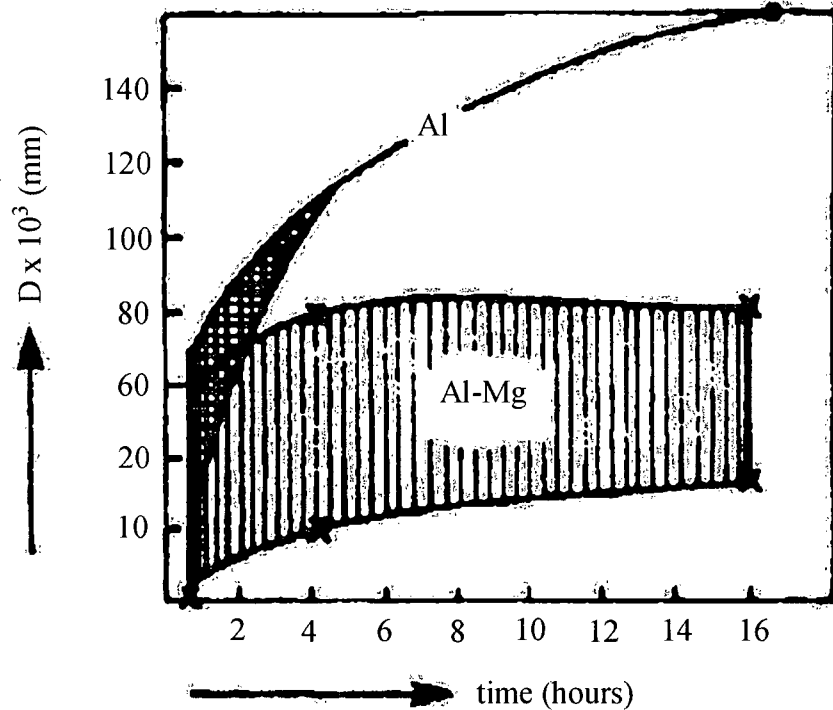
Figure 2.8 - Grain growth in Al and Al-Mg [33].

2.2.5 Effect of Particles

In general, particles have three important effects on recrystallisation: the stored energy and hence the driving force for recrystallisation may be increased by increasing the dislocation density surrounding a particle, large particles may act as nucleation sites for recrystallisation and small particles may exert a significant pinning effect on both low and high angle grain boundaries [9].

Sellars [7] found there was a critical diameter of particles at which lattice rotations in the matrix around coarse particles can occur during hot deformation. The critical particle diameter for Al-1%Mg aluminum alloys has been estimated by:

$$p_c = \frac{3.7 \times 10^5}{(T \cdot Z)^{\frac{1}{3}}} \tag{2.10}$$

where p_c is the critical diameter below which particle site nucleation cannot occur, T is the deformation temperature and Z is the Zener-Hollomon parameter. Since there will be

a distribution of particle sizes in a given material the only potential nucleation sites have a diameter greater than the critical diameter, thus static recrystallisation will be greatly influenced by the particle distribution as well as the deformation conditions. The approximate conditions where particle site nucleation (PSN) is active, shown in Figure 2.9 [5,9,17].
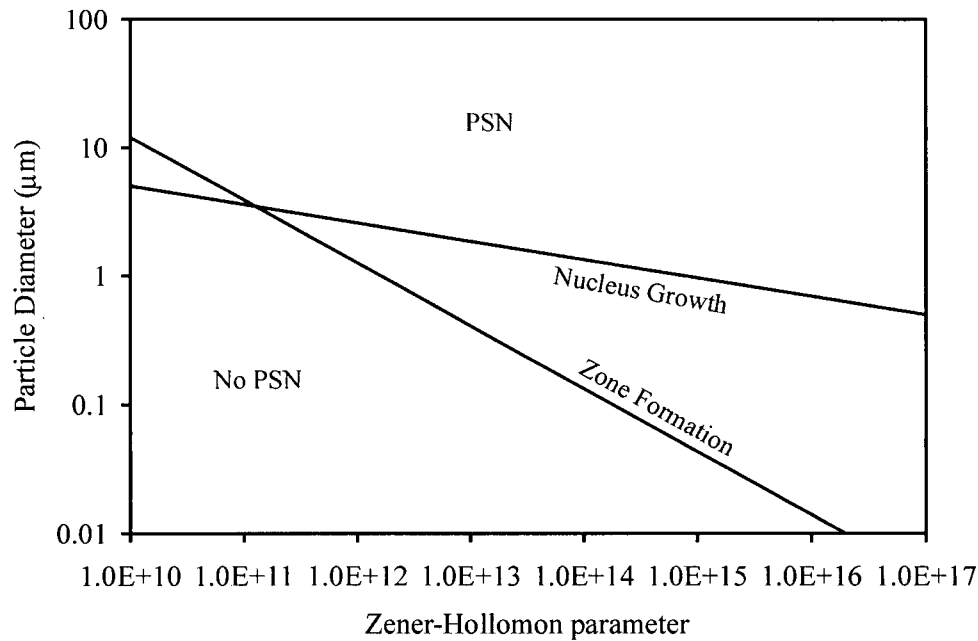
Figure 2.9 - The effect of deformation conditions on PSN for aluminum alloys [5,9].

Kannan et al. [34] have found that recrystallisation and recrystallised grain sizes in aluminum alloys are related to the amount and distribution of second-phase particles in the matrix. Hard particles, larger than a critical size, can serve as sites of recrystallisation, in doing so they influence the recrystallised grain size. Kannan et al. [34] report this critical particle size to be 1 to 2 μm for most aluminum alloys; particles smaller than this critical size can negatively affect the recrystallisation kinetics by Zener drag pressure.

In general, all particles exert a Zener drag pressure, P_Z, on moving boundaries, which restricts their migration. This relationship is given below:

26

$$P_Z = \beta \cdot \gamma \cdot \left(\frac{f}{r} \right) \qquad\qquad (2.11)$$

where β is 3/2 [7,35], γ is the surface energy (in kJ), f is the particle volume fraction and r is the particle size (in μm). Both the sub-grain boundaries in the unrecrystallised substructure and grain boundaries of new recrystallised grains are subject to Zener drag. Since both recrystallisation and grain growth are influenced by particle dispersion there are opposite effects on the final grain size. The drag pressure on sub-grain boundaries by the fine particles leads to a coarser recrystallised grain size by preventing the activation of some potential nucleation sites. As a result, Kannan *et al.* [34] have determined the critical size of the nucleus for recrystallisation, r^*, to be the following:

$$r^* = \frac{K \cdot \gamma}{(P_D - P_Z)} \qquad\qquad (2.12)$$

where K is a geometric constant, γ is the surface energy, P_D is the driving pressure for recrystallisation and P_Z is the Zener pressure. Therefore with increasing Zener drag pressure fewer nucleation sites are activated resulting in an increased recrystallised grain size.

2.3 Mathematical Models Developed for Hot Rolling of Aluminum

There have been a number of models that have been developed for both breakdown rolling [3], tandem hot rolling [1,2,4,5,7] and a combination of both roughing and tandem rolling [20] to predict the microstructure for multi-pass rolling of aluminum and various methods of validation have been used.

2.3.1 Approaches for Modelling Microstructure in Multi-Pass Operations

The multi-pass, breakdown rolling model developed by van der Winden [3] calculated the driving force for recrystallisation of AA3004/AA3104 by calculating an average strain rate for the first 10 passes. The total driving force is then estimated by assuming the total reduction of the first 10 passes occurred during a single pass. The

average values for the strain rate and temperature are calculated in the same manner by using the strain fraction for each pass as a weighting function, shown here for strain rate:

$$\bar{\dot{\varepsilon}}_{1-10} = \frac{1}{\varepsilon_{10}} \cdot \sum_{i=1}^{10} \varepsilon_i \cdot \dot{\varepsilon}_i \qquad (2.13)$$

where i represents the pass number. The average strain rate and temperature values are then applied to obtain an average Z value, which is then used in the JMAK-based microstructure equations.

Vatne *et al.* [4,20] developed a multi-pass, tandem hot rolling model for AA3004 and AlMgMn aluminum alloys. A total number of nucleation sites were after the nth pass was formulated in the following manner:

$$N_{TOT}^n = N_{PSN}^n + X_{X-1}\left(N_C^n + N_{GB}^n\right) + \sum_{i=0}^{n-2} X_i \cdot \left[\prod_{j=i+1}^{n-1} \left(1 - X_j\right) \right] \cdot \left[N_C^{i+1,\dots,n} + N_{GB}^{i+1,\dots,n} \right]$$

$$(2.14)$$

where N_x is the type of nucleation site (i.e. x=PSN, cube or grain boundary), n is the pass number, X is the recrystallised fraction, $N_x^{i+1,\dots,n}$ is the number of sites that have survived the passes (i+1) to (n-1) without recrystallising (expressed as a function of grain size, sub-grain size, texture) and N_x^n is due to the areas that recrystallised in the pass prior to the nth pass. The recrystallisation kinetics were calculated by applying the assumption of site saturation and a random distribution of nucleation sites. The recrystallised fraction and recrystallised grain size then become a function of the number of nucleation sites.

Using the modified JMAK approach and plane strain compression experimental results to tune the model, the model predictions for a generic rolling schedule are shown in Figure 2.10. The initial strip thickness for the model was 600 mm and the strip was reduced in 14 passes to a thickness of 2.5 mm. This model simulated the entire hot rolling process, including both roughing and hot tandem rolling.
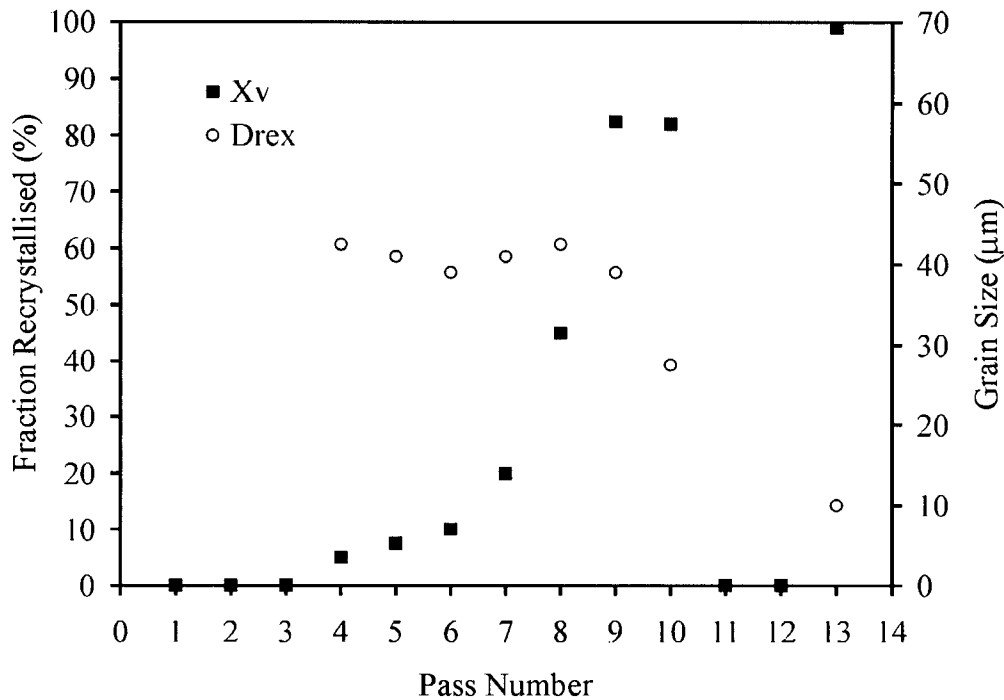
Figure 2.10 - Vatne *et al.* [20] model predictions for multipass hot rolling of Al-Mg-Mn alloy.

2.3.2 Validation of the Models

There have been a few different ways that the hot rolling models have been validated. Primarily the models have either been validated against industrial data, such as Wells *et al.* [2] or against lab scale experimental data using either plane strain compression testing, such as Vatne *et al.* [4,20].

It is difficult to measure industrial hot rolling parameters during the actual rolling of the material because the high speeds of the strip. Therefore the only parameters that can be measured industrially during the rolling are the temperatures, using pyrometers, and the rolling loads, using force transducers typically located under the work roll bearing blocks. Unfortunately pyrometers are not very accurate while the force transducers will only give an average rolling load. Wells *et al.* [2] validated their model against industrial temperature and rolling load measurements. Table 2.5 shows the comparison of predicted and measured temperatures and load at each stand of a four stand tandem hot rolling mill.

29

Table 2.5 - Percent difference between model predictions and industrial measurements for each stand [2].

Alloy	Stand 1		Stand 2		Stand 3		Stand 4	
	Temp.	Loads	Temp.	Loads	Temp.	Loads	Temp.	Loads
AA5182	0	16.6	1.7	7.4	0.3	19.4	-	-
AA5052	0.2	0.3	1.0	11.6	1.9	26.3	5.3	37.0

As can be seen from Table 2.5, the temperature predictions are reasonable, unfortunately the rolling load predictions are only reasonable for the first stand. In addition to the temperature and rolling load comparisons, the Wells model was also validated against recrystallised grain size and recrystallisation texture. Since it is impossible to stop the strip immediately after the last roll the microstructure measurements are taken at some distance past the last stand. Figure 2.11 shows the recrystallised grain size predictions compared to the industrial measurements results for the AA5052 model. Figure 2.12 shows the comparison of the Cube and S texture components model predictions against industrial measurements. These predictions show good agreement with the experimental data for a given distance from the last stand.
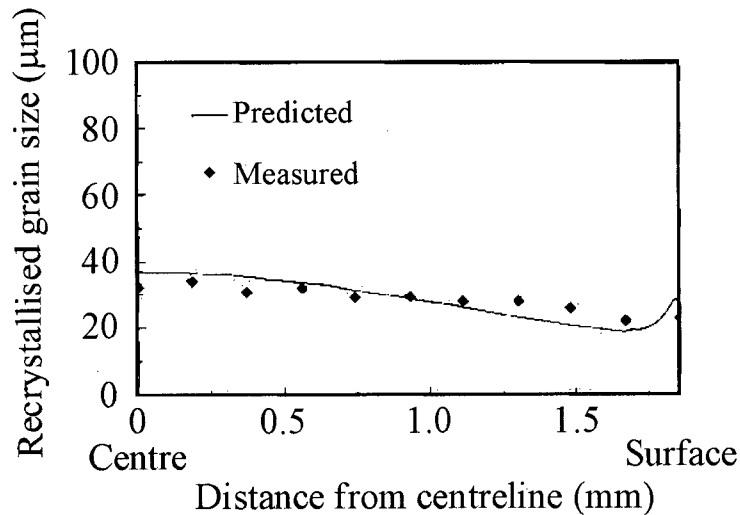
Figure 2.11 - Wells *et al.* [2] recrystallised grain size validation.
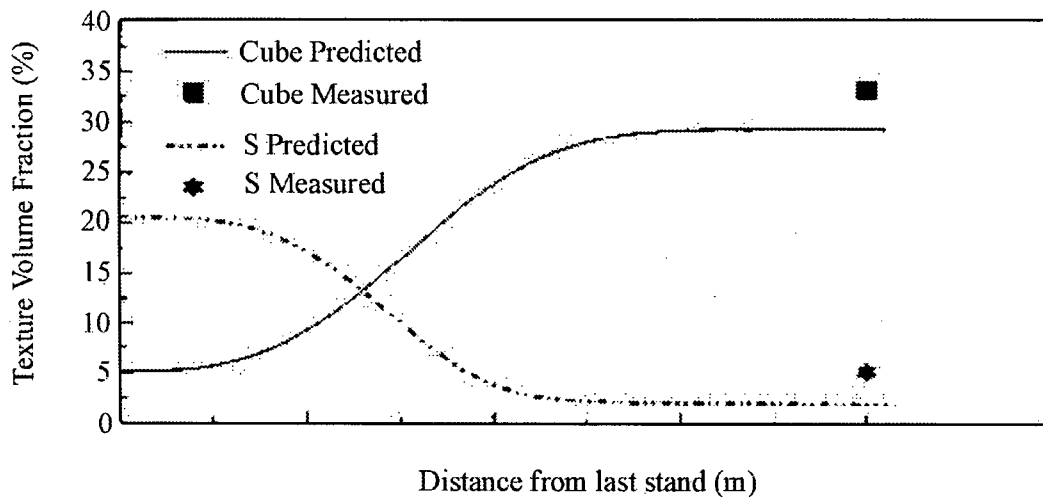
Figure 2.12 - Wells *et al.* [2] texture validation.

Puchi *et al.* [36] validated their mathematical model of an industrial hot rolling operation against industrial rolling loads, shown in Figure 2.13.
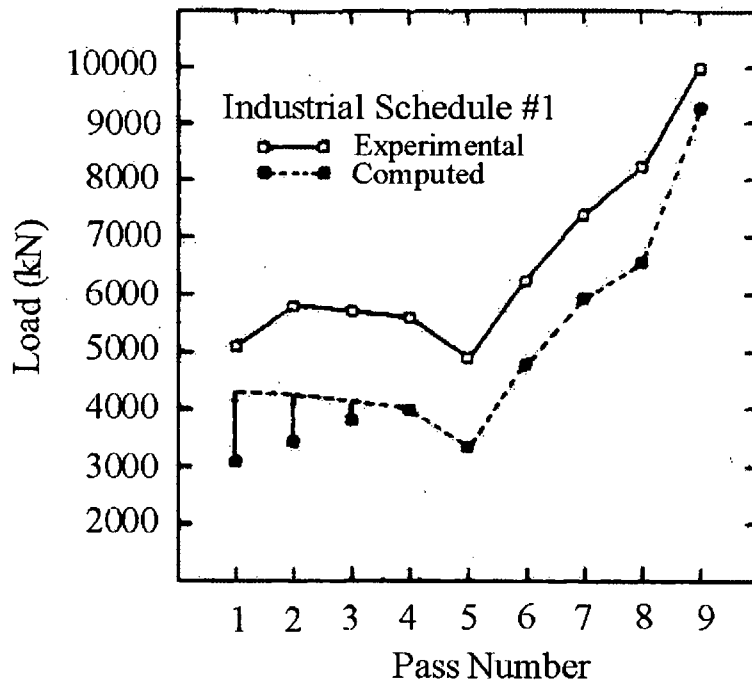
Figure 2.13 - Comparison of Puchi *et al.* [36] load predictions to industrial measurements.

31

As can be seen in Figure 2.13, the predicted load is consistently lower than the measured loads. Unfortunately there was no indication that the microstructure predictions were validated against industrial data.

The Vatne *et al.* [4,20] model was validated using plane strain compression testing. In addition to the recrystallised grain size, shown in Figure 2.6, the volume fraction of cube grains was also compared to experimental data, shown in Figure 2.14.
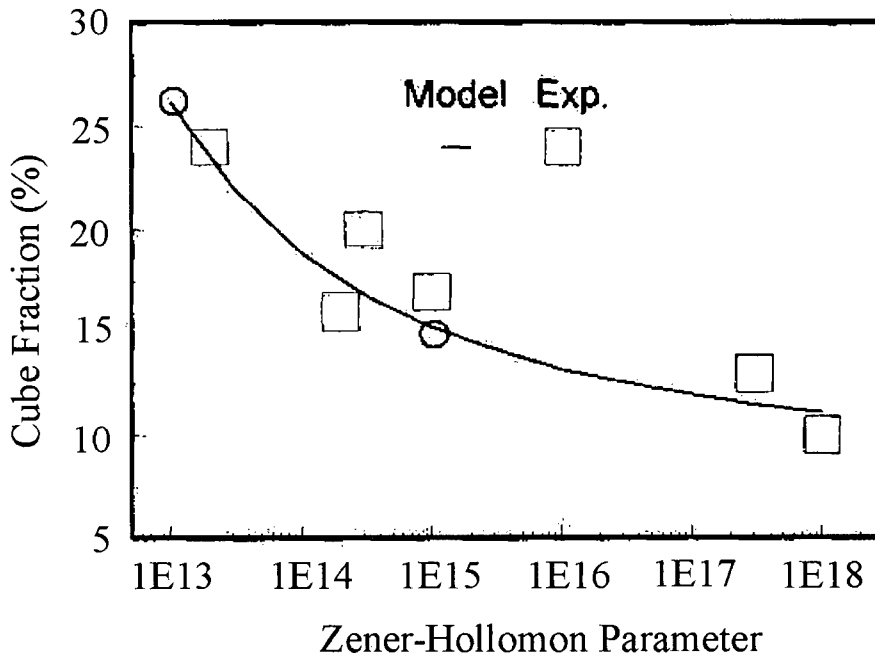
Figure 2.14 - Vatne *et al.* [4,20] texture validation.

Similar to the Wells model [2], the texture predictions are quite good and the Vatne *et al.* model [4,20] is capable of predicting texture for a variety of deformation conditions.

2.4 Summary

The evolution of microstructure during hot rolling operations is a complex interaction among rolling parameters. Hot rolling parameters that are particularly important are the deformation temperature and strain rates that are generally combined into the Zener-Hollomon parameter. Other hot rolling parameters that affect the recrystallisation are initial grain size and strain experienced by the material.

The modelling of recrystallisation of aluminum alloys can be simplified slightly by only considering static recrystallisation. The JMAK approach has been effective at modelling hot deformation under constant strain rate and temperature conditions. However in the absence of industrially validated recrystallisation models, it is impossible to identify which temperature and strain rate to use in the microstructure models to represent what occurred in the rolling process.

2.5 References

1   Wells, M.A., Lloyd, D.J., Samarasekera, I.V., Brimacombe, J.K. and Hawbolt, E.B. "Modeling the microstructural changes during hot tandem rolling of AA5XXX aluminum alloys: part I. Microstructural evolution" Met and Mat. Trans, Vol. 29B, pp. 611-620, 1998

2   Wells, M.A., Lloyd, D.J., Samarasekera, I.V., Brimacombe, J.K. and Hawbolt, E.B. "Modeling the microstructural changes during hot tandem rolling of AA5XXX aluminum alloys. Part III. Overall model development and validation" Meta and Mat Trans., Vol. 29B, pp. 709-720, June, 1998

3   van der Winden, M.R. "Laboratory simulation and modelling of the break-down rolling of AA3104", Ph.D. Thesis, Sheffield University, 1999

4   Vatne, H.E. and Nes, E. "A model for recrystallisation kinetics, texture and grain size applied to multipass hot rolling of an AlMgMn aluminium alloy" Comp. Mat. Sci, Vol. 7, pp. 5-10, 1996

5   Sellars, C.M., Humphreys, F.J., Nes, E. and Juul Jensen, D. "Microstructural modelling of industrial thermomechanical processing" <u>Numerical Predictions of Deformation Processes and the Behaviour of Real Materials</u>, pp. 109-133, 1994

6   Chen, B.K., Choi, S.K. and Thomson, P.F. "Simulation of evolution of microstructure in a thermo-mechanical analysis of the hot rolling of aluminium" <u>Res Mechanica</u>, 31, pp. 455-469, 1991

7   Sellars, C.M. "Modelling microstructural development during hot rolling" <u>Mat. Sci. and Tech.</u>, Vol. 6, pp. 1072-1081, 1990

8   Doherty, R.D. "Recrystallisation of deformed metals (primary)" <u>Encyclopedia of materials science and engineering</u>, edited by Bever, vol. 6, pp. 4108-4112, 1986

9   Humphreys, F.J. and Hatherly, M. "Recrystallisation and related annealing phenomena" Pergamon Press, New York, 1996

10   McQueen, H.J. and Conrod, K. "Recovery and recrystallisation in the hot-working of aluminum alloys" <u>Microstructural Control in Aluminum Alloys: Deformation, Recovery and Recrystallization</u>, pp. 197-219, 1986

11   Blum, W., Zhu, Q., Merkel, R. and McQueen, H.J. "Evolution of grain structure in hot torsion of Al-5Mg-0.7Mn (AA5083)" <u>Mater. Sci. Forum</u>, Vol. 217-222, pp. 611-616, 1996

12   McQueen, H.J. and Belling, J. "Comparison of hot working constitutive analysis of AA5083 and AA5182" <u>Thermec '97</u>, pp. 965-971, 1997

13   McQueen, H.J. "Elevated temperature behaviour of 5083" <u>J. Mat. Eng. Performance</u>, Vol. 10, pp. 164-172, 2001

14   Byrne, J.G. "Recovery, recrystallisation and grain growth" The MacMillan Company, New York, 1965

15   Raghunathan, N. and Sheppard, T. "Microstructural development during annealing of hot rolled Al-Mg alloys" <u>Mat. Sci. and Tech.</u>, Vol. 5, pp. 542-547, 1989

16   Raghunathan, N., Zaidi, M.A. and Sheppard, T. "Recrystallisation kinetics of Al-Mg alloys AA 5056 and AA 5083 after hot deformation" <u>Mat. Sci. and Tech.</u>, Vol. 2, pp. 938-945, 1986

17 Furu, T., Shercliff, H.R., Sellars, C.M. and Ashby, M.F. "Physically-based modelling of strength, microstructure and recrystallisation during thermomechanical processing of Al-Mg alloys" Mat. Sci. Forum, Vol. 217-222, pp. 453-458, 1996

18 Marthinsen, K., Fridy, J.M., Rouns, T.N., Lippert, K.B. and Nes, E. "Characterisation of 3-D particle distributions and effects on recrystallisation kinetics and microstructure" Scrip. Mater., Vol. 39, No. 9, pp. 1177-1183, 1998

19 Gutierrez, I. and Fuentes, M. "Influence of the microstructural changes occurring during steady-state hot deformation on static recrystallisation kinetics and recrystallised grain size of commercial aluminum" Recrystallisation '90, edited by T. Chandra, pp. 807-812, 1990

20 Vatne, H.E., Marthinsen, K., Orsund, R. and Nes, E. "Modeling recrystallisation kinetics, grain sizes and textures during multipass hot rolling" Met. and Mat Trans., Vol. 27A, pp. 4133-4144, 1996

21 Vatne, H.E. and Wells, M.A. "Microstructure modelling of industrial hot rolling processes – the state of the art and the challenges ahead" Light Metals (Canada), pp. 593-609, 1999

22 Humphreys, F.J. "A new analysis of recovery, recrystallisation, and grain growth" Mat. Sci. and Tech., Vol. 15, pp. 37-44, Jan., 1999

23 Humphreys, F.J. "A unified theory of recovery, recrystallisation and grain growth, based on the stability and growth of cellular microstructures – I. The basic model" Acta. Mater., Vol. 45, No. 10, pp. 4231-4240, 1997

24 Furu, T., Shercliff, H.R., Baxter, G.J. and Sellars, C.M. "The influence of transient deformation conditions on recrystallisation during thermomechanical processing of an Al-1% Mg alloy" Acta Mater., Vol. 47, pp. 2377-2389, 1999

25 Baxter, G.J., Furu, T., Zhu, Q., Whiteman, J.A. and Sellars, C.M. "The influence of transient strain-rate deformation conditions on the deformed microstructure of aluminum alloy Al-1%Mg" Acta Mater., Vol. 47, No. 8, pp. 2367-2376, 1999

26 Davies, C.H.J. "The cellular automaton simulation of static recrystallisation" Institute of Materials (UK), pp. 178-184, 1996

27   Spittle, J.A. and Brown, S.G.R. "A 3D cellular automaton model of coupled growth in two component systems" Acta Matell. Mater., No. 6, pp. 1811-1815, 1994

28   Davies, C.H.J. and Hong, L. "The cellular automaton simulation of static recrystallisation in cold-rolled AA1050" Scripta Mater., Vol. 40, No. 10, pp. 1145-1150, 1999

29   Davies, C.H.J. "Intelligent materials design and processing: simulating microstructural evolution during metal processing" Canadian Institute of Mining, Metallurgy and Petroleum, The Brimacombe Memorial Symposium (Canada), pp. 685-694, Oct. 2000

30   Marx, V., Reher, F.R. and Gottstein, G. "Simulation of primary recrystallisation using a modified three-dimensional cellular automaton" Acta Mater., Vol. 47, No. 4, pp. 1219-1230, 1999

31   Hesselbarth, H.W. and Gobel, I.R. "Simulation of recrystallisation by cellular automata" Acta Metall., Vol. 39, No. 9, pp. 2135-2143, 1991

32   Geiger, J., Roosz, A. and Barkoczy, P. "Simulation of grain coarsening in two dimensions by cellular automaton" Acta Mater., Vol. 49, pp. 623-629, 2001

33   Ryum, N. and Embury, J.D. "A comment on the recrystallisation behaviour of Al-Mg alloys" Scandinavian Journal of Metallurgy, No. 11, pp. 51-54, 1982

34   Kannan, K., Vetrano, J.S. and Hamilton, C.H. "Effects of alloy modification and thermomechanical processing on recrystallisation of Al-Mg-Mn alloys" Met. and Mat. Trans., vol. 27A, pp. 2947-2957, Oct., 1996

35   Nes, E., Ryum, N. and Hunder, O. "On the Zener drag" Acta Metall., Vol. 33, No. 1, pp. 11-22, 1985

36   Puchi, E.S., Beynon, J. and Sellars, C.M. "Simulation of hot rolling operations on commercial aluminum alloys" Thermec '88, Tokyo, June 6-10, edited by Tamura, E.I, Iron and Steel Society, pp. 572-579, 1988

Chapter 3   Scope and Objectives

3.1 Scope of Research Program

As microstructure evolution is strongly dependent upon the distribution of strain, strain rate and temperature in the roll bite and the temperature in the subsequent interstand region, the research program was required to consider both the thermal and plastic strain distribution through the roll bite as well as the thermal distribution in the interstand region. The goal of this research was to develop a model capable of predicting the microstructure evolution in an AA5083 aluminum alloy strip after a single stand in a hot rolling mill.

To achieve this goal a mathematical model was developed to predict the distribution of strain, strain rate and temperature through the roll bite and thickness of the strip using the commercial finite element software package, ABAQUS™. Empirical relationships, taken from the literature and based on the JMAK equation were integrated into the model to predict the microstructure evolution (i.e. fraction recrystallised) in the interstand region. ABAQUS™ has excellent built-in non-linear heat transfer and stress analysis capabilities but does not have the ability to predict microstructure. This capability was added through "user-defined subroutines" which employ empirical relationships between stress, strain and temperature to predict the evolution of microstructure.

Experimental measurements from a pilot scale rolling mill were obtained for validation of the models and to ensure industrial relevance. Samples were instrumented with thermocouples to measure temperature and scored with a 1.6 mm by 1.6 mm grid on the side of the sample to measure through-thickness strain before being rolled in the CORUS Multi-mill rolling facility. Temperature data from the thermocouples in the experimental strips and the strain measured in the sample were used to validate the thermal/mechanical models. After the rolling, the strip was sectioned and the microstructure was characterised and compared to the model predictions.

Mechanical property data necessary for the individual models was supplied by CORUS from plane strain compression (PSC) testing data. Thermal property data was taken from literature sources. A sensitivity analysis was performed on some of these variables to determine their effect on the microstructure.

3.2 Objectives

The objectives of this study include the following:

- Formulate, develop and verify a mathematical model capable of predicting the temperature, strain and strain rates in hot rolled AA5083 aluminum alloy.
- Identify and integrate an appropriate microstructure model for the interstand region into the rolling model.
- Assess the sensitivity of the microstructure equations to the deformation conditions present during hot rolling.
- Validate the model against pilot scale rolling mill experiments.

Although mathematical models describing the microstructural evolution during hot tandem rolling have been developed previously [1-4], the uniqueness of the present study lies in the choice of AA5083 aluminum alloy, the incorporation of the microstructure calculation directly into the finite element code for the interstand region and the validation of the microstructure predictions using a pilot scale rolling mill. The microstructure equations available in the literature have typically been developed on lab scale tests with constant strains, temperatures and strain rates. Hence their applicability to an industrial rolling operation is questionable since in hot rolling the strains, temperatures and strain rates are constantly changing both through the thickness of the strip but also within the duration of the roll bite [5]. To date, there have not been any studies that have identified the appropriate input parameters to the microstructure equations which reflect the stored energy in the material due to hot deformation, i.e. the roll bite average values versus the roll bite exit values. Also, none of the models have validated the microstructure and temperature predictions against industrial data.

38

3.3 References

1   Wells, M.A., Lloyd, D.J., Samarasekera, I.V., Brimacombe, J.K. and Hawbolt, E.B. "Modeling the microstructural changes during hot tandem rolling of AA5XXX aluminum alloys: part I. Microstructural evolution" <u>Met and Mat. Trans</u>, Vol. 29B, pp. 611-620, 1998

2   Wells, M.A., Lloyd, D.J., Samarasekera, I.V., Brimacombe, J.K. and Hawbolt, E.B. "Modeling the microstructural changes during hot tandem rolling of AA5XXX aluminum alloys. Part III. Overall model development and validation" <u>Meta and Mat Trans.</u>, Vol. 29B, pp. 709-720, June, 1998

3   van der Winden, M.R. "Laboratory simulation and modelling of the break-down rolling of AA3104", Ph.D. Thesis, Sheffield University, 1999

4   Chen, B.K., Choi, S.K. and Thomson, P.F. "Simulation of evolution of microstructure in a thermo-mechanical analysis of the hot rolling of aluminium" <u>Res Mechanica</u>, 31, pp. 455-469, 1991

5   Jupp, S.P., Wells, M.A., Maijer, D. and van der Winden, M.R. "Development of a mathematical model using ABAQUS to simulate industrial hot tandem rolling of AA5XXX aluminum alloys" <u>Minerals, Metals and Materials Society/AIME, EPD Congress 2001 (USA)</u>, pp. 287-301, 2001

Chapter 4 Model Development

Thermomechanical modelling of hot rolling of aluminum is a fully coupled problem that is highly non-linear because of the interactions between temperature, strain and strain rates. Based on the modelling work reviewed, the finite element method (FEM) provides a convenient procedure to mathematically model the development of the thermal and strain distribution which occur in the rolling process and which has a strong influence on the resulting recrystallised microstructure [1]. The commercial finite element software, ABAQUS™, was chosen because it provides highly developed non-linear solution capabilities, as well as a well-documented method for extending the program's capabilities.

The rolling model that was developed was applied to two applications. The first application was for an AA5056 aluminum alloy using the same conditions modelled by Chen *et al.* [1] and Wells *et al.* [2], against which the ABAQUS™ results could be compared. The second application was for an AA5083 aluminum alloy that simulated the CORUS Multi-mill rolling facility. The general components employed in the rolling model incorporating the combined thermo-mechanical (i.e. deformation) and microstructure models is shown in Figure 4.1.
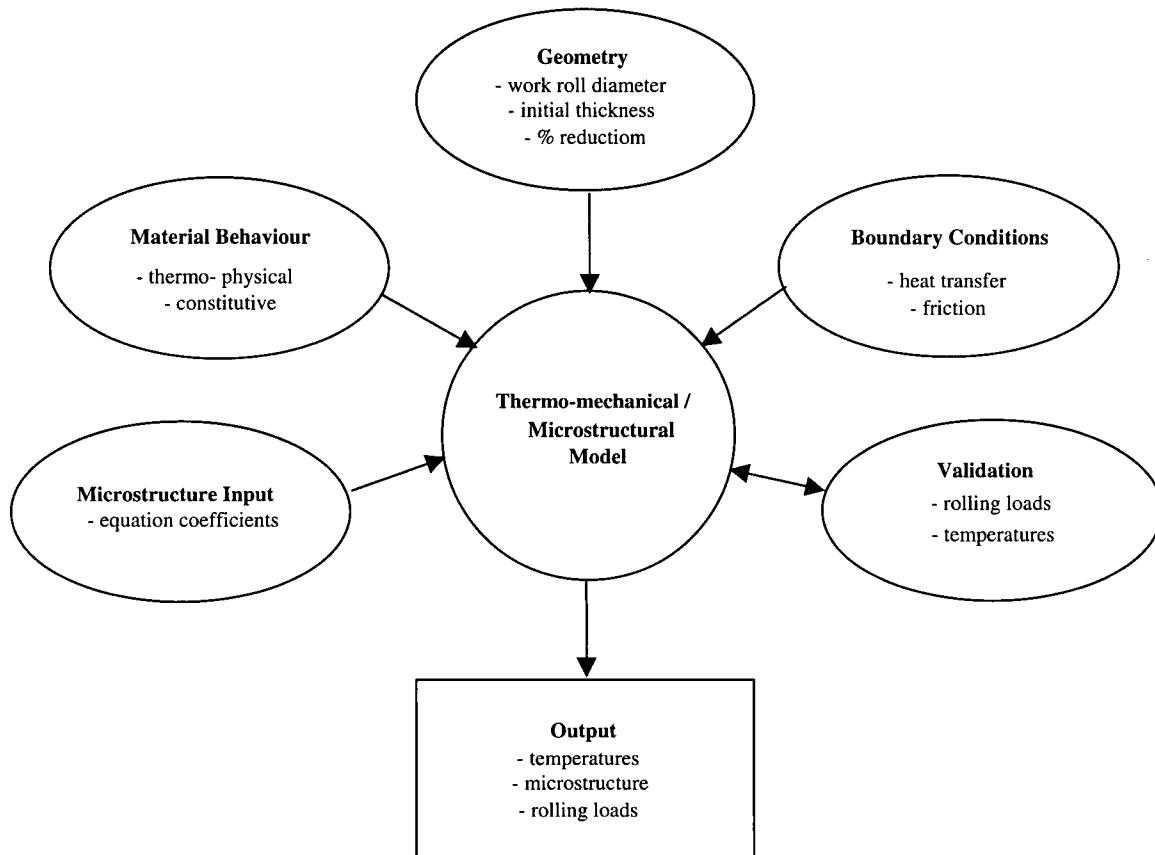
Figure 4.1 - Modelling components.

4.1 Thermo-Mechanical Model

A rolling model was developed to simulate a single stand of the hot rolling process for aluminum alloys using ABAQUS™. ABAQUS™ uses the Newton-Raphson numerical technique to solve the non-linear equilibrium equations and the temperatures are integrated using a backwards-difference scheme [3].

4.1.1 Mathematical Formulation

The integral statements necessary for the finite element approximations solved by ABAQUS™ are developed from the principle of virtual work, which states that for a stress field that is in equilibrium within the body, the work-rate inside the deforming body equals the work-rate done by the surface traction's for all velocity fields that are continuous and continuously differentiable.

41

Based on the principal of virtual work, the following equation is used by ABAQUS™ [3] to model the deformation process during hot rolling:

$$\int_S [t] \cdot [\delta u] dS + \int_V [f] \cdot [\delta u] dV = \int \sum [\sigma] \cdot \left(\frac{\partial [\delta u]}{\partial [x]} \right) dV \tag{4.1}$$

where [t] is the traction force matrix per unit area, [δu] is the displacement field, [f] is the force matrix per unit volume, [σ] is the true stress or Cauchy stress matrix and [x] is the direction matrix (i.e. x, y, z directions).

During the hot rolling process the temperature distribution within the strip is calculated using the unsteady-state heat conduction equation, according to:

$$\frac{\partial}{\partial x} \left(k \cdot \frac{\partial T}{\partial x} \right) + \frac{\partial}{\partial y} \left(k \cdot \frac{\partial T}{\partial y} \right) + \dot{Q} = \rho \cdot C_p \cdot \frac{\partial T}{\partial t} \tag{4.2}$$

where ρ is the strip density (in kg m^{-3}), C_p is the specific heat (in J kg^{-1} °C^{-1}), T is the temperature of the strip (in °C), t is the time (in s), k is the thermal conductivity of the strip (in Wm^{-1}°C^{-1}) and $\dot{Q}$ is the rate of heat generation due to plastic deformation (in W m^{-3}). The rate of heat generation per unit volume due to plastic work has been quantified as [1]:

$$\dot{Q} = \eta \cdot \dot{\bar{\varepsilon}} \cdot \bar{\sigma}_{flow} \tag{4.3}$$

where η is an efficiency term, $\dot{\bar{\varepsilon}}$ is the effective strain rate (in s^{-1}) and $\bar{\sigma}_{flow}$ is the effective flow stress (in MPa). The model assumes that 95% of the plastic work is transformed into heat. Equation 4.2 can be discretised and written in matrix form, as follows [4]:

$$[C_P]\{\dot{T}\} + [K_C]\{T\} = \{Q\} \tag{4.4}$$

where [C$_P$] is the heat capacity matrix, $\{\dot{T}\}$ is the rate of temperature change vector, [K$_C$] is the heat conduction matrix, {T} is the temperature vector and {Q} is the heat flux vector.

4.1.2 Model Geometry

The primary components of a general rolling model consists of two objects, the work roll and the strip. Employing symmetry conditions in the strip, only the top half of the strip is simulated. Previous models [2] have shown that the thermal effects in the work roll do not extend beyond the 5 mm thickness. In order to obtain steady-state rolling conditions in the strip, only a quarter section of the work roll is needed. Therefore to reduce computational time, a work roll geometry of 90° by 5 mm thick was chosen, as shown in Figure 4.2.
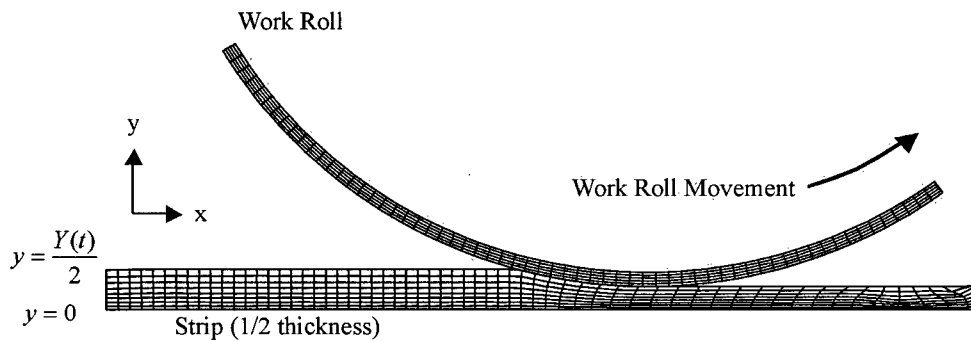
Figure 4.2 - Work roll and strip configuration in ABAQUS™.

The type of elements used in the ABAQUS™ simulations for both the strip and the work roll elements were 4-node bilinear plane strain elements. The use of plane strain elements is based on the assumption that deformation in the z-direction is negligible, which is a reasonable assumption for the centre of the strip.

For the AA5056 study, the portion of the strip modelled was initially 25 cm long and 14 mm thick with 60 elements in the longitudinal direction and 8 elements through the thickness. The through thickness elements had a bias ratio of 2 with the mesh density coarser at the surface than in the center in order to more easily accommodate the greater strain at the surface. The work roll was 350 mm in diameter and modelled with 5 elements in the radial direction and 61 elements in the circumferential direction.

43

For the AA5083 study the work roll diameter was 400 mm to simulate the CORUS Multi-mill rolling facility. This geometry was modelled with 5 elements in the radial direction and 90 elements in the circumferential direction. The initial thickness of the strip was 9.6 mm. The strip geometry was modelled with 75 elements in the longitudinal direction and 4 elements through the thickness. The through thickness elements had a bias ratio of 2 with the mesh density finer at the surface than in the center. The length of the modelled strip was also set to 25 cm, which had previously been found to be a sufficient length to obtain steady-state conditions within the strip. This mesh density corresponded to approximately 4 square millimetres per element.

4.1.3 Material Properties

The work roll was defined as a purely elastic material with a modulus of 200 GPa. The large differences in elastic moduli between the work roll and the strip enables the work roll to behave as a virtually rigid material. The properties of the steel work roll are shown in Table 4.1 [1].

Table 4.1 - Steel work roll properties [1].

Elastic Modulus (GPa)	Density (kg m^{-3})	Heat Capacity (J kg^{-1} K^{-1})	Thermal Conductivity (W m^{-1} K^{-1})
200	7860	460	46

The strip was assumed to behave as an elastic-viscoplastic material. Due to the large variations in temperatures and strain rates throughout the process it was necessary to define the strip's plastic behaviour as a function of temperature and strain rate. As a result, a hyperbolic sine equation (shown in Equation 4.5) was used to populate a matrix ABAQUS™ used this matrix to obtain the flow stress for a given temperature and strain rate by linear interpolation, shown in Appendix A.

$$\dot{\varepsilon} = A \cdot \left[\sinh(\alpha \cdot \sigma)\right]^n \cdot \exp\left(-\frac{Q_{def}}{R \cdot T_{def}}\right) \qquad (4.5)$$

In Equation 4.5, $\dot{\varepsilon}$ is the strain rate (in s^{-1}), A is a material constant, α is the stress multiplier, σ is the flow stress (in Pa), n is the exponent, Q_{def} is the activation energy of deformation (in $J\ mol^{-1}$), R is the gas constant ($J\ mol^{-1}\ K^{-1}$) and T_{def} is the deformation temperature (in K). The coefficients of the hyperbolic sine equation are material-dependent and are summarised in Table 4.2 for the two aluminum alloys modelled [1,5].

Table 4.2 - Summary of hyperbolic sine constants for AA5056 [1] and AA5083 [5].

Material	A	α (MPa^{-1})	n	Q_{def} (kJ mol^{-1})
AA5056	1.02×10^{10}	0.015	4.82	166.9
AA5083	2.87×10^{8}	0.04	2.26	162.5

The constitutive equation for the AA5083 aluminum alloy was taken from Sheppard [5] which best matched the plane strain compression data of the AA5083 material supplied by CORUS. Equation 5 was used to calculate the flow stress under the same strain rate and temperature conditions as the plane strain compression tests performed by CORUS. These flow stresses are compared to the measured results [6] in Figure 4.3. As can be seen from Figure 4.3, Sheppard's hyperbolic sine equation adequately represents the CORUS AA5083 material behaviour.
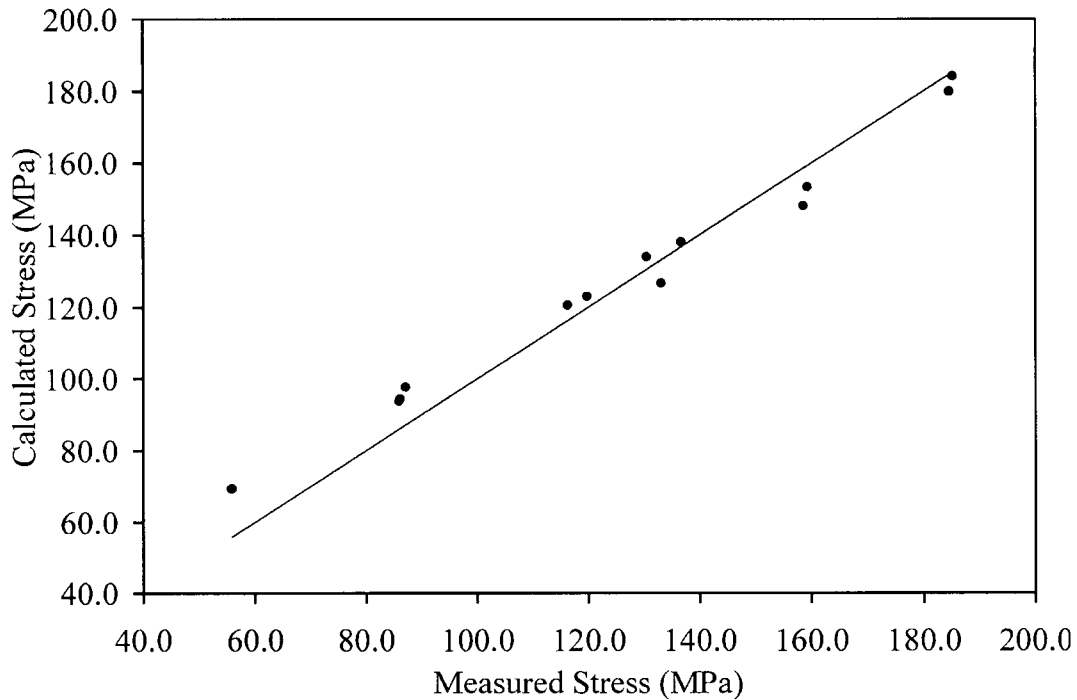
Figure 4.3 - Comparison of experimentally measured stress vs. the calculated stress using Sheppard's equation for AA5083.

The properties of thermal conductivity and heat capacity for the AA5056 strip, shown in Table 4.3, were based on literature values [1] and were assumed to be temperature independent. The thermal properties for AA5083, shown in Table 4.4, were assumed to be the same as AA5052 [7]. The elastic modulus and density of the strip were taken to be constant at 70 GPa and 2700 kg m^{-3} respectively.

Table 4.3 - Strip thermal properties for the AA5056 model [1].

Heat Capacity (J kg^{-1} K^{-1})	Thermal Conductivity (W m^{-1} K^{-1})
900	200

Table 4.4 - Strip thermal properties as a function of temperature for the AA5083 model [7].

Temperature (°C)	Heat Capacity (J kg^{-1} K^{-1})	Thermal Conductivity (W m^{-1} K^{-1})
14	930.0	143.4
280	990.0	167.1
306	1010.0	170.2
410	1050.0	174.1
505	1160.0	185.4

4.1.4 Boundary Conditions

Thermal boundary conditions for the rolling model were selected to describe the interface heat transfer conditions at the strip centreline, the inside radius of the work roll and at the interface between the strip and work roll.

Symmetry conditions have been assumed about the centreline of the strip for both rolling simulations. Referring to Figure 4.2, the thermal boundary condition for symmetry can be expressed as:

$$-k \cdot \frac{\partial T}{\partial y} = 0 \quad @ \ t>0; \ y=0 \tag{4.6}$$

where k is the thermal conductivity of the strip. A displacement boundary condition was also applied to prevent movement of the centreline in the y-direction.

The adiabatic thermal boundary condition at the inside radius of the work roll has been represented by:

$$-k \cdot \frac{\partial T}{\partial r} = 0 \quad @ \ t>0, \ r = r_i \tag{4.7}$$

where k is the thermal conductivity of the work roll (in W m^{-1} K^{-1}). To ensure this condition is valid the model thickness of the work roll must be sufficient to avoid increases in temperature along the inner radius.

47

The thermal boundary condition between the strip and the work roll can be expressed as:

$$-k \cdot \frac{\partial T}{\partial y} = h \cdot \left(T_{strip} - T_{workroll} \right) \quad @ \ t>0; \ y = \frac{Y(t)}{2} \tag{4.8}$$

where k is the thermal conductivity of the strip (in W m^{-1} K^{-1}) and h is the interface heat transfer coefficient at the interface (in W m^{-2} K^{-1}).

For the AA5056 study the interface heat transfer was assumed to be independent of pressure [1] and was set to a constant value of 20 kW m^{-2} °C^{-1}. The magnitude of this interface heat transfer coefficient is significantly lower than other values found in the literature [8-10]. From the literature it was found that the interface heat transfer coefficient is dependent upon the interface pressure [8-11]. For the AA5083 study the interface heat transfer coefficient was taken to be a function of pressure using the following relationship [11]:

$$h = 11.394 \cdot P + 137.53 \tag{4.9}$$

where h is the interface heat transfer coefficient (in kW m^{-2} °C^{-1}) and P is the interface pressure (in kg mm^{-2}).

A survey of the literature [12-16] revealed that no particular interface friction model has been shown to any more accurate than any other model. Following Chen *et al.* [1], interface friction was modelled using Coulomb friction, whereby the magnitude of the frictional force is proportional to the normal force. The Coulomb friction model is the default friction behaviour in ABAQUS™ [3], given by:

$$\tau_{crit} = \mu \cdot P \tag{4.10}$$

where τ_{crit} is the critical shear stress at which sliding starts (in Pa), μ is the coefficient of friction and P is the pressure (in Pa). A coefficient of friction of 0.3, employed by Chen *et al.* [1], was used for both studies since 0.3 is generally considered adequate to approximate hot rolling friction conditions [17].

The work roll elements are rigid with respect to the centre of the work roll, i.e. the axis of rotation. This enables the amount of reduction in the strip and the work roll velocity to be controlled by the single node located at the centre of the work roll.

4.1.5 Rolling Simulation in ABAQUS™

As previously discussed, the model developed in ABAQUS™ consists of two separate entities, the strip and the work roll. To accomplish the rolling simulation, two steps are necessary. In the beginning of the first step the work roll is above, but not in contact with the strip. The work roll is then lowered to obtain the desired strip reduction, pinching the head of the strip against the centreline. The second step consists of rotating the work roll at the desired radial velocity. The strip is drawn into the roll bite by the surface interaction between the strip and the work roll. The second step is finished after the work roll has rotated far enough for the entire strip to exit the roll bite. The interstand region is simulated with a third step where the strip cools and a user-defined subroutine calculates the recrystallised fraction.

4.1.6 Model Parameter Sensitivity

A sensitivity analysis of some of the AA5056 model parameters was done to determine their impact on the model results. Model parameters that were examined included: mesh density, interface heat transfer coefficient and interface friction coefficient.

Two effects of mesh density were considered, through the thickness and along the length. The effect of the axial mesh density on the model results is shown in Figure 4.4. The effect of the through-thickness mesh density is shown in Figure 4.5.

49
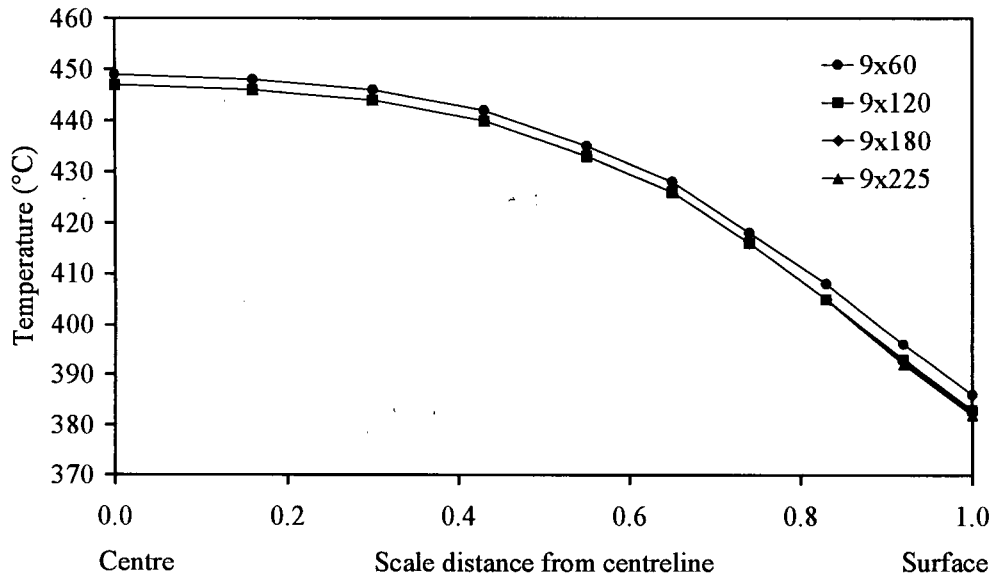
Figure 4.4 - Axial mesh density sensitivity analysis with 9 elements through-thickness.
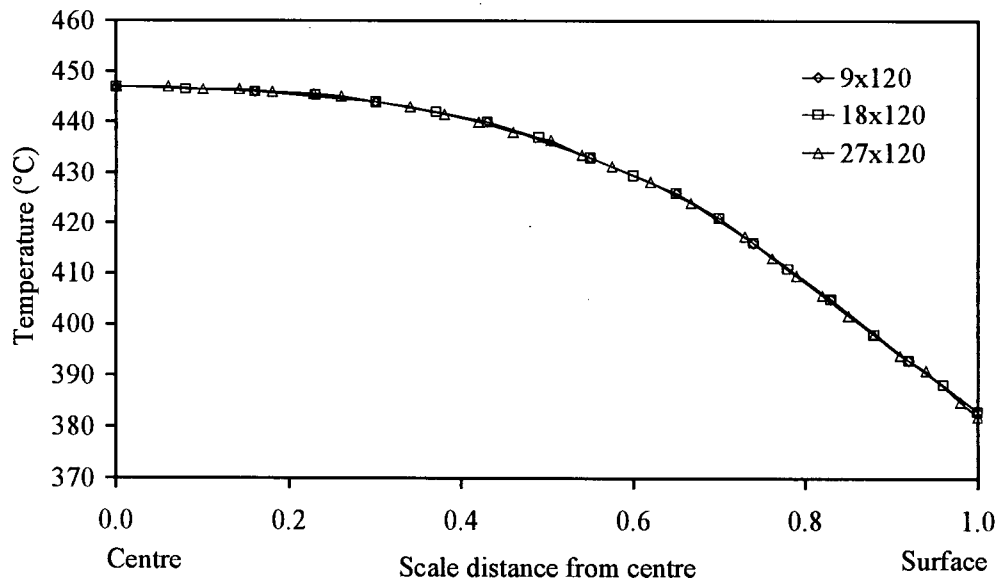
Figure 4.5 - Through-thickness mesh density sensitivity analysis with 120 axial elements.

Figure 4.4 indicates that more than 120 elements along the length of the strip do not have a significant effect on the results. Figure 4. shows that increasing the number of

elements through the thickness of the strip did not have a significant effect on the results. Therefore it was concluded that a sufficient mesh density for this model was 9 elements through the thickness by 120 elements along the length, which corresponds to an average area of 3.22 square millimetre per element.

The effects of the interface heat transfer coefficient on the temperature and strain predictions were determined by adjusting the interface heat transfer coefficient by ~25%. The effect of the interface heat transfer coefficient on the temperature predictions are shown in Figure 4.6. The sensitivity analysis shows that decreasing the interface heat transfer coefficient by 25% has a moderate effect on the predicted temperature while increasing the interface heat transfer coefficient by 25% causes little change in the surface temperature. Figure 4.7 shows that the changing the interface heat transfer coefficient has very little influence on the predicted strain profile.
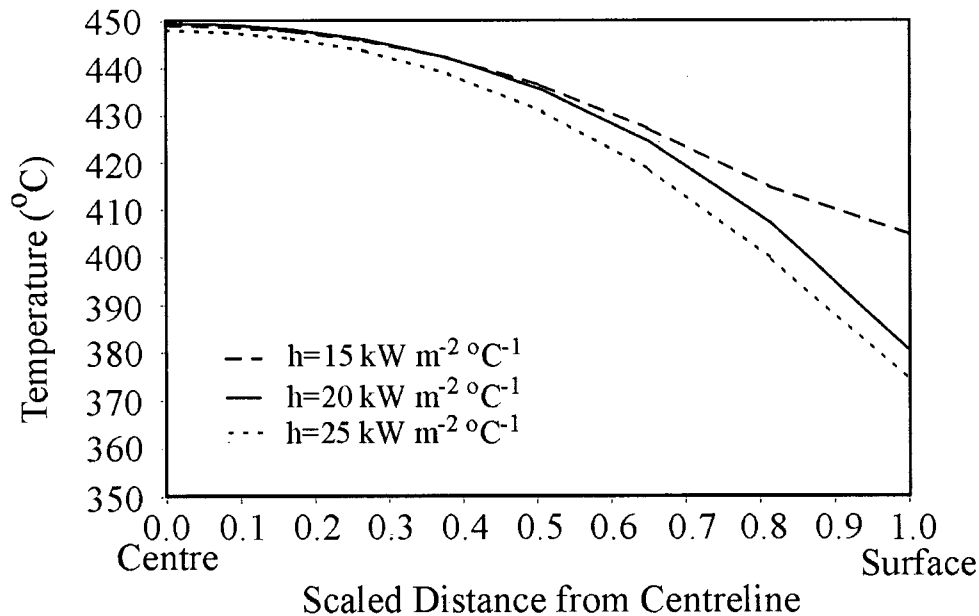
Figure 4.6 - Effect of interface heat transfer coefficient on temperature predictions.
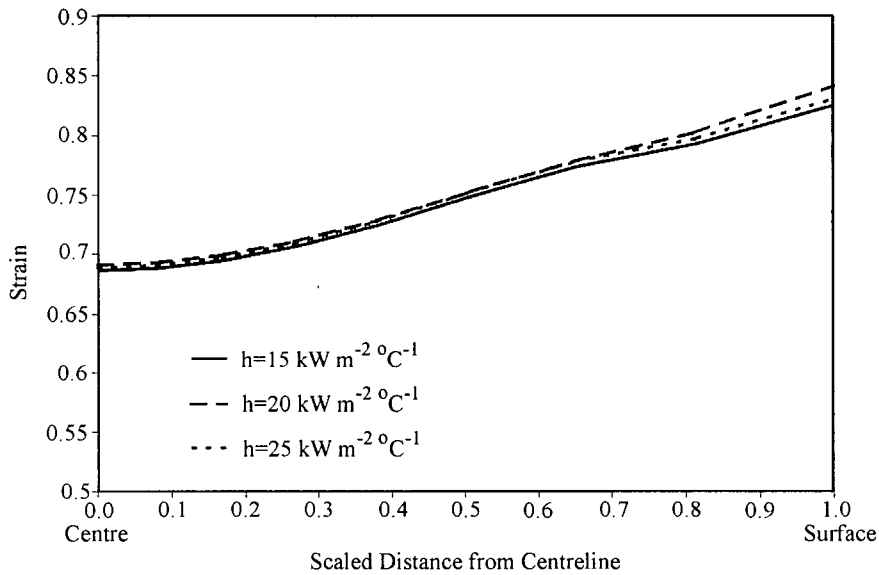
Figure 4.7 - Effect of interface heat transfer coefficient on strain predictions.

A similar sensitivity analysis was performed on the coefficient of friction. The coefficient of friction was adjusted approximately 35%, the predicted temperature response is shown in Figure 4.8. This sensitivity analysis showed that the temperature profile has very little dependence on the friction coefficient, with the exception of the 0.577 friction coefficient near the surface. The increased surface temperature for the 0.577 friction coefficient is a result of the increased strain experienced by the surface at the higher values for the coefficient of friction. As can be seen in Figure 4.9, the coefficient of friction has a large effect on the strain at the surface. This can be explained by the resulting shear forces between the work roll and the strip, which results in large changes in surface strain.
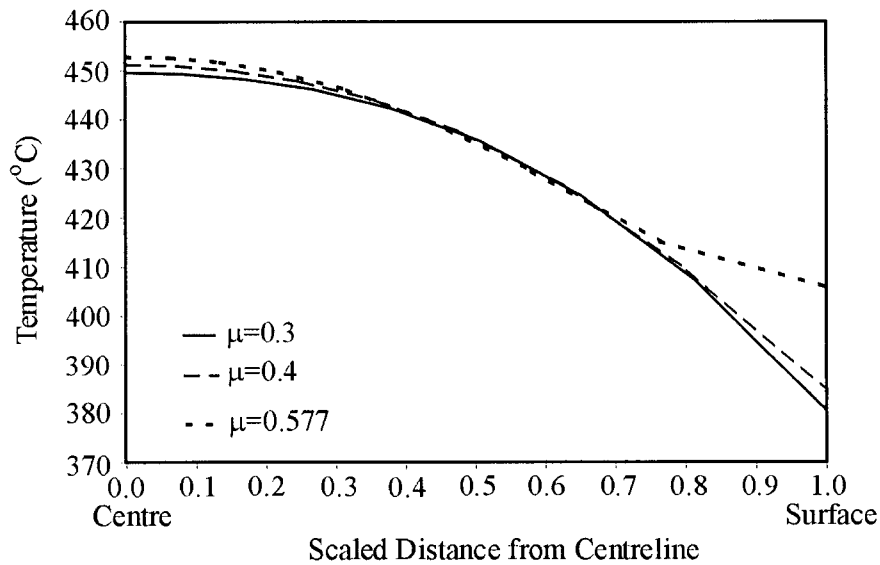
Figure 4.8 - Effect of friction on temperature pedictions.
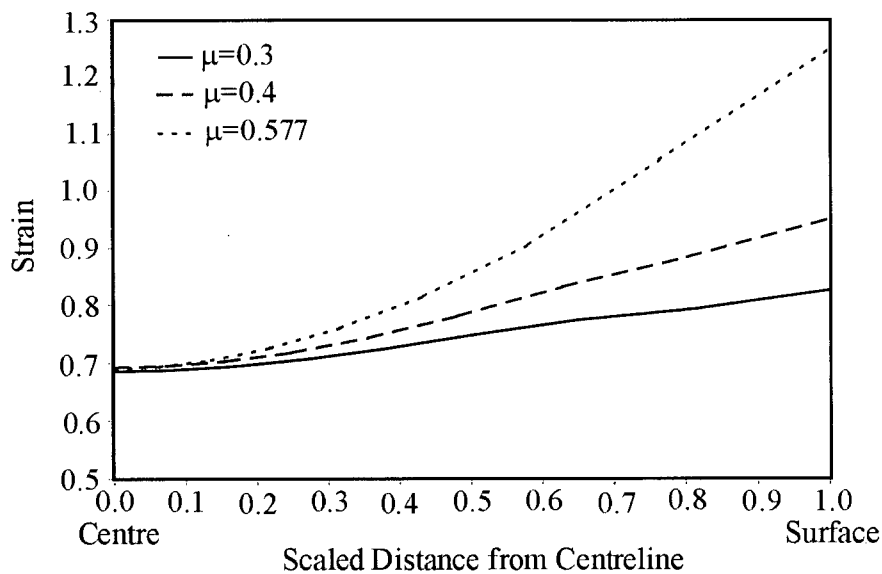
Figure 4.9 - Effect of friction on strain predictions.

4.2 Microstructure Model

The recrystallisation behaviour of the AA5083 aluminum alloy strip was modelled using semi-empirical relationships derived by Raghunathan et al. [18,19] based on the JMAK theory. Components of this model include: the recrystallised fraction, the Zener-Hollomon parameter and time to 50% recrystallisation.

53

4.2.1 Static Recrystallisation Microstructure Predictions

The recrystallised fraction, X_V, for isothermal conditions can be predicted using the Avrami-type equation given by [1,4,2,18,19]:

$$X_v = 1 - \exp\left(-0.693\left(t/t_{0.5}\right)^n\right)$$ (4.11)

where t is the transformation time, $t_{0.5}$ is the time to 50% recrystallisation and n is the JMAK exponent which is equal to 2 for both AA5056 and AA5083. The equation to estimate $t_{0.5}$ is given by Raghunathan *et al.* [19] as:

$$t_{0.5} = \frac{a \cdot d_o^b \cdot Z^d \cdot \exp\left(Q_{rex}/RT_{rex}\right)}{c}$$ (4.12)

where d_0 is the initial grain size (in μm), Z is the Zener-Hollomon parameter (in s^{-1}), Q_{rex} is the activation energy of recrystallisation (in J mol^{-1}), R is the gas constant (in J mol^{-1} K^{-1}) and T_{rex} is the recrystallisation temperature (in K). The different coefficients for the time to 50% recrystallisation are summarised in Table 4.5.

Table 4.5 - Time to 50% recrystallisation coefficients.

Material	a	b	c	d	Q_{rex} (kJ/mol)	Q_{def} (kJ/mol)
AA5056	9.1×10^{-12}	1.58	$0.0286 + 1.8\,\varepsilon^2$	-0.38	212	166.9
AA5083	2.7×10^{-10}	2.45	$9.73 + 3.82\varepsilon^2$	-0.58	183	175

where ε is the von Mises plastic equivalent strain. The Zener-Hollomon parameter, which is an estimate of the amount of stored energy, is given by:

$$Z = \dot{\varepsilon} \cdot \exp\left(\frac{Q_{def}}{R \cdot T_{def}}\right)$$ (4.13)

where $\dot{\varepsilon}$ is the strain rate (in s^{-1}), Q_{def} is the activation energy of deformation (in kJ mol^{-1}), R is the gas constant (in J $mol^{-1}K^{-1}$) and T_{def} is the deformation temperature (in K).

4.2.2 Incorporating Microstructure Predictions into ABAQUS™

For the AA5083 model, the microstructure equations from the literature were employed in a user-defined subroutine written for ABAQUS™. The subroutine used the average values of temperature and strain rate during the roll bite to make microstructure predictions. These parameters, along with the von Mises plastic equivalent strain at the roll bite exit, can be used as input to calculate the recrystallised fraction.

In commercial rolling operations, isothermal conditions are never present as there is continuous cooling by convection/radiation of the strip between rolling stands. In order to be able to apply isothermal recrystallisation equations, a temperature compensated time parameter, W, has been successfully employed by a number of researchers [2,19]. Equations 4.15 through 4.17 summarise this approach.

$$X_V = 1 - \exp\left(-0.693 \cdot \left(\frac{W}{W_{0.5}}\right)^n\right) \tag{4.15}$$

$$W = \sum_i \partial t_i \cdot \exp\left(-\frac{Q_{rex}}{R \cdot T_i}\right) \tag{4.16}$$

$$W_{0.5} = a \cdot d_o^b \cdot \varepsilon^c \cdot Z^d \tag{4.17}$$

In Equations 4.15-4.17, δt_i is the time increment (in s), T_i is the instantaneous temperature (in K), d_0 is the initial grain size (in μm), ε is the strain, Z is the Zener-Hollomon parameter (in s^{-1}), n is the JMAK exponent and a to d are the $t_{0.5}$ coefficients from above. In general, the additivity condition requires that the transformation at any given temperature be a function only of the amount of transformation product already present and the transformation temperature [20].

4.3 Summary

A model simulating the hot rolling of aluminum was developed to predict the temperature, strain and strain rates through the roll bite. In general, the work roll geometry can be a 90° section by 5 mm thick with most work roll diameters for a hot rolling of aluminum simulation. Typically the through-thickness mesh density for the work roll can be 1 element per millimetre and the radial mesh density should be sufficient to ensure a relatively smooth arc. The strip geometry can have a variable thickness and a 25 cm length is generally sufficient to obtain steady-state conditions but will have some dependence upon the initial thickness.

Different hyperbolic sine equations were employed to populate the required rate dependent plasticity matrices in ABAQUS™ for the AA5056 and the AA5083 models. The remaining properties of the steel work roll and the aluminum strip were taken from the literature.

The interface heat transfer coefficient was found to have some effect on the temperature strain predictions and therefore on the microstructure predictions. The AA5056 model employed a constant interface heat transfer coefficient of 20 kW m^{-2} °C^{-1} while the AA5083 model employed a relationship between interface heat transfer coefficient and pressure which results in an interface heat transfer coefficient in the range of 200-450 kW m^{-2} °C^{-1}. The coefficient of friction used in both models was 0.3, which has been recommended from literature sources.

The rolling simulation in ABAQUS™ required two steps; the first step pinched the head of the strip while the second step was the actual rolling step. A third step to simulate the interstand region was added for microstructure calculations. From these steps ABAQUS™ predicts temperature, strain and strain rate through the thickness of the strip as it is being deformed in the roll bite. This information was then fed into the user-defined subroutines to calculate the changes in microstructure in the interstand region using equations taken from the literature. The microstructure changes for non-isothermal can be estimated using a temperature-compensated time parameter.

4.4 References

1   Chen, B.K., Choi, S.K. and Thomson, P.F. "Simulation of evolution of microstructure in a thermo-mechanical analysis of the hot rolling of aluminium" Res Mechanica, 31, pp. 455-469, 1991

2   Wells, M.A., Lloyd, D.J., Samarasekera, I.V., Brimacombe, J.K. and Hawbolt, E.B. "Modeling the microstructural changes during hot tandem rolling of AA5XXX aluminum alloys. Part III. Overall model development and validation" Meta and Mat Trans., Vol. 29B, pp. 709-720, June, 1998

3   "ABAQUS™ Theory Manual" Hibbitt, Karlsson & Sorensen, Inc., 1998

4   Wells, M.A. "Mathematical modelling of the microstructure and texture changes during hot tandem rolling of AA5182 and AA5052 aluminum alloys" Ph.D. Thesis, University of British Columbia, 1995

5   Sheppard, T. "Extrusion processing of aluminium alloys" Proceedings 8th Light Metal Congress, edited by Jeglitsch, pp. 301-311, 1987

6   CORUS Plane Strain Compression Data

7   Roebuck, B. "Physical properties of representative engineering alloys for high rate deformation modelling" NPL Report, CMMT(A) 283, September, 2000

8   Devadas, C., Samarasekera, I.V. and Hawbolt, E.B. "The thermal and metallurgical state of steel strip during hot rolling: Part I. Characterisation of heat transfer coefficient" Met Trans, 22A, 307-319, Feb., 1991

9   Fletcher, J.D. and Beynon, J.H. "Heat transfer conditions in roll gap in hot strip rolling" Iron and Steelmaking, 23, no. 1, 1996

10   Samarasekera, I.V. "The importance of characterising heat transfer in hot rolling of steel strip" Proc. Int. Symp. on the Mathematical Modelling of the Hot Rolling of Steel, pp. 148-167, Aug., 1990

11   Hlady, C.O., Brimacombe, J.K., Samarasekera, I.V. and Hawbolt, E.B. "Heat transfer in the hot rolling of metals" Met and Mat Trans, 26B, 1019-1027, Oct., 1995

12   Bay, N. and Wanheim, T. "Real area of contact between a rough tool and a smooth workpiece at high normal pressures" Wear, 38, pp. 225-234, 1976

13   Lenard, J.G. and Malinowski, Z. "Measurement of friction during the warm rolling of aluminum" J. Mat. Proc. Tech., Vol. 39, pp. 357-371, 1993

14   Beynon, J.H. "Tribology of hot metal forming" New Directions in Tribology, pp. 135-139, 1997

15   Korzekwa, D.A. and Beaudoin, A.J. "Modeling the effects of friction and geometry on deformation path during hot rolling of aluminum" Hot Deformation of Aluminum Alloys II, edited by Bieler, Lalli and MacEwan, pp. 317-328, 1998

16   Lee, J.D. and Chen, Y.P. "Non-steady-state elastic-plastic behaviour of metal forming (rolling) with a generalized friction law" Theor. Appl. Frac. Mech., Vol. 33, pp. 93-99, 2000

17   Wusatoski, Z. "Fundamentals of rolling" Pergamon Press, pp. 62, 1969

18   Raghunathan, N. and Sheppard, T. "Microstructural development during annealing of hot rolled Al-Mg alloys" Mat. Sci. and Tech., Vol. 5, pp. 542-547, 1989

19   Raghunathan, N., Zaidi, M.A. and Sheppard, T. "Recrystallisation kinetics of Al-Mg alloys AA 5056 and AA 5083 after hot deformation Mat. Sci. and Tech., Vol. 2, pp. 938-945, 1986

20   Hawbolt, E.B., Chau, B. and Brimacombe, J.K. "Kinetics of austenite-pearlite transformation in eutectoid carbon steel" Met. Trans., Vol. 14A, pp. 1803-1815, September, 1983

Chapter 5   Rolling Experiments

A series of rolling experiments were conducted at the CORUS Multi-mill to validate the ABAQUS™ hot rolling model developed and ensure that it reflects what occurs during hot rolling. These experiments consisted of rolling samples of AA5083 aluminum alloy under a variety of temperature, strain and strain rate conditions. The conditions varied during rolling included: the entry temperature of the strip into the roll bite, the reduction experienced by the strip and the velocity of the work rolls. Data collected during the experiments included temperatures of the strip at the centreline, through-thickness strains, average rolling loads and final microstructures.

5.1 Pilot Scale Experimental Rolling Mill

A series of rolling experiments were conducted using CORUS Multi-mill, a pilot scale experimental rolling facility, in IJmuiden, Netherlands. Temperature data during rolling was collected with thermocouples embedded in the samples and rolling loads were measured from load cells on the work roll bearing blocks. The surface of the work roll was preheated to 90°C using circulating oil that was heated to 135 °C. The diameter of the work rolls was 400 mm.

The layout of the CORUS Multi-mill is shown in Figure 5.1. The furnace, capable of heating the samples to the required temperature in approximately 40 minutes, was located approximately 15 metres from the work rolls. The data acquisition computer was located approximately halfway between the furnace and the work rolls to minimise the required length of the thermocouple leads. The quench tank was located approximately 1.5 metres from the roll bite exit.

59
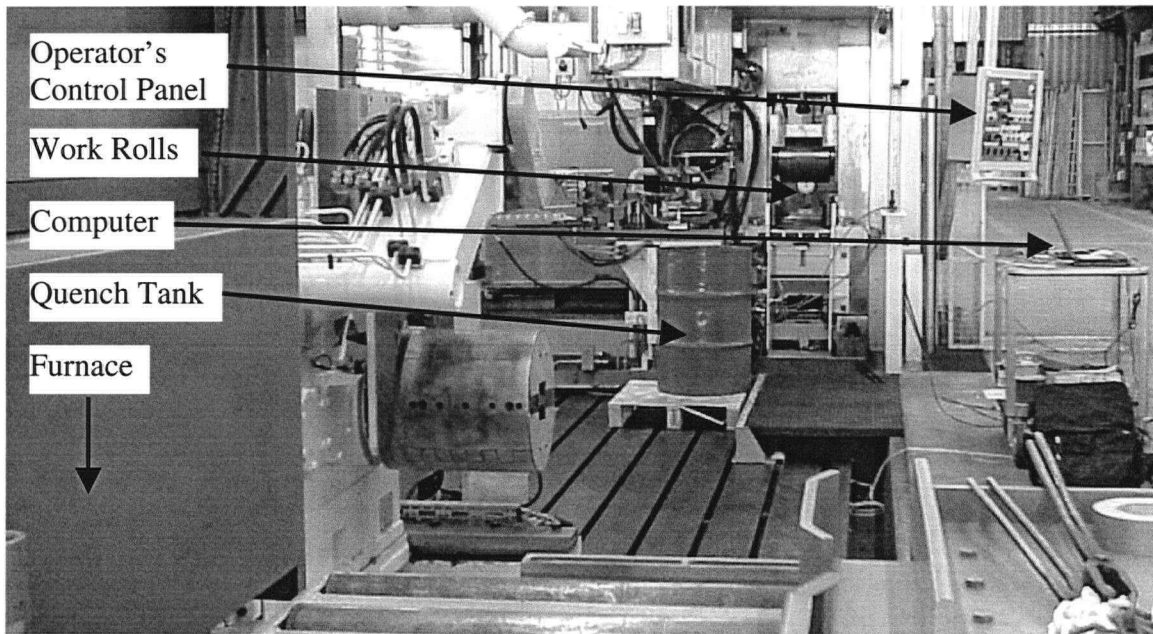
Figure 5.1 - CORUS Multi-Mill layout.

5.2 Sample Description and Instrumentation

Samples of the AA5083 aluminum alloy were supplied by CORUS for testing. This material was D.C. cast in sheet ingots 500 mm thick that were subsequently breakdown rolled to 20 mm. To ensure a uniform starting microstructure the material was heat-treated for 4 hours at 450°C before final machining to 9.6 mm thickness. The initial microstructure for the surface and the centreline is shown in Figure 5.2.
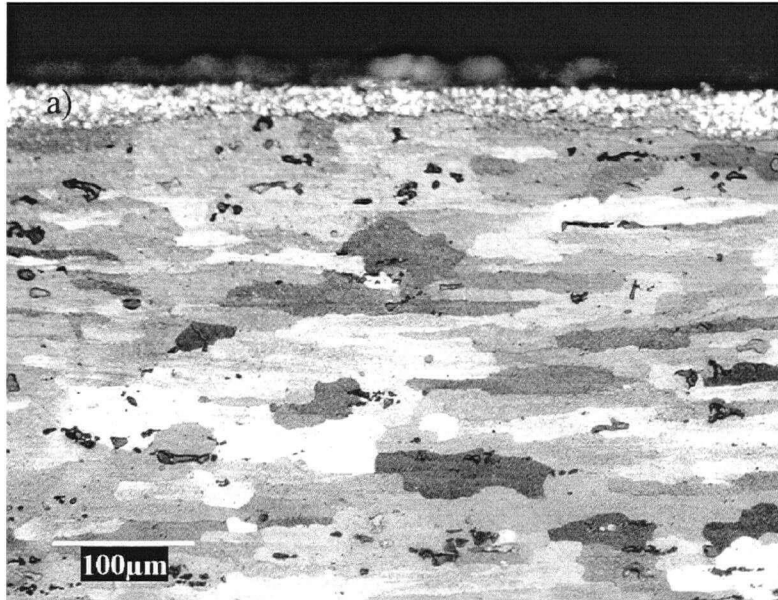
a) Surface
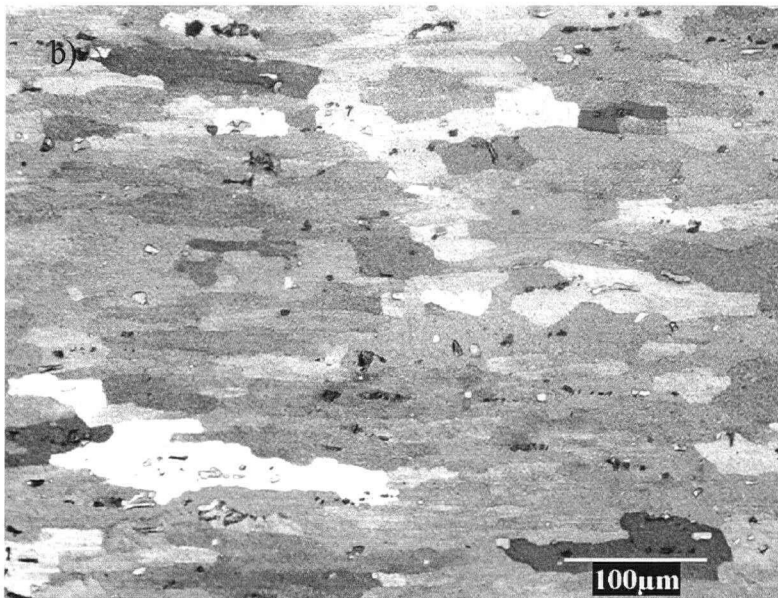
b) Centreline

Figure 5.2 - Initial sample microstructure after being annodized using Barker's reagent
and viewed under polarised light at 20x magnification. a) Surface b) Centreline.

As can be seen from Figure 5.2, the initial microstructure shows elongated grains along the horizontal axis with little variation in grain size from centreline to surface. The elongated nature of the starting grains will have a large effect on the final microstructure due to the increased grain boundary area that acts as recrystallised grain nucleation sites [1]. Using image analysis, the average equivalent starting grain size was determined to be 35.03 μm with a standard deviation of 18.62 μm. However, the elongated nature of the grains has been quantified by a length-to-breadth ratio of 3.9. The average length of the grains was 77.2 μm. The chemistry of the AA5083 samples is shown in Table 5.1.

Table 5.1 - AA5083 sample chemistry in wt %.

Al	Mg	Mn	Si	Fe	Cr
Remainder	4.5	0.7	0.3	0.3	0.15

5.2.1 Sample Instrumentation

The nominal sample dimensions were 200 mm wide by 500 mm long by 9.6 mm thick. The majority of the samples were instrumented with two Type K intrinsic thermocouples for redundant centreline temperature measurements. One of the samples was also instrumented using two surface thermocouples in addition to the centreline thermocouples. The details of the thermocouple locations are shown in Figure 5.3. The starting dimensions measured prior to testing each sample are summarised in Appendix B.
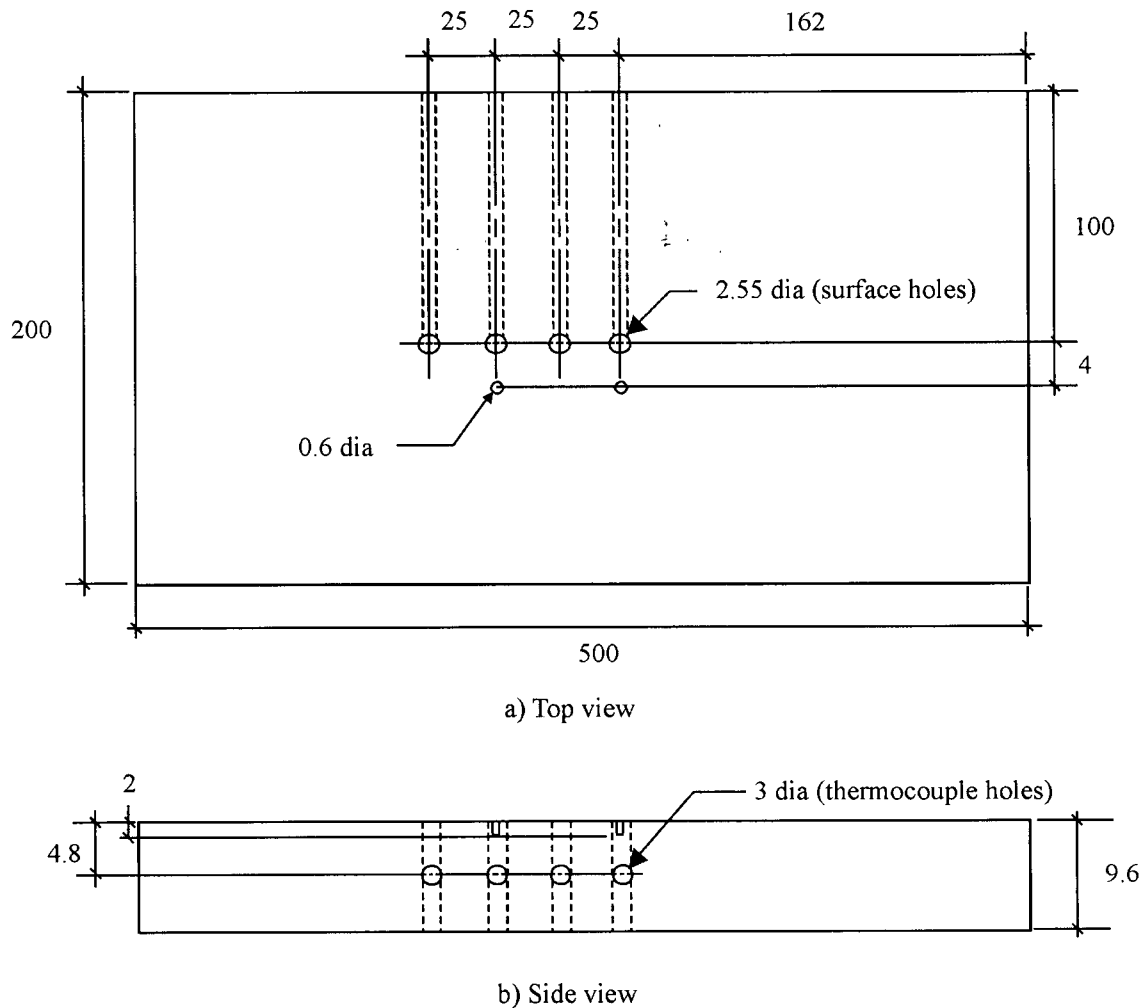
Figure 5.3 - Schematic diagram of the rolling samples. All dimensions are in millimetres, drawing not to scale: a) Top view b) Side view.

The difference between an intrinsic and an extrinsic thermocouple is how the thermocouple "circuit" is completed. In an extrinsic thermocouple, the two leads are welded into a "bead". An intrinsic thermocouple uses the sample material to complete the circuit. The advantage of an intrinsic thermocouple over an extrinsic thermocouple is the increased speed of the thermal response due to the reduced electrical resistance with the absence of the bead at the thermocouple junction.

To accurately locate the thermocouples, holes 3 mm in diameter were drilled in the side of the sample to the middle of the sample. Holes 2.55 mm in diameter were then drilled through the sample. The centreline thermocouples were positioned using two 2.5

mm diameter AA5182 plugs of equal length. The surface thermocouples were attached by centre-punching the thermocouple wires into small holes on the surface. Details of the thermocouple arrangements are shown in Figure 5.4.

a) Centreline

Thermocouple hole
Metal-clad thermocouple
Plugs
Thermocouple wires

b) Surface

Point of contact
Thermocouple hole
Metal-clad thermocouple
Surface hole
Thermocouple wires
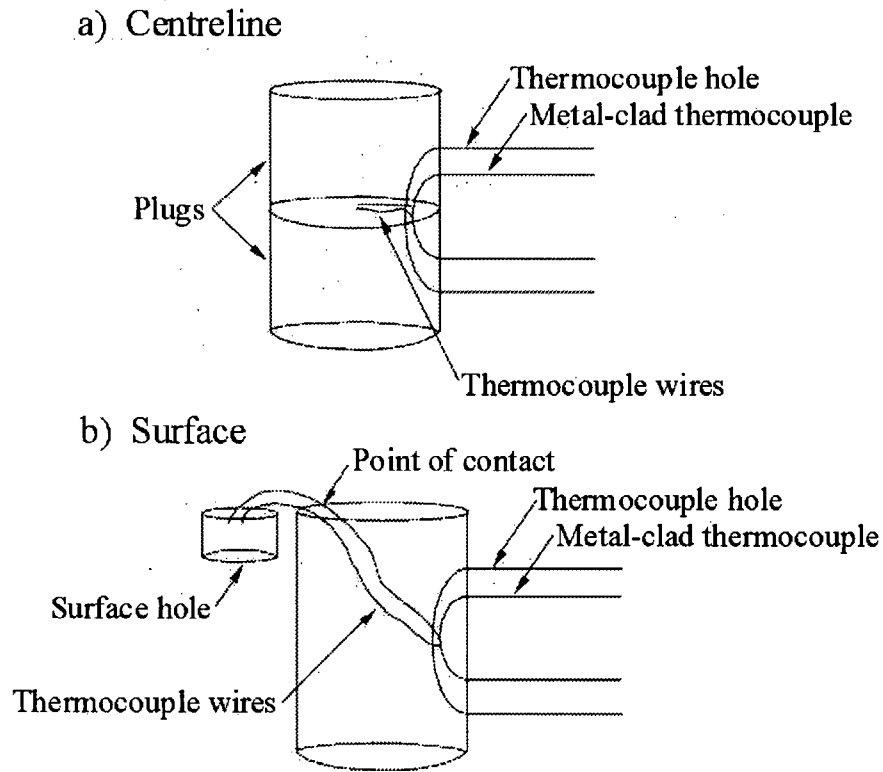
Figure 5.4 - Thermocouple placement details: a) Centreline thermocouple, b) Surface thermocouple.

The frequency with which the temperature data was collected depended upon the number of thermocouples in any given sample. The effect of the number of recorded signals on the data collection frequency is shown in Table 5.2. This shows that there is a drastic drop in the recording frequency with the increasing number of thermocouple signals.

Table 5.2 - Effect of the number of recorded signals on data collection frequency.

Number of Thermocouple Signals	Number of Rolling Load Signals	Data Collection Frequency (Hz)
1	2	1742
2	2	811
4	2	270

A physically based strain measurement technique was developed whereby the sample edge was scored with a grid on the edge of the sample, shown in Figure 5.5. The grid line spacing was 1.6 mm centre-to-centre, along both the x- and y-directions.
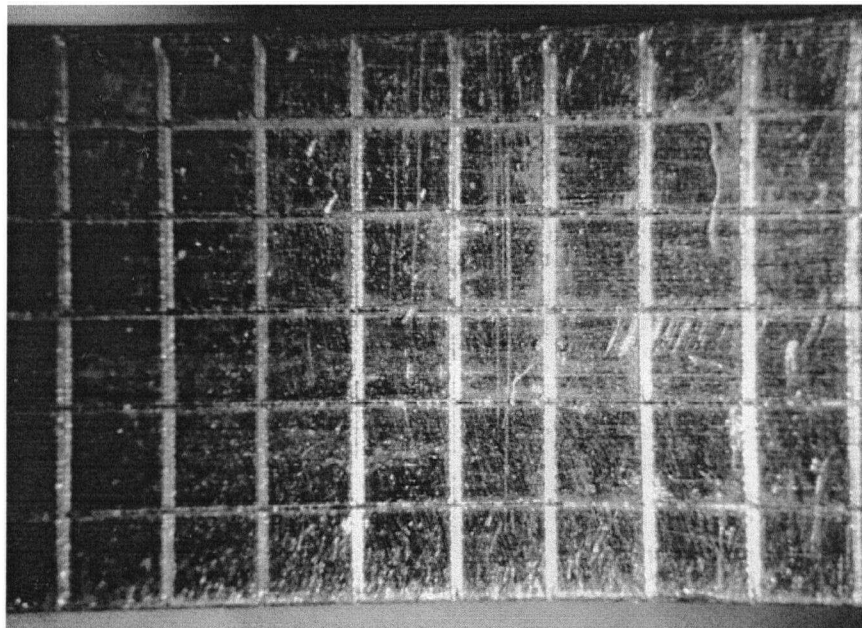
Figure 5.5 - Initial grid scored on sample edge (8x magnification).

A schematic of the two jigs that were used to scribe the surface is shown in Figure 5.6. Scribing the surface took place in two steps, the first step included scribing the vertical lines followed by the second step to scribe the horizontal lines. The jigs were constructed to have the middle line of the horizontal line jig as close as possible to the centreline of the samples. Approximately 20 mm in length of each sample was scribed with the 1.6 mm grid.
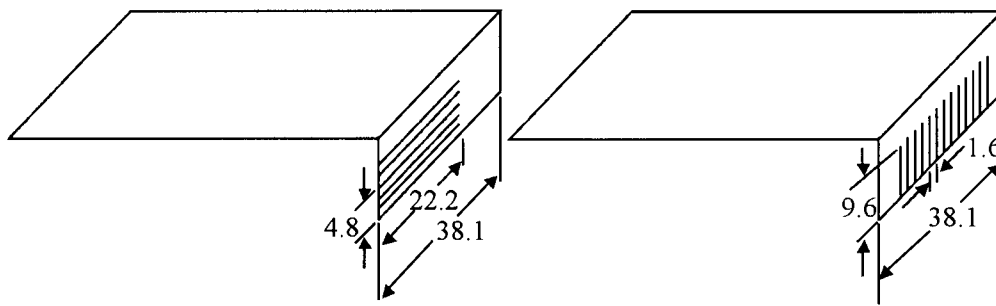
Figure 5.6 - Schematic of strain grid jigs. All dimensions are in mm, drawing not to scale.

5.2.2 Mill Instrumentation

The rolling loads were measured via load cells located between the upper work roll and hydraulic cylinders on both sides of the set-up. The hydraulic cylinders controlled the height of the roll bite gap. The precision of each load cell is 0.1% [2]. The work roll velocity was determined by multiplying the RPM (measured with a tachometer located on the drive shaft) by the work roll diameter. In addition to the thermocouple data collection system, the rolling load data was collected at 10 Hz by the Multi-mill control system.

5.3 Experimental Rolling Procedure

The experimental rolling procedure consisted of heating the samples to the required temperature in the furnace with very short holding times before rolling. The sample was then removed from the furnace and manually transferred to the roll bite entrance. The sample was then manually fed into the roll bite while the thermocouple leads were held clear. After exiting the roll bite the sample was quenched in the quench tank. A series of samples were processed in the manner under varying conditions, as shown in Table 5.3.

Table 5.3 - Plant trial matrix.

Sample ID	h_{in} (mm)	h_{out} (mm)	% Reduction	T_{entry} (°C)	Mean $\dot{\varepsilon}$ (s^{-1})
C	9.6	7.19	25	460	22.23
I	9.6	5.73	40	448	14.93
K	9.6	7.28	24	397	11.70
L	9.6	7.30	24	390	22.23
O	9.6	7.31	24	320	22.23
P	9.6	7.39	23	315	11.70

At the time of the plant trial, the automatic oil emulsion lubrication system was not operating. As a result, the oil emulsion lubricant was manually applied to the top work roll before each run.

5.4 Experimental Results

The experimental data of temperature and rolling loads was collected during rolling. Through-thickness strain and final microstructures were examined on sectioned samples taken after rolling and quenching. The final dimensions of the samples were measured and are summarised in Table 5.4.

Table 5.4 - Final sample dimensions after rolling.

Sample ID	Width (mm)	Length (mm)	Thickness (mm)
C	200.5	657	7.19
I	201.4	855	5.73
K	200.6	651	7.28
L	200.6	650	7.30
O	200.4	630	7.31
P	200.3	638	7.39

5.4.1 Thermal Response and Rolling Loads

The rolling environment is extremely electrically noisy, primarily due to the presence of induction motors driving the work rolls. This results in a noisy thermocouple signal, which was smoothed using a 3-point and 5-point moving average. The raw thermocouple data is compared to the smoothed data in Figure 5.7.
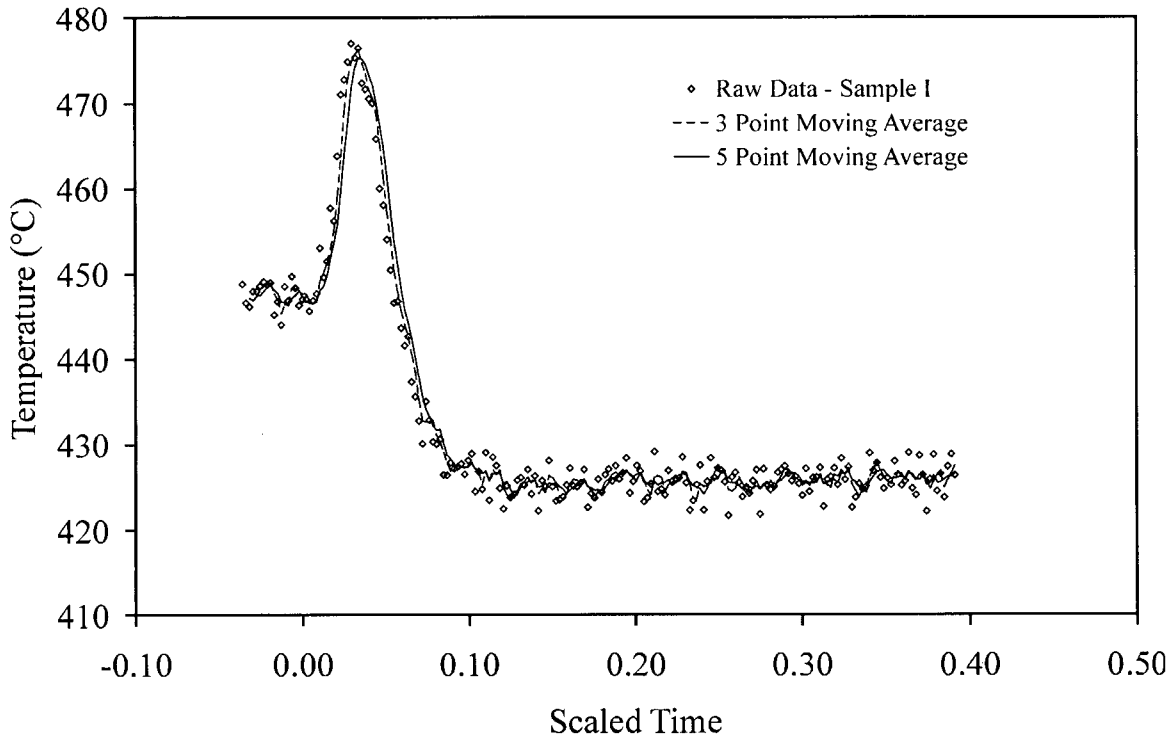
Figure 5.7 - Sample I centreline raw temperature data versus filtered data.

As can be seen, the raw temperature data varies by approximately 7 °C. The 3- and 5-point moving average reduces this variation to approximately 5 °C. However the 5-point moving average causes the peak temperature to shift slightly in time, therefore the 3-point moving average was chosen for comparison purposes with the model predictions.

Pressure transducers on the bearing blocks of the work rolls measured the rolling loads. The resulting signal provided the average rolling load for the sample. The experimental average rolling loads are summarised in Table 5.5.

Table 5.5 - Summary of experimental average rolling loads.

Sample ID	Average Rolling Load (kN)
C	n/a
I	1330
K	1073
L	1036
O	1215
P	1228

5.4.2 Microstructure Characterisation

Upon exiting the work roll the samples were quenched, with typical quench rates on the order of 200 °C s^{-1}. The time to quench varied as a result of the sample handling. The times from roll bite exit to quench are summarised in Table 5.6.

Table 5.6 - Summary of times to quench.

Sample ID	Time to Quench (s)
C	3
I	15
K	8
L	3
O	3
P	4

The samples were polished to 1 μm and anodized using Barker's reagent. To reveal the grain structure the samples were examined under polarized light. The resulting microstructure for Sample I at the centreline and the surface are shown in Figure 5.8.

69
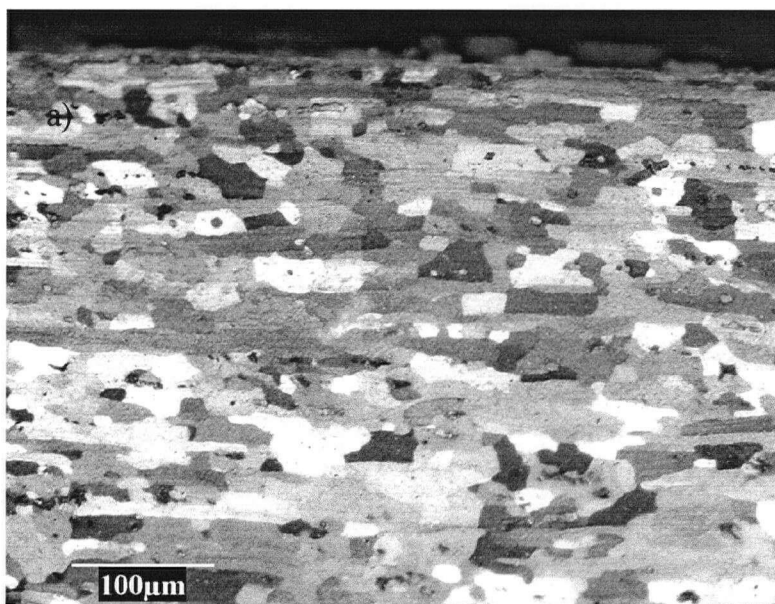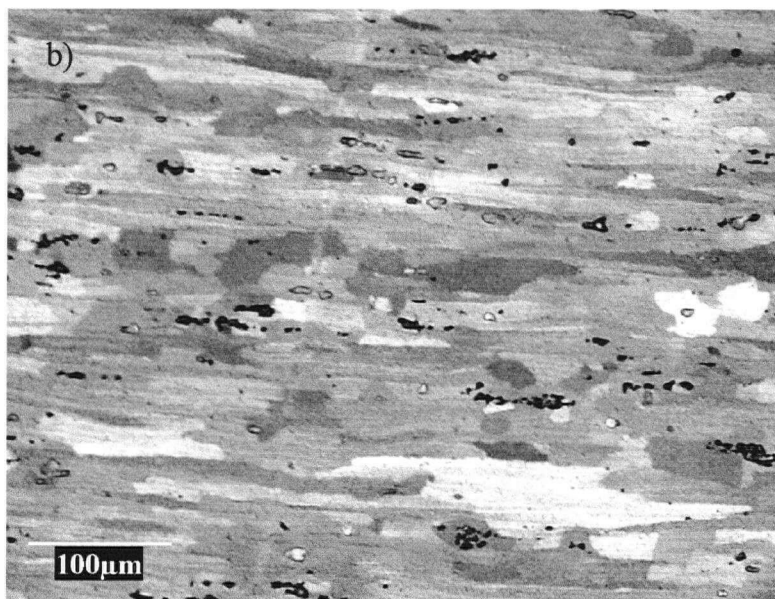
a) Surface

b) Centreline

Figure 5.8 - Sample I rolled microstructure after being anodized using Barker's reagent and viewed under polarised light at 20x magnification. a) Surface b) Centreline.

As can be seen from Figure 5.8 there is a significant variation in the amount of recrystallisation from centreline to surface. The ASTM Standard E 562-89 was used to determine the recrystallised fraction. ASTM Standard E 562-89 describes a systematic manual point counting procedure for statistically estimating the volume fraction of an identifiable constituent (i.e. recrystallised grains) from sections through the microstructure by means of a point grid. In determining the recrystallised fractions, grains clearly defined were considered recrystallised while the remaining grains were considered unrecrystallised. The recrystallised fraction measurements using ASTM Standard E 562-89 are summarised in Table 5.7.

Table 5.7 – Summary of measured recrystallised fractions.

Sample ID	Location	X_V	Standard Deviation
C	Surface	0.794	0.060
	Centre	0.073	0.024
I	Surface	0.828	0.041
	Centre	0.059	0.020
K	Surface	0.549	0.071
	Centre	0.072	0.015
L	Surface	0.390	0.050
	Centre	0.042	0.012
O	Surface	0.442	0.063
	Centre	0.118	0.019
P	Surface	0.690	0.074
	Centre	0.188	0.028

5.4.3 Strain Characterisation

The strain experienced by the sample was characterised using the grid scored on the edge of the sample prior to rolling. The through-thickness strain in the sample was characterised by the change in the grid spacing, shown in Figure 5.9. The new dimensions of the grid lines were measured manually. By knowing the original dimensions of the grid, the true strain in the x- and y-directions can be calculated using the following equation:

$$\varepsilon = \ln \frac{l_{final}}{l_{initial}} \tag{5.1}$$

where ε is the true strain, l_{final} is the final length of the line (in mm) and $l_{initial}$ is the starting length of the line (in mm). The engineering shear strain (γ) is estimated by the new angle, in radians, of the parallelogram defined by each grid section [3] whereas the true strain (ε_{xy}) is $\gamma/2$. The strain measurements are shown schematically in Figure 5.10, with the results summarised in Table 5.8. Since the halfway line of the scored grid may not actually fall on the exact centreline of the sample, the strains at any given through-thickness location have been taken as the average of both sides of the centreline.
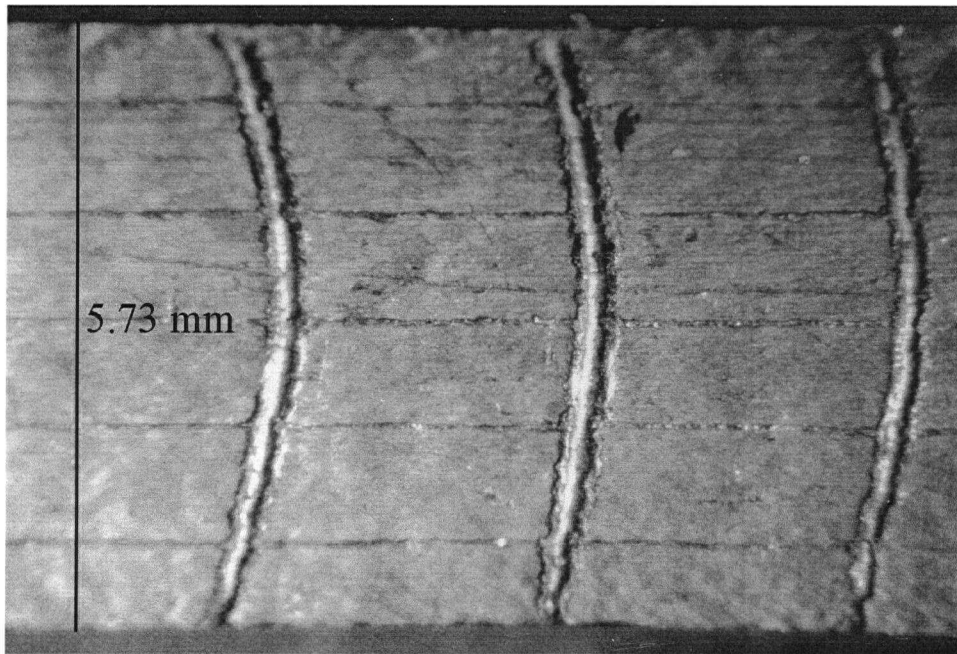
Figure 5.9 – Sample I through-thickness strain distribution.
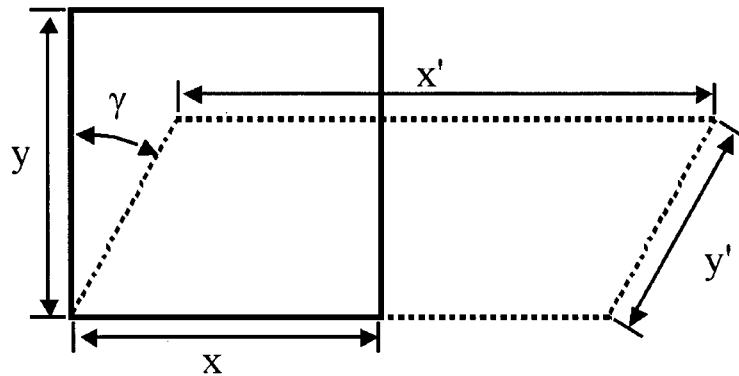
Figure 5.10 - Locations of strain measurements.

As can be seen from Figure 5.9, the scored lines in the y-direction have been widened as a result of the rolling process. The increased width of these lines introduces a greater amount of error into the strain calculations. The accuracy of the measurements was taken as ±0.5 mm based on the accuracy of the ruler used. This length was then multiplied by the magnification to determine the actual length. The accuracy in locating the corners of the deformed grid was taken as ±1 mm. The overall tolerance was taken as the summation of these accuracies.

The shear strain is increasing from centre to surface as a result of the frictional forces between the work roll and the surface of the strip whereas the strains in the x- and y-direction are relatively uniform, as would be expected under plane strain conditions. From Mohr's circle the principal strains can be calculated using the analytical expression shown in Equation 5.1.

$$\varepsilon_{1or2} = \frac{\varepsilon_x + \varepsilon_y}{2} \pm \sqrt{\left(\frac{\varepsilon_x - \varepsilon_y}{2}\right)^2 + \varepsilon_{xy}^2} \qquad 5.1$$

The principal strains can then be used to calculate the von Mises equivalent strain using the Equation 5.2.

$$\bar{\varepsilon} = \left(\frac{2}{3} \left(\varepsilon_1^2 + \varepsilon_2^2 \right) \right)^{1/2}$$
5.2

Table 5.8 - Summary of experimental strain measurements.

Sample ID	Scaled Distance	ε_x	ε_y	ε_{xy}	ε_1	ε_2	$\bar{\varepsilon}$
C	0.00	0.34	-0.36	0.045	0.343	-0.363	0.41
	0.33	0.32	-0.32	0.060	0.325	-0.325	0.38
	0.67	0.35	-0.40	0.067	0.356	-0.406	0.44
I	0.00	0.61	-0.46	0.060	0.613	-0.463	0.63
	0.34	0.63	-0.41	0.103	0.640	-0.420	0.63
	0.72	0.63	-0.77	0.136	0.643	-0.783	0.83
K	0.00	0.30	-0.34	0.036	0.302	-0.342	0.37
	0.33	0.33	-0.34	0.046	0.333	-0.343	0.39
	0.63	0.32	-0.29	0.061	0.326	-0.296	0.36
L	0.00	0.32	-0.35	0.045	0.323	-0.353	0.39
	0.35	0.33	-0.29	0.067	0.335	-0.295	0.36
	0.69	0.33	-0.29	0.058	0.335	-0.295	0.36
O	0.00	0.25	-0.26	0.056	0.256	-0.266	0.30
	0.36	0.30	-0.31	0.054	0.305	-0.315	0.36
	0.69	0.32	-0.31	0.082	0.330	-0.320	0.38
P	0.00	0.30	-0.29	0.027	0.301	-0.291	0.34
	0.34	0.28	-0.26	0.036	0.282	-0.262	0.31
	0.63	0.31	-0.29	0.046	0.314	-0.294	0.35

5.5 Summary

Experimental rolling trials were successfully conducted at the CORUS Multi-mill in IJmuiden, Netherlands using an AA5083 aluminum alloy supplied by CORUS. Two different initial temperatures, two different work roll velocities and two different reductions were examined for a total of six experiments. From these trials, data and samples were collected for use in characterising the microstructure, through-thickness strain, through-thickness temperatures and rolling loads from materials with different thermomechanical histories.

5.6 References

1   Humphreys, F.J. and Hatherly, M. "Recrystallisation and related annealing phenomena" Pergamon Press, New York, 1996

2   Corus Research, Development and Technology, "Introduction to the research mill of CORUS R,D&T" January 4th, 2000

3   Ruoff, A.L. "Introduction to materials science" Prentice-Hall, New Jersey, pp. 39-40, 1972

Chapter 6   Results and Discussion

Validation of the model developed within ABAQUS™ consisted of two steps. The first step involved validating the model predictions against data published in the literature using two other finite element method codes that simulated the rolling of an AA5056 aluminum alloy.   This step was used to validate the rolling algorithm for temperature, strain and strain rate predictions.   The second step involved validating the model against experimental measurements using the CORUS Multi-mill pilot scale rolling facility located in IJmuiden, Netherlands.   The pilot facility was used to roll AA5083 aluminum alloy samples.   The second step was used to validate the microstructure predictions calculated based on the model temperature, strain and strain rate predictions.

6.1   Model Validation Against Literature Data

The ABAQUS™ rolling model simulated the hot rolling process for a strip 28 mm thick with a work roll diameter of 350 mm at an entry temperature of 415 °C and a mean strain rate of 4.2 s^{-1}. For this application, only the temperature and strain distributions were predicted.   The results of the ABAQUS model were compared to the results of the literature models developed by Wells *et al.* [1] and Chen *et al.* [2].   The roll bite exit temperature profiles are compared in Figure 6.1 and the roll bite exit strain profiles are compared in Figure 6.2.
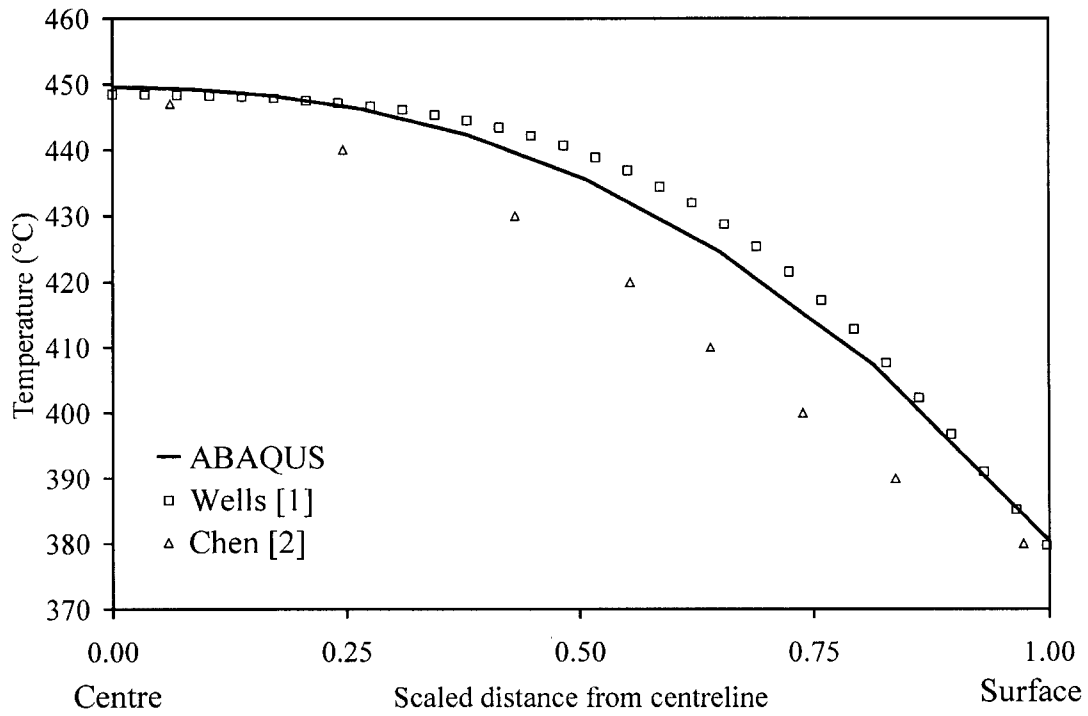
Figure 6.1 - Temperature profile comparison.
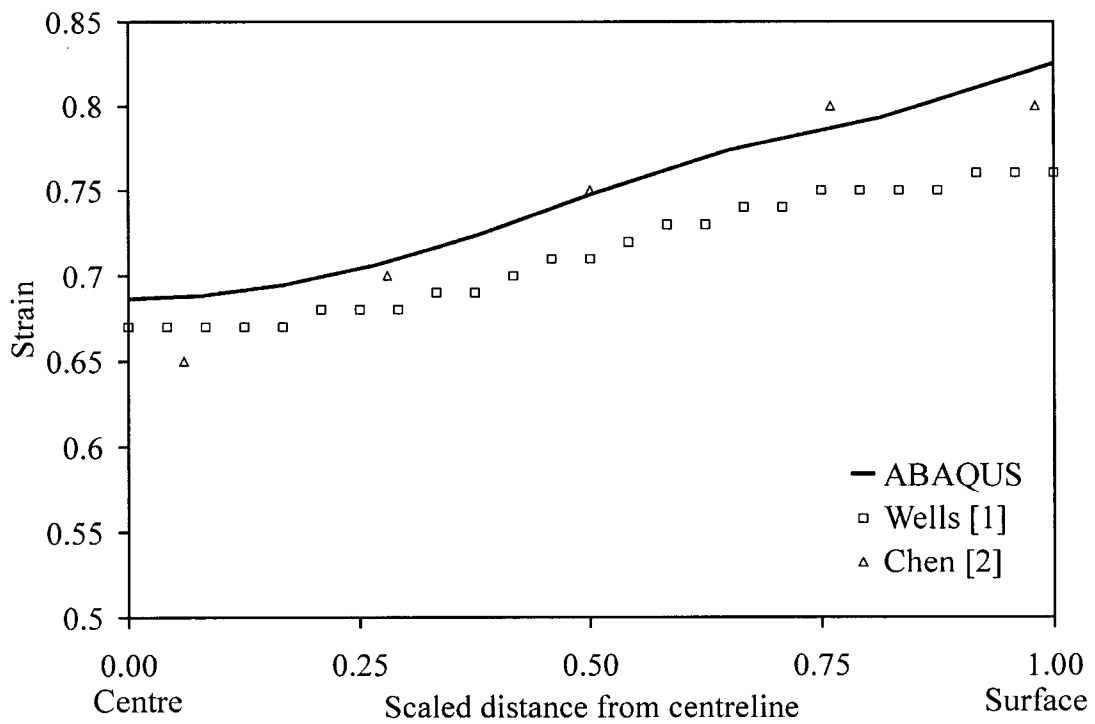
Figure 6.2 - Strain profile comparison.

77

The temperature profile at the roll bite exit, shown in Figure 6.1, is the result of heat generated due to plastic deformation and the quenching of the strip surface by the work rolls. The strain profile, shown in Figure 6.2, is the result of the friction interaction between the surface of the strip and the work roll. Since the ABAQUS™ model predictions were similar to the literature model predictions ABAQUS was considered to be able to describe the thermal and mechanical aspects of rolling.

6.2 Model Validation Against Experimental Measurements

The second application of the ABAQUS model was to analyse experiments performed using the pilot-scale CORUS Multi-Mill. For this application the microstructure evolution was considered, in addition to the temperature and deformation that occurred in the roll bite. The ABAQUS™ model was validated against experimentally measured rolling loads, temperatures, strains and microstructure.

6.2.1 Temperature Comparisons

The centreline temperatures were recorded for all of the samples. In addition, the surface temperature of Sample P was also recorded. A comparison of the temperature predictions to the experimental data for Sample I are shown in Figure 6.3.
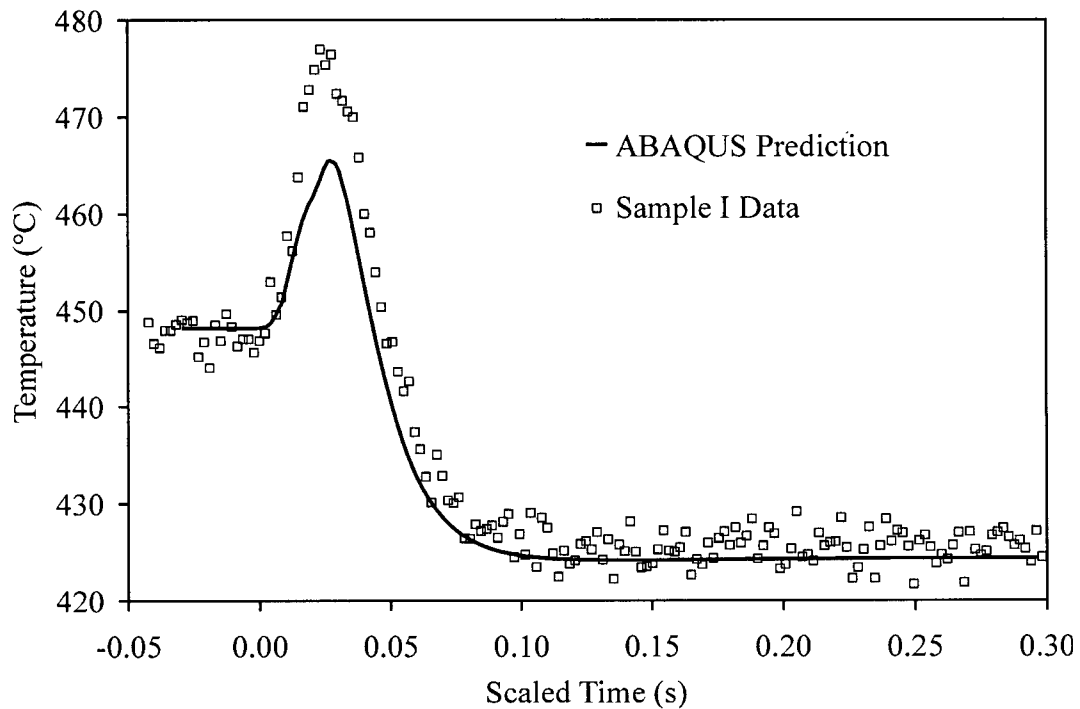
Figure 6.3 - ABAQUS™ temperature through the roll bite predictions versus experimental data for the centreline of Sample I. (T_{entry}=448 °C, $\bar{\dot{\varepsilon}}$ =14.93 s^{-1}, % reduction=40).

As can be seen from Figure 6.3, the maximum difference between predicted and experimental temperatures occurs once the peak temperature is reached and is approximately 11 °C, which corresponds to a 2.3% difference. There are two possible reasons for this difference: 1) the model does not generate enough heat due to plastic work, and 2) the boundary condition at the surface is extracting too much heat and here the predicted temperature is lowered than that measured.

A comparison of the predicted temperatures to the experimental data for the conditions experienced for Sample P, including both centreline and surface profiles, are shown in Figure 6.4.

79
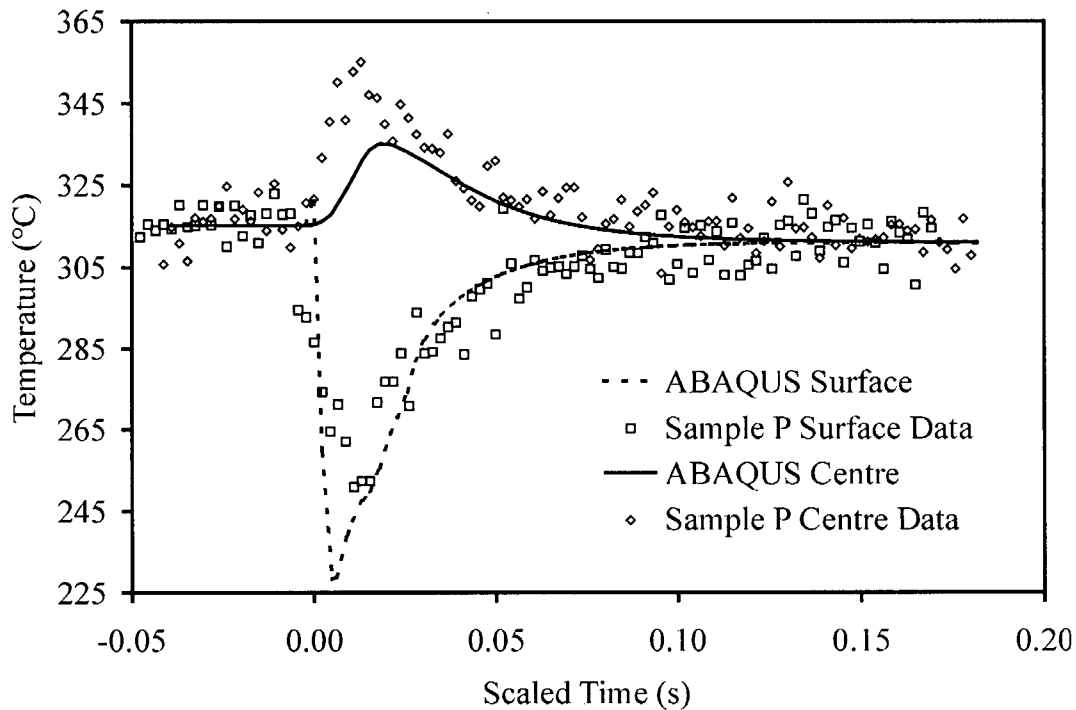
Figure 6.4 - ABAQUS™ temperature through the roll bite predictions versus experimental data for Sample P. (T_{entry}=315 °C, $\bar{\dot{\varepsilon}}$ =11.7 s^{-1}, % reduction=24).

As can be seen from Figure 6.4, the maximum difference between the model predictions and the experimental data occurs at the surface and is approximately 28 °C, which corresponds to a difference of 11%. The model predictions along the centreline more closely match the experimental data with the maximum temperature difference of 16 °C, which corresponds to a difference of 4.6%. The difference in the predicted and measured temperature profiles at the surface can be explained by two variables. The first variable is the boundary condition used at the surface to quantify the heat extracted by the work roll in the form of a heat transfer coefficient which appears to be slightly too high. The second variable is how the temperature was measured during the experiments. The thermocouple used to collect the data was an intrinsic Type-K thermocouple that provides a rapid response but there is an inevitable delay that will offset the temperature profile by a small amount. The data acquisition rate for Sample P was reduced to 273 Hz since more temperature signals were logged. This corresponds to a reduced number of data points collected through the roll bite. With the reduced number of points the signal noise

becomes a more important factor since there are fewer data points for the filtering algorithm. The true temperature of the sample will now fall within are larger range. Since the time spent by the sample in the roll bite is very short, another effect of the slower data collection rate is the possibility that the minimum temperature reached by the surface is not actually recorded. Considering the variation in temperature that is possible within the experimental data, the model prediction for the surface temperature is a reasonable match. Overall, the model temperature predictions through the roll bite are reasonable and the thermal aspects of the roll bite model can be considered validated.

The temperature drop between the roll bite exit and the quench has been calculated assuming a convective heat transfer coefficient between the surface of the strip and the environment of 12.5 W m^{-2} °C^{-1} with a measured ambient temperature during the plant trials of 35 °C. A comparison of the recorded temperature drop and the predicted temperature drop is shown for Sample I in Figure 6.5.
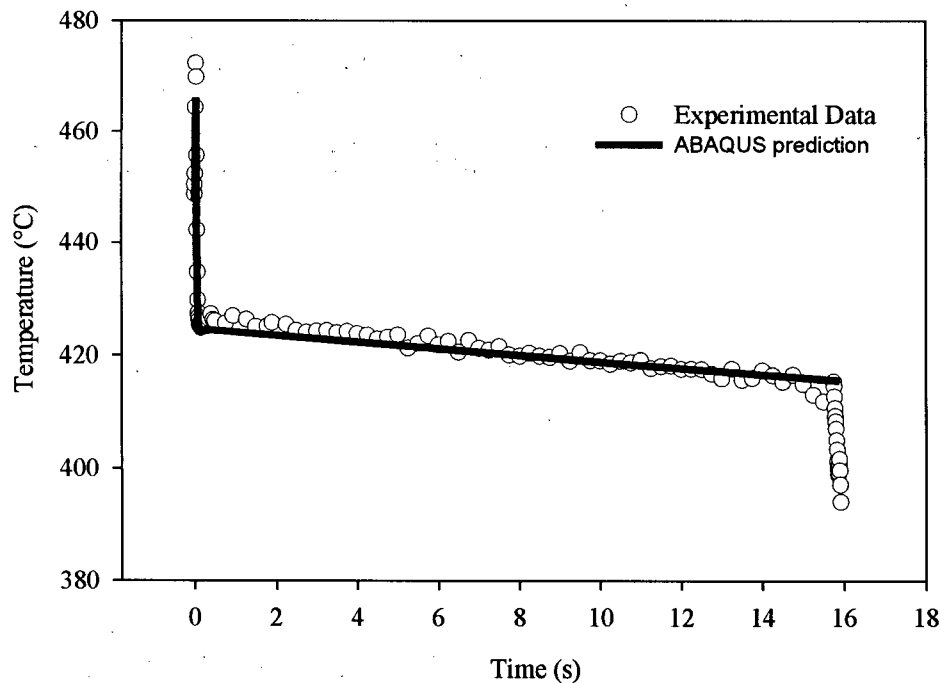
Figure 6.5 - Thermal profile between roll bite exit and quench for Sample I.

81

As can be seen from Figure 6.5, a convective heat transfer coefficient adequately describes the heat lost by the samples to the environment upon exiting the roll bite compared to the experimental data.

6.2.2 Through-Thickness Strain Comparisons

The experimental through-thickness strain was recorded by means of scoring the edge of the sample. Since the maximum amount of spread was 0.7 % in Sample I, plane strain conditions have been achieved and the strains measured at the edge are representative of the model strain predictions at the centre of the sample. A source of error in the strain measurements is the thickness of the scored lines themselves and the actual through-thickness locations.

The experimental samples have been rolled to approximately two different strain levels. Sample C has been rolled to 40 % reduction while the remaining samples have been rolled to roughly 24 % reduction. The through-thickness von Mises equivalent strains are compared to the model plastic equivalent predictions for Samples I and P in Figures 6.6 and 6.7 respectively.
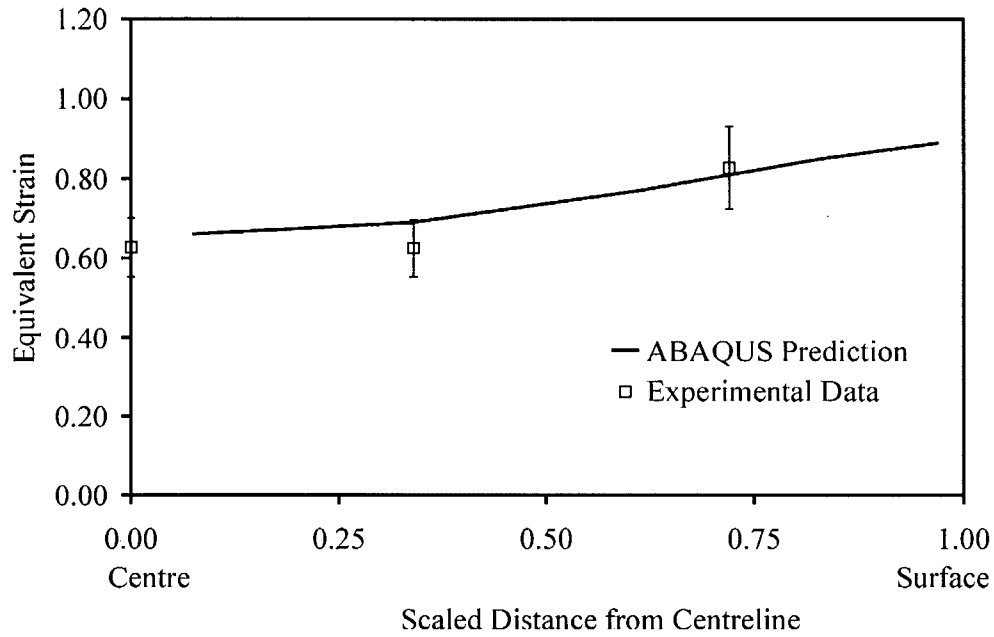
Figure 6.6 – ABAQUS™ plastic equivalent predictions versus experimental plastic equivalent data for Sample I through-thickness strains. T_{entry}=448°C, $\bar{\dot{\varepsilon}}$ =14.7 s^{-1}, % reduction=40%.
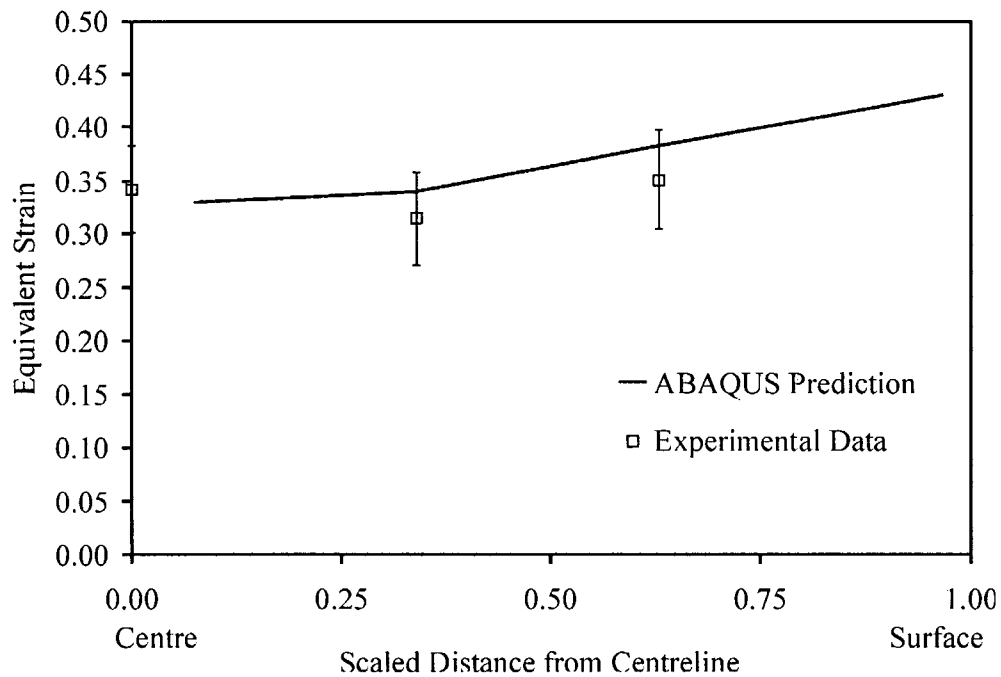
Figure 6.7 - ABAQUS™ predictions versus experimental data for Sample P through-thickness strains. T_{entry}=315 °C, $\bar{\dot{\varepsilon}}$ =11.7 s^{-1}, % reduction=24%.

From Figures 6.6 and 6.7, the von Mises equivalent through-thickness equivalent strains calculated from the experimental data agree quite well with the plastic equivalent strains predicted by the ABAQUS model. The individual strain components for Sample P are compared to the experimental measurements in Figure 6.8. Similar to the through-thickness equivalent strains of Sample I, the predicted trend of increasing plastic equivalent strains toward the surface agrees quite well with the experimental data that indicates that the friction coefficient of 0.3 adequately represents the friction conditions that exist between the work roll and the strip surface however the relative magnitude of the shear strain would indicate that the friction conditions in the model could be improved.
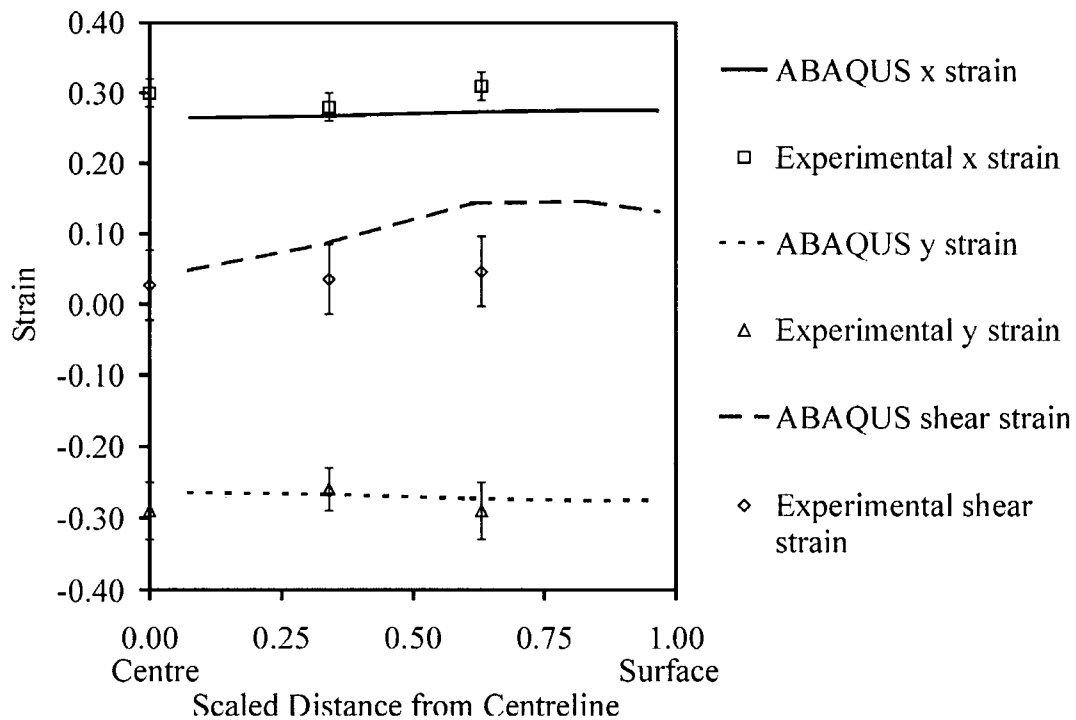
Figure 6.8 - Individual strain component comparison for Sample P. T_{entry}=315 $^{\circ}$C, $\bar{\dot{\varepsilon}}$ =11.7 s^{-1}, % reduction=24%.

84

6.2.3 Rolling Load Comparisons

During hot rolling, the interaction between the work roll and the strip surface results in what is known as a friction hill, shown in Figure 6.9, where the pressure increases through the roll bite to a maximum at the neutral point before decreasing. The neutral point is the location in the roll bite where the velocity of the strip matches the velocity of the work roll.
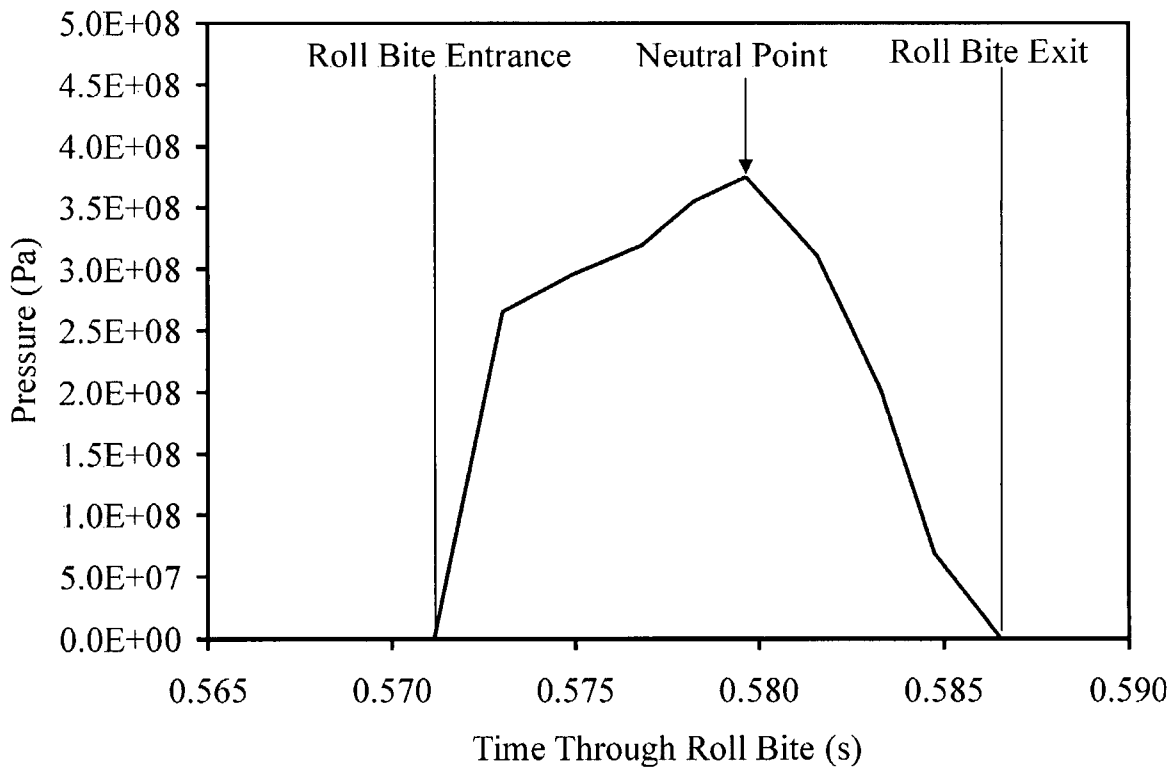
Figure 6.9 – Pressure distribution through the roll bite for a surface node predicted by ABAQUS™ for Sample O.

The pressure experienced by a surface node through the roll bite is shown in Figure 6.9. The average rolling load predicted by ABAQUS™ becomes the average pressure for a surface node multiplied by the contact area, i.e. the width of the strip by the roll bite angle. The experimentally measured rolling loads are the average rolling load during the entire sample. The experimental rolling loads are compared to the ABAQUS™ rolling loads in Table 6.1.

85

Table 6.1 – Experimental and ABAQUS rolling load comparison.

Sample ID	Experimental (kN)	ABAQUS™ (kN)	% Difference
C	n/a	1037	-
I	1330	1059	-20.4
K	1073	1114	3.7
L	1036	1017	-1.8
O	1215	1223	0.7
P	1228	1296	5.2

Overall, with the exception of Sample I, ABAQUS™ appears to be able to satisfactorily predict the average rolling loads. Factors that affect the rolling loads include: constitutive behaviour, friction conditions, strain rate and temperature. With the exception of Samples I and L, the ABAQUS™ model over-predicts the rolling loads. As shown earlier, the friction conditions in the model were adequately simulated since the predicted equivalent strains were in good agreement with the experimental equivalent strains. A comparison of predicted temperatures against the experimental temperatures indicated that the model under-predicted the temperature at both the surface and centre of the sample. This helps to explain why the model predicted rolling loads tend to be higher than those measured since the strength of AA5083 aluminum alloy increases with decreasing temperature. The significant difference in the predicted versus the experimental rolling loads for Sample I does not have an immediate explanation since the primary difference between Sample I and the remaining samples is the increased amount of reduction; otherwise the temperature and strain rate conditions (i.e. work roll velocities) are in the same range. Considering this, there may be a flaw in the code that is only apparent at the higher reductions. Possible explanations include an increased amount of elastic strain or some work hardening at the higher reduction that is not accounted for in the model. Both of these explanations can be addressed through the

choice of the hyperbolic sine equation to model the constitutive behaviour and the possibility that it may not be the optimum method at the higher reductions.

6.2.4 Microstructure

The fraction recrystallised was quantified at the surface and the centre for each of the samples after quenching using the ASTM Standard E 562-89. Fraction recrystallised predictions using Raghunathan's equation for AA5083, Equation 4.12. Average values of temperature and strain rate, along with exit values of strain predicted by the ABAQUS™ rolling model are compared to the fraction recrystallised measurements in Table 6.2.

Table 6.2 - Model predictions for fraction recrystallised compared to experimental results for the centreline using the exit values for deformation temperature and strain rate along with the exit strain.

Sample ID	Z	$t_{0.5}$ (s)	t (s)	Predicted X_V	Measured X_V	% Diff.
C	3.05×10^{12}	0.92	3	0.999	0.073	92.7
I	2.24×10^{12}	2.78	15	1.000	0.059	94.1
K	1.70×10^{13}	9.57	8	0.384	0.072	81.3
L	2.65×10^{13}	4.00	3	0.322	0.042	87.0
O	1.57×10^{15}	13.19	3	0.035	0.118	-237.1
P	4.83×10^{14}	67.29	4	0.002	0.188	-9300.0

As can be seen in Table 6.2 with the exception of Sample O, it appears that the equation developed by Raghunathan is not able to predict the fraction recrystallised. Therefore a sensitivity analysis on the process (i.e. temperature and strain rate) and material parameters (i.e. initial grain size) along with the model fitting (i.e. "a", "b" and "d" from Equation 4.12) were done using Sample P centreline as the base case. The base case parameters are summarised in Table 6.3.

Table 6.3 - Base case (Sample P) parameters for sensitivity analysis.

Material/Processing Parameters			Fitting Parameters		
d_o (μm)	$\bar{\varepsilon}$ (s^{-1})	T_{def} (°C)	a	b	d
70	11.7	315	2.7×10^{-10}	2.45	-0.58

The sensitivity analysis was done by adjusting each of the parameters by ±25%, then comparing the resulting fraction recrystallised to that predicted in the base case. The results of the sensitivity analysis for the material/processing parameters are shown in Table 6.4.

Table 6.4 - Fraction recrystallised equation sensitivity analysis results for material/processing parameters.

Parameter	Change (%)	Value	X_V Result	% Diff.
d_o	+25	87.5 μm	0.007	71.4
d_o	-25	52.5 μm	0.086	97.7
$\bar{\varepsilon}$	+25	14.63 s^{-1}	0.028	92.9
$\bar{\varepsilon}$	-25	8.78 s^{-1}	0.016	87.5
T_{def}	+25	393 °C	0.000	∞
T_{def}	-25	236 °C	1.000	99.8

As can be seen from Table 6.4, the material/processing parameter that has the greatest effect on the fraction recrystallised prediction is the deformation temperature.

88

Table 6.5 - Fraction recyrstallised equation sensitivity analysis results for model fitting parameters.

Parameter	Change (%)	Value	X_V Result	% Diff.
a	+25	3.34×10^{-10}	0.014	85.7
a	-25	2.03×10^{-10}	0.038	94.7
b	+25	3.06	0.000	∞
b	-25	1.84	0.980	99.8
d	+25	-0.725	1.000	99.8
d	-25	-0.435	0.000	∞

As can be seen in Table 6.5, the fitting parameters that have the strongest influence on the fraction recrystallised prediction are the exponent for the Zener-Hollomon parameter ("d") and the exponent for the initial grain size ("b").

Since the Raghunathan equation was unable to accurately predict the fraction recrystallised in the experimental samples, an attempt was made to modify the coefficients in the equation to better reflect the experimental data. This was done by using the JMAK equation to calculate the $t_{0.5}$ from the experimental data. In order to do this, it was assumed that there was negligible temperature loss after rolling and prior to the quench. The resulting $t_{0.5}$ values are summarised in Table 6.6.

The $t_{0.5}$ values in Table 6.6 were then plotted against the Zener-Hollomon parameter to determine whether a relationship between the exit deformation and the resulting microstructure exits, as shown in Figure 6.10.

Table 6.6 - Summary of calculated $t_{0.5}$ based on the experimental data.

| Sample ID	Location	$t_{0.5}$ (s)
C	Surface	2.00
	Centre	9.07
I	Surface	9.41
	Centre	50.65
K	Surface	7.46
	Centre	24.23
L	Surface	3.55
	Centre	11.93
O	Surface	3.27
	Centre	7.04
P	Surface	3.08
	Centre	7.30
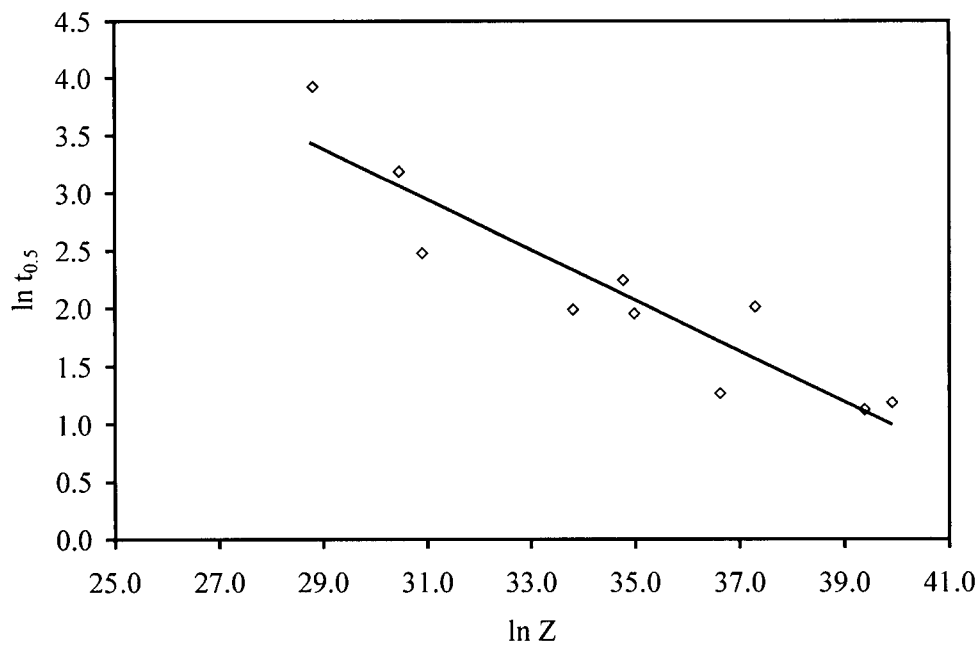
Figure 6.10 - Measured ln $t_{0.5}$ plotted against exit deformation conditions used in the Zener-Hollomon parameter.

This was done for roll bite exit deformation conditions along with the average strain rate. The straight line, that fits the data reasonably well, indicates that there is a relationship between the deformation conditions and the $t_{0.5}$. Unfortunately, due to the lack of data and the questionable nature of the data that was available it was not feasible to determine new curve fitting constants. The variation in sample chemistries and the significantly different experimental conditions that were experienced between this study and that by Raghunathan significantly influence the microstructure predictions. Therefore, the predictions based on these equations are not realistic and further tests under the pilot-scale rolling conditions would be required to develop new equations for $t_{0.5}$ in order to accurately predict the microstructure.

6.3 Summary

The ABAQUS™ model was validated in two steps. The first validation step was a literature rolling simulation to investigate only the through-thickness strain and temperature distributions to validate the model algorithm applied to the ABAQUS™ rolling simulation. The ABAQUS™ model was found to adequately simulate the conditions described by the literature models. The second validation step was the simulation of the CORUS Multi-mill against which experimental data could be compared to the model. Components of the ABAQUS™ model that were compared to experimental data were rolling loads, through-thickness strains, temperatures and microstructure data.

The ABAQUS™ model was shown to adequately simulate the hot rolling process under a variety of rolling conditions with the exception of the microstructure predictions. The microstructure model was not able to consistently describe the experimental microstructure. A sensitivity analysis on the input parameters to the microstructure equations revealed that the deformation temperature was the most influential parameter followed by the initial grain size. The parameters of strain and strain rate do not have a dramatic influence on the fraction recrystallised predictions.

The equations developed by Raghunathan were not able to predict the fraction recrystallised for the conditions experienced by the samples in the pilot-scale rolling mill. In order to be able to accurately predict the fraction recrystallised a series of experiments under the pilot-scale rolling conditions would be required to develop a new $t_{0.5}$ equation.

6.4 References

1   Wells, M.A., Lloyd, D.J., Samarasekera, I.V., Brimacombe, J.K. and Hawbolt, E.B. "Modeling the microstructural changes during hot tandem rolling of AA5XXX aluminum alloys. Part III. Overall model development and validation" Meta and Mat Trans., Vol. 29B, pp. 709-720, June, 1998

2   Chen, B.K., Choi, S.K. and Thomson, P.F. "Simulation of evolution of microstructure in a thermo-mechanical analysis of the hot rolling of aluminium" Res Mechanica, 31, pp. 455-469, 1991

Chapter 7   Summary and Conclusions

A mathematical model has been developed to predict the rolling loads and evolution of the through-thickness temperature, microstructure and strain in an aluminum strip during a single hot rolling stand.   The semi-empirical equations describing the microstructure focused primarily on the commercially significant AA5083 aluminum alloy although the thermomechanical model used to predict the through-thickness temperature and strain was applied to both AA5083 and AA5056 aluminum alloys.

The overall model includes a plasticity component to predict the strain, strain rate and temperature distribution in the strip as it is being rolled, as well as a component to predict the microstructure and temperature distribution in the strip in the time between the roll bite exit and quench.   Validation of the model using experimental data from a pilot scale rolling mill indicated that it gave reasonable predictions for the rolling loads, temperature and strain.   However, the model proved less successful in predicting the recrystallised fraction.

7.1 Plasticity Model (ABAQUS™)

The plasticity model was developed using a commercial finite element package ABAQUS™, a 2-D transient model which couples the thermal and deformation phenomenon that occur during strip rolling.   One of the strengths of this model is that the only tuning that was done for the thermal and deformation models was the choice of constitutive behaviour equations that were taken from the literature and agreed well with independent experimental data.   Using this model it was found that:

- ABAQUS™ was able to reasonably simulate the temperature and strain distribution in the strip when compared to other finite element models (i.e. MARC and DEFORM) and experimental data.

- The friction boundary condition using a Coulomb friction coefficient is reasonable since the model predicted strain distribution was similar to the experimental measurements.

- The assumed heat transfer coefficient appears to be slightly too high as the model predicted temperature profile under-predicts the experimental temperature profile.

- For the experimental mill the convective heat transfer coefficient outside the roll bite was found to be 12.5 $W\,m^{-2}\,{}^{\circ}C^{-1}$.

7.2 Microstructure Model

The user-defined subroutine within the ABAQUS™ finite element model includes semi-empirical equations that describe the through-thickness fraction recrystallised. The semi-empirical equation used to model the fraction recrystallised in an AA5083 aluminum alloy after hot deformation was taken from the literature. This equation, based on Raghunathan's work, relies on temperature, strain and strain rate information during rolling as input. Using this equation the following conclusions were drawn:

- Although qualitatively, Raghunathan's microstructure model was able to predict the gradient in fraction recrystallised from the centre to surface, quantitatively the difference between the model and measured data was unacceptable with the model over-predicting the fraction recrystallised.

- A sensitivity analysis on material/processing parameters showed that the deformation temperature had the strongest influence on the fraction recrystallised predictions.

- A sensitivity analysis on the fitting coefficients indicated that the initial grain size and Zener-Hollomon exponents have a major influence on the fraction recrystallised predictions.

- Based on the experimental data, a relationship does exit between the roll bite exit deformation conditions and the time to 50% recrystallisation. Unfortunately there was insufficient data to determine what the equation coefficients should be to accurately predict the time to 50% recrystallisation.

7.3 Future Work

The model developed in this investigation provides a basis for the scientific visualization of the effects of process parameters on the microstructure formation during hot rolling of AA5083 aluminum alloys. Suggestions for future work to improve the model's capabilities include:

1. Improved quantification of the starting microstructure for parameters such as grain size distribution and particle distribution.

2. Conduct a series of tests under the pilot-scale rolling conditions to determine the relationship between deformation conditions and the microstructure.

3. Further investigate the cause for the significant difference between the model predictions and measured values for roll force.

4. Integration of a more sophisticated microstructural model including texture evolution for AA5XXX alloys. Two separate approaches could be taken. First, a Cellular Automaton approach and second, a more traditional approach such as that done by Wells [1] or Vatne [2].

5. Extend the model's capability to multi-stand, including a method to account for the retained strain characteristic of partially recrystallised microstructures.

6. More experimental surface data is required to refine the roll bite heat transfer coefficient.

7.4 References

1   Wells, M.A., Lloyd, D.J., Samarasekera, I.V., Brimacombe, J.K. and Hawbolt, E.B. "Modeling the microstructural changes during hot tandem rolling of AA5XXX aluminum alloys: part I. Microstructural evolution" Met and Mat. Trans, Vol. 29B, pp. 611-620, 1998

2   Vatne, H.E. and Nes, E. "A model for recrystallisation kinetics, texture and grain size applied to multipass hot rolling of an AlMgMn aluminium alloy" Comp. Mat. Sci, Vol. 7, pp. 5-10, 1996

Appendix A

Table A.1 - ABAQUS look-up table for rate-dependent plasticity.

Strain Rate (s^{-1})	Temperature (°C)	Flow Stress (Pa)	Strain Rate (s^{-1})	Temperature (°C)	Flow Stress (Pa)
0.0001	150	2.109E+08	20	325	1.965E+08
0.0001	175	1.824E+08	20	350	1.820E+08
0.0001	200	1.569E+08	20	375	1.686E+08
0.0001	225	1.340E+08	20	400	1.562E+08
0.0001	250	1.133E+08	20	425	1.447E+08
0.0001	275	9.444E+07	20	450	1.340E+08
0.0001	300	7.728E+07	20	475	1.240E+08
0.0001	325	6.164E+07	25	150	3.484E+08
0.0001	350	4.752E+07	25	175	3.199E+08
0.0001	375	3.513E+07	25	200	2.944E+08
0.0001	400	2.487E+07	25	225	2.715E+08
0.0001	425	1.706E+07	25	250	2.508E+08
0.0001	450	1.158E+07	25	275	2.319E+08
0.0001	475	7.915E+06	25	300	2.147E+08
1	150	3.128E+08	25	325	1.990E+08
1	175	2.843E+08	25	350	1.845E+08
1	200	2.588E+08	25	375	1.711E+08
1	225	2.359E+08	25	400	1.587E+08
1	250	2.152E+08	25	425	1.472E+08
1	275	1.963E+08	25	450	1.365E+08
1	300	1.791E+08	25	475	1.265E+08
1	325	1.633E+08	30	150	3.504E+08
1	350	1.488E+08	30	175	3.219E+08
1	375	1.355E+08	30	200	2.965E+08
1	400	1.231E+08	30	225	2.735E+08
1	425	1.116E+08	30	250	2.528E+08
1	450	1.009E+08	30	275	2.339E+08
1	475	9.089E+07	30	300	2.167E+08
5	150	3.306E+08	30	325	2.010E+08
5	175	3.021E+08	30	350	1.865E+08
5	200	2.766E+08	30	375	1.731E+08
5	225	2.537E+08	30	400	1.607E+08
5	250	2.330E+08	30	425	1.492E+08
5	275	2.141E+08	30	450	1.385E+08
5	300	1.969E+08	30	475	1.285E+08
5	325	1.811E+08	35	150	3.522E+08
5	350	1.666E+08	35	175	3.237E+08
5	375	1.533E+08	35	200	2.982E+08
5	400	1.409E+08	35	225	2.752E+08

Strain Rate (s^{-1})	Temperature (°C)	Flow Stress (Pa)	Strain Rate (s^{-1})	Temperature (°C)	Flow Stress (Pa)
5	425	1.294E+08	35	250	2.545E+08
5	450	1.187E+08	35	275	2.356E+08
5	475	1.087E+08	35	300	2.184E+08
10	150	3.383E+08	35	325	2.027E+08
10	175	3.098E+08	35	350	1.882E+08
10	200	2.843E+08	35	375	1.748E+08
10	225	2.614E+08	35	400	1.624E+08
10	250	2.406E+08	35	425	1.509E+08
10	275	2.218E+08	35	450	1.402E+08
10	300	2.046E+08	35	475	1.302E+08
10	325	1.888E+08	40	150	3.536E+08
10	350	1.743E+08	40	175	3.251E+08
10	375	1.609E+08	40	200	2.996E+08
10	400	1.485E+08	40	225	2.767E+08
10	425	1.370E+08	40	250	2.560E+08
10	450	1.263E+08	40	275	2.371E+08
10	475	1.163E+08	40	300	2.199E+08
15	150	3.428E+08	40	325	2.041E+08
15	175	3.143E+08	40	350	1.896E+08
15	200	2.888E+08	40	375	1.763E+08
15	225	2.659E+08	40	400	1.639E+08
15	250	2.451E+08	40	425	1.524E+08
15	275	2.263E+08	40	450	1.417E+08
15	300	2.091E+08	40	475	1.317E+08
15	325	1.933E+08	45	150	3.549E+08
15	350	1.788E+08	45	175	3.264E+08
15	375	1.654E+08	45	200	3.009E+08
15	400	1.530E+08	45	225	2.780E+08
15	425	1.415E+08	45	250	2.573E+08
15	450	1.308E+08	45	275	2.384E+08
15	475	1.208E+08	45	300	2.212E+08
20	150	3.460E+08	45	325	2.055E+08
20	175	3.175E+08	45	350	1.910E+08
20	200	2.920E+08	45	375	1.776E+08
20	225	2.690E+08	45	400	1.652E+08
20	250	2.483E+08	45	425	1.537E+08
20	275	2.295E+08	45	450	1.430E+08
20	300	2.122E+08	45	475	1.330E+08

Appendix B

Table B.1 - Starting sample dimensions.

Sample ID	Width (mm)	Length (mm)	Thickness (mm)
C	200.0	496.2	9364
I	200.0	496.2	9.67
K	200.0	496.2	9.65
L	200.0	496.5	9.62
O	200.0	496.5	9.58
P	200.0	496.2	9.61

APPENDIX C
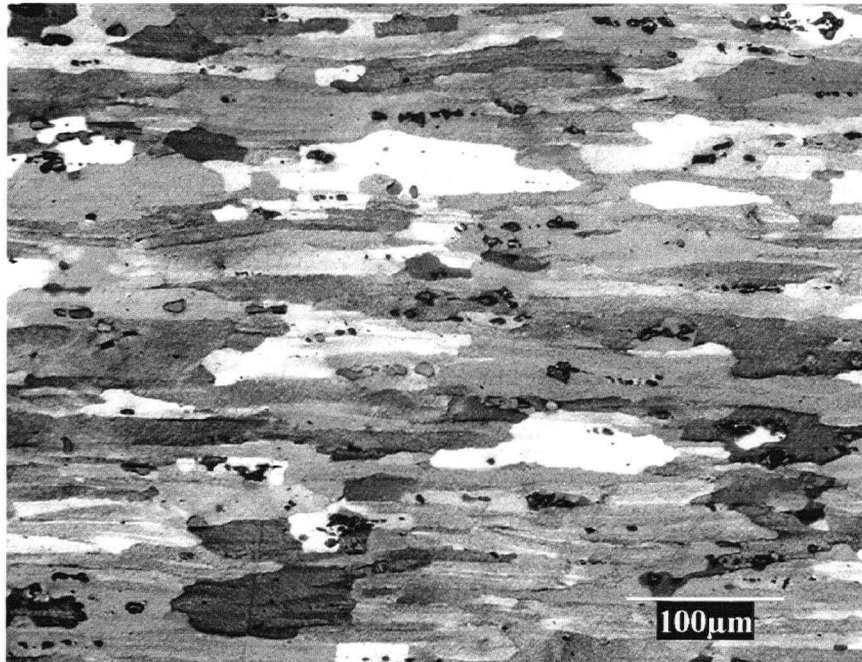
a) Centreline
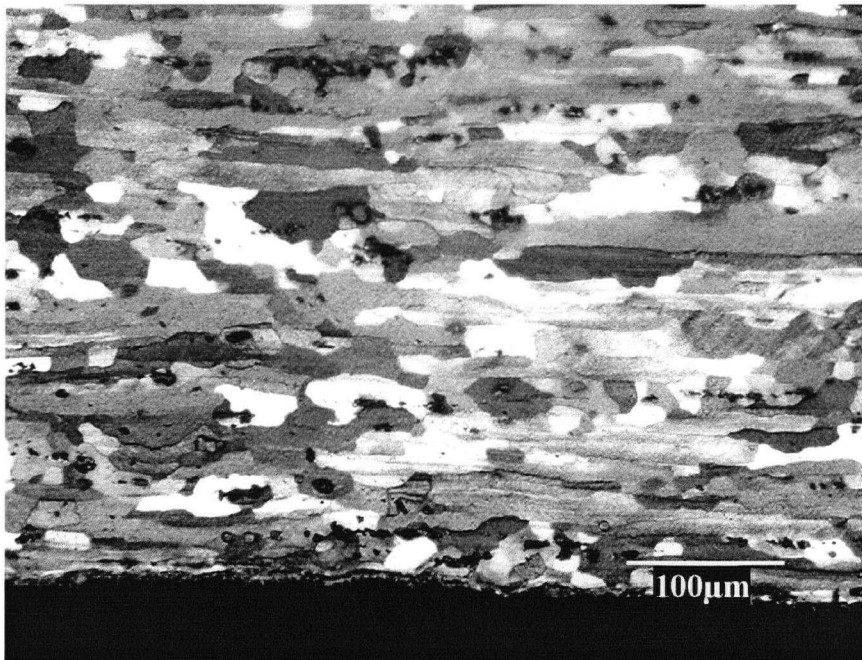
b) Surface

Figure C.1 - Sample C deformed microstructure after being annodized using Barker's reagent and viewed under polarised light at 20x magnification. a) Centreline b) Surface.
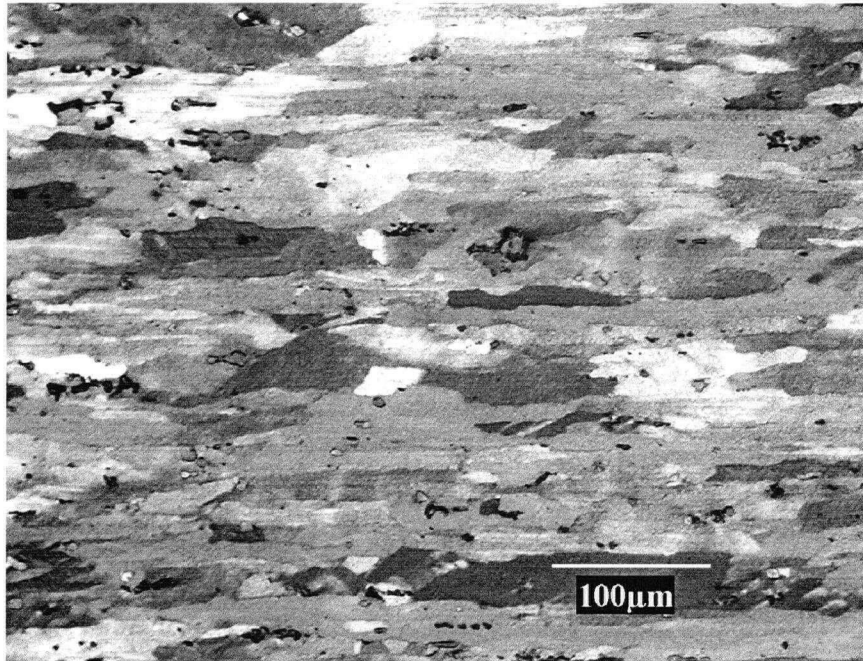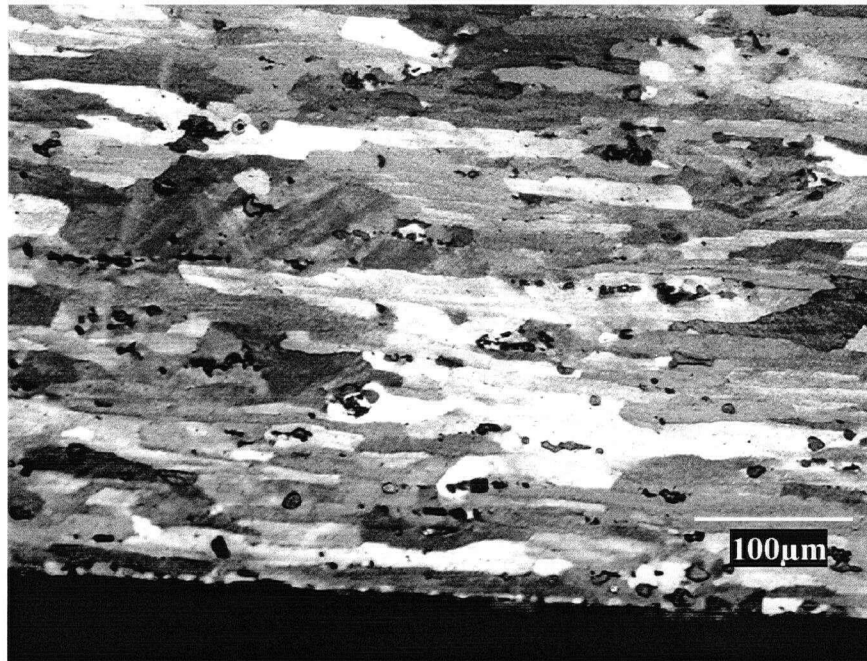
a) Centreline

b) Surface

Figure C.2 - Sample K deformed microstructure after being annodized using Barker's reagent and viewed under polarised light at 20x magnification. a) Centreline b) Surface.
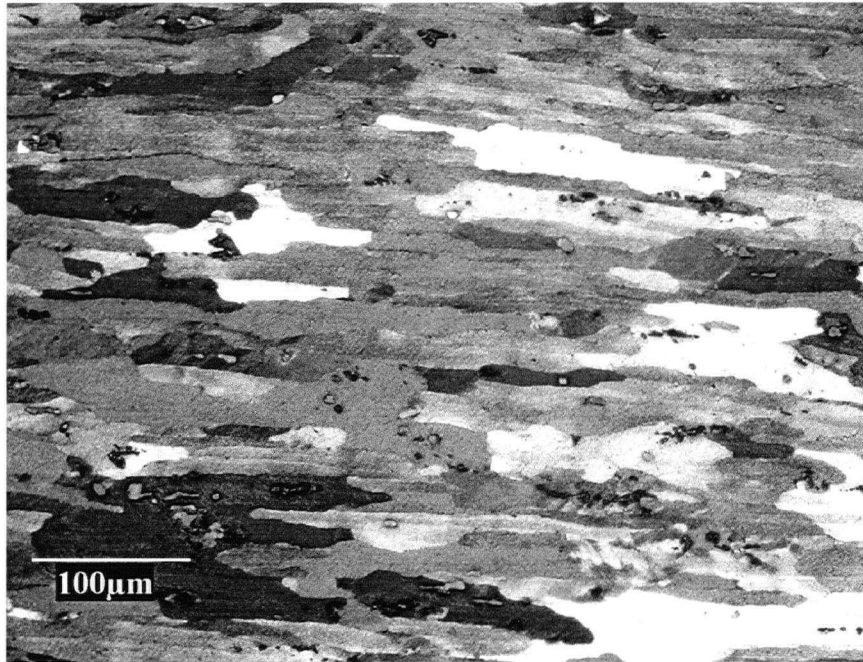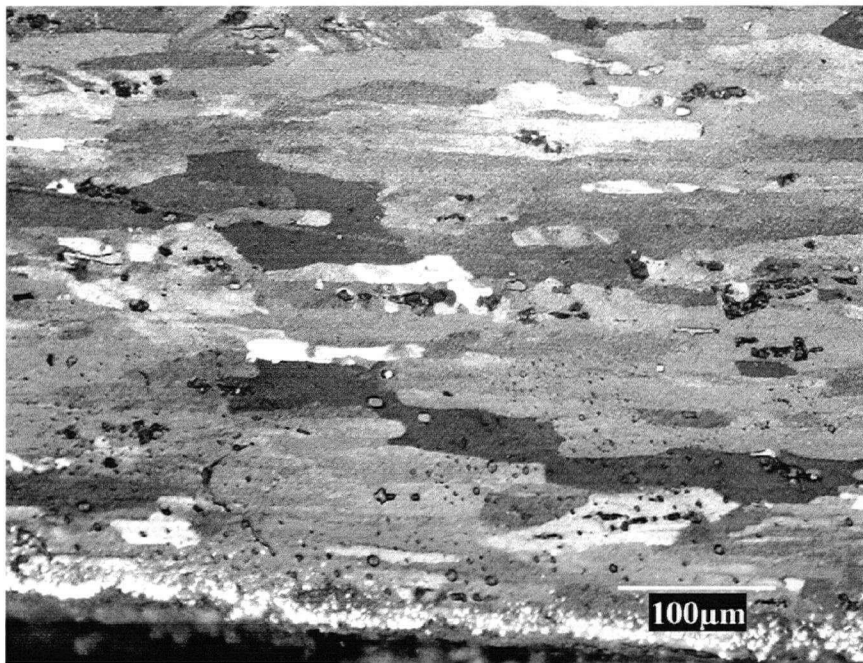
a) Centreline

b) Surface

Figure C.3 - Sample L deformed microstructure after being annodized using Barker's reagent and viewed under polarised light at 20x magnification. a) Centreline b) Surface.
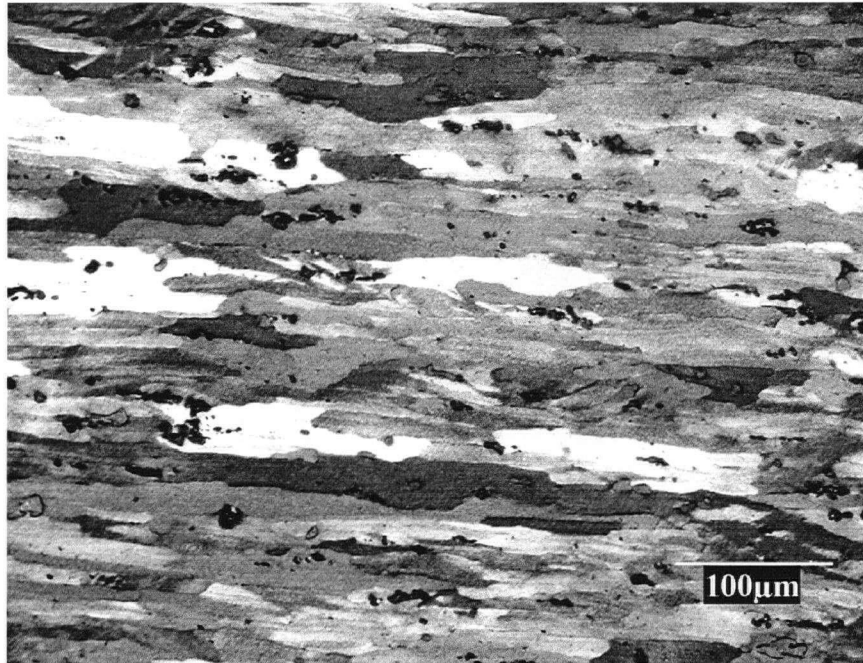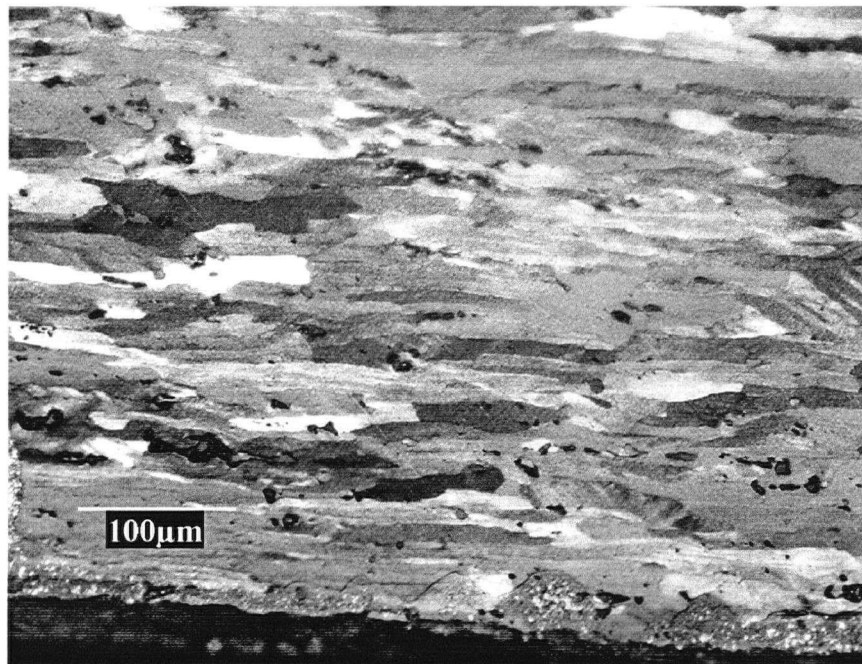
a) Centreline

b) Surface

Figure C.4 - Sample O deformed microstructure after being annodized using Barker's reagent and viewed under polarised light at 20x magnification. a) Centreline b) Surface.
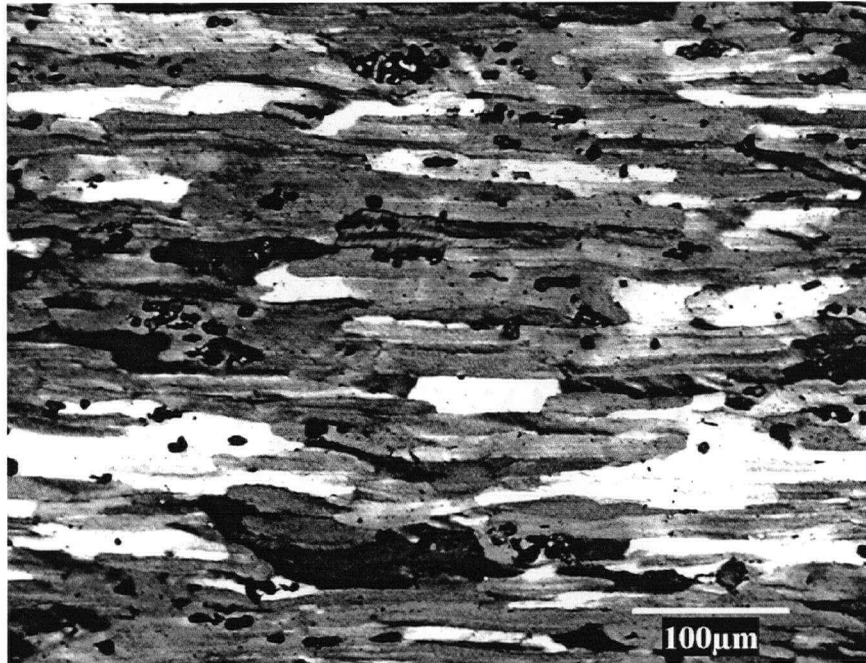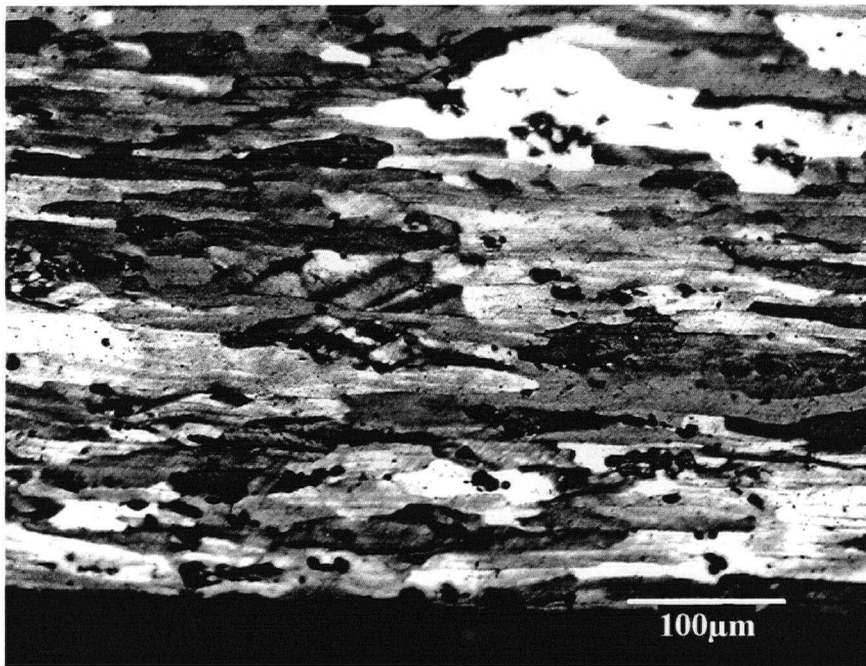
a) Centreline

b) Surface

Figure C.5 - Sample P deformed microstructure after being annodized using Barker's reagent and viewed under polarised light at 20x magnification. a) Centreline b) Surface.

103